34

PHARMACODYNAMICS

BEOM SOO SHIN, DHAVAL SHAH, AND JOSEPH P. BALTHASAR
University at Buffalo, The State University of New York, Buffalo, New York

Contents

34.1 Introduction
34.2 Overview
34.3 "Static" Models of Pharmacological Response
  34.3.1 Drug–Receptor Binding
  34.3.2 E_{max} Model
  34.3.3 Sigmoid E_{max} Model (Hill Equation)
34.4 "Kinetic" Models of Pharmacological Response
  34.4.1 Direct Effect Models
  34.4.2 Indirect Response Models
  34.4.3 Transduction Models
  34.4.4 Irreversible Effects
  34.4.5 Tolerance Models
34.5 Conclusion
Acknowledgments
References

34.1 INTRODUCTION

Pharmacodynamics refers to the study of relationships between drug concentrations and pharmacological effects. The mathematical description of these relationships, through the use of appropriate *pharmacodynamic models*, facilitates the characterization and comparison of candidate drugs, facilitates the rational selection of appropriate dosing regimens, and assists in the investigation and identification of

Preclinical Development Handbook: ADME and Biopharmaceutical Properties,
edited by Shayne Cox Gad
Copyright © 2008 John Wiley & Sons, Inc.

the mechanisms associated with drug action. This chapter is structured to provide an overview and a catalog of mathematical models that may be employed to characterize drug pharmacodynamics. Section 34.2 provides a brief overview of the analysis of pharmacodynamic data, Section 34.3 reviews mathematical models used to relate fixed (e.g., steady-state) drug concentrations to drug effects, and Section 34.4 covers basic and advanced models that relate the time course of drug exposure to the time course of drug effects. Section 34.5 provides a brief summary of the chapter.

34.2 OVERVIEW

Pharmacodynamics can be defined as the study of the relationships between the systemic exposure of drug and its biological action. Upon intravascular or extravascular administration, the drug enters the systemic circulation directly or with an absorption phase. Once the drug reaches the systemic circulation, drug is distributed into various organs and then eliminated by metabolism and excretion. *Pharmacokinetics* refers to the investigation of the rates and extent of drug absorption, distribution, metabolism, and excretion, and *pharmacokinetic models* allow description of the relationship between drug dosing and the time course of drug concentrations in the body. The combination of pharmacokinetic models with pharmacodynamic models, which relate drug exposure to drug response, allows for the characterization and prediction of the relations hips between the timing of drug administration and the time course of drug effects (Fig. 34.1). The main differences between pharmacokinetics and pharmacodynamics are summarized in Table 34.1 [1].

Pharmacological responses are initiated by binding of drug molecule with proteins (e.g., enzymes, receptors) or, in certain cases, DNA. The intensity of the drug response is altered as a function of the administered dose, with a higher receptor–drug binding generally producing a greater response. At a certain point, the response may be saturated and the relationship between drug concentration and response becomes nonlinear. In 1927, Clark [2] first introduced the drug–receptor binding concept into pharmacodynamics. It was suggested that the quantitative effect of acetylcholine was mediated by a receptor-binding process. Clark's occupancy theory was elaborated by Ariens and De Groot [3] and Stephenson [4] and became a fundamental basis for the field of pharmacodynamics. Upon long-term infusion or multiple dosing, drug concentrations in each area of the body will approach a steady state, where concentrations are constant with time. In such cases, drug response may be assumed to be "static" or time invariant. Section 34.3 of this chapter discusses several mathematical models that have been developed to describe static drug concentration–response relationships, including the E_{max} and the sigmoid E_{max} model.

Although static models are useful in some situations, "kinetic" models, which relate the time course of drug concentration to the time course of drug response, provide a much more complete characterization of drug pharmacodynamics, and kinetic models often provide great insight into the underlying mechanisms responsible for drug effects. Kinetic models of drug response are reviewed in Section 34.4. The simplest of the kinetic models, *direct effect models*, assume a direct relationship

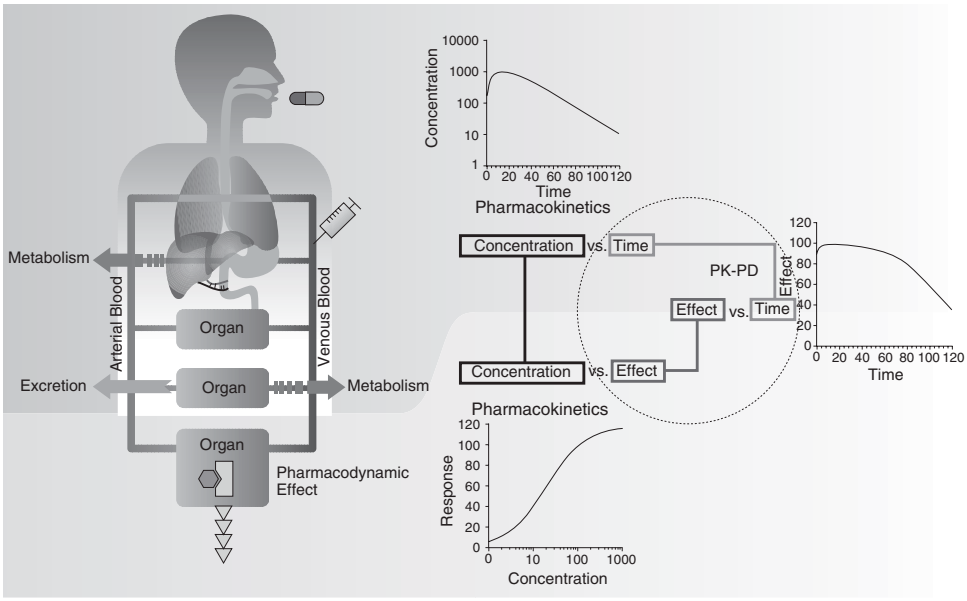


FIGURE 34.1 Representative diagram for relationship between pharmacokinetics and pharmacodynamics. Pharmacokinetics mainly deals with the time course of drug absorption (A), distribution (D), metabolism (M), and elimination (E). Pharmacodynamics deals with the drug effect as a function of drug concentration. Pharmacokinetic and pharmacodynamic (PKPD) modeling combines the two processes to allow prediction and characterization of the time course of drug effects.

TABLE 34.1 Main Differences Between Pharmacokinetics and Pharmacodynamics

Characteristics	Pharmacokinetics	Pharmacodynamics
Broad definition	What body does to the drug	What the drug does to the body
Influence	Affected by interactions throughout the whole body	Affects specific drug receptors/ signaling pathways
Determinants	Typically governed by simple physiologic determinants	Typically determined by complex, nonlinear response and control pathways
Linearity	Typically linear	Typically nonlinear
Initial condition	Baseline concentrations are zero prior to drug dosing	Nonzero baseline response prior to drug dosing

between drug concentrations in plasma and drug response. In many cases, drug responses are delayed relative to the time course of drug concentrations in plasma. Several models have been developed to describe mechanisms responsible for this delay. For example, the *biophase model* assumes that the delay between the time course of drug concentrations in plasma and the time course of drug effect is due to the kinetics of drug distribution to the site of drug action (i.e., the biophase). *Indirect effect models* assume that the delay is related to the production

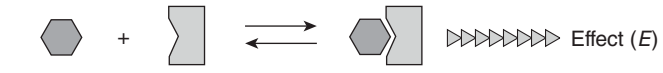
or elimination of endogenous substances related to the observed drug effect, and *transduction models* attempt to describe a cascade of signaling events that act as intermediates between drug–receptor binding and drug response. Section 34.4 also introduces pharmacodynamic models that may be used to characterize irreversible drug responses (e.g., cytotoxicity) and complexities including tolerance and sensitization.

34.3 "STATIC" MODELS OF PHARMACOLOGICAL RESPONSE

Drug response is initiated by the interaction of drug with biomolecules (e.g., receptors, enzymes, DNA) at the biophase. Unfortunately, in most cases, it is difficult or impossible to measure drug concentrations at the biophase and, consequently, pharmacodynamic models typically attempt to relate drug effects to drug concentrations in plasma. However, such relationships are confounded by any disequilibrium that exists between drug concentrations in plasma and drug concentrations at the biophase. Concerns associated with distribution delays may be overcome by the use of *steady-state* drug concentrations. Upon long-term intravenous infusion, a steady state may occur, where drug concentrations in all sites in the body, including plasma and the biophase, remain constant with time. Under these circumstances, a unique, monotonic relationship between drug concentrations in plasma and drug concentrations at the biophase may be assumed. Following administration of drug at a variety of infusion rates, sufficient data may be available to develop relationships between steady state concentrations and the magnitude of drug effect. Due to the nature of the steady state, these relationships may be considered to be time invariant or "static," and these relationships are unable to describe the time course of drug response. This section introduces drug–receptor binding theory and several static pharmacodynamic models, including the E_{max} model, the log-linear E_{max} model, and the sigmoid E_{max} model.

34.3.1 Drug–Receptor Binding

The biological action of a drug is initiated by the interaction of the drug with free receptor, which may be expected to follow the law of mass action:



R and D represent free receptor and drug; DR and E represent the drug–receptor complex and the effect of drug, respectively. The brackets [ ] signify the representation of molar concentrations. Typically, the following assumptions are made for this equation:

1. The interaction is reversible.
2. The receptor, drug, and drug–receptor complex are in equilibrium.

3. The receptor contains one binding site for the drug.
4. The drug and receptor interact rapidly to form the drug–receptor complex.

At equilibrium,

$$K_D = \frac{[D][R]}{[DR]} \tag{34.1}$$

where K_D is the equilibrium dissociation constant for the drug–receptor complex.

The total concentration of receptor, $[R_T]$, is the sum of bound and free receptors.

$$[R_T] = [R] + [DR] \tag{34.2}$$

By rearranging Eq. 34.2, we have

$$[R] = [R_T] - [DR] \tag{34.3}$$

By substituting Eq. 34.3 into Eq. 34.1, the following equation is obtained:

$$K_D = \frac{([R_T] - [DR]) \times [D]}{[D][R]} = \frac{[R_T][D] - [DR][D]}{[DR]} \tag{34.4}$$

And by Rearranging Eq. 34.4, we have

$$[DR] = \frac{[R_T][D]}{K_D + [D]} \tag{34.5}$$

In 1954, Ariens and De Groot [3] proposed the concept that drug–receptor complex [DR] is linearly proportional to the effect of drug. According to this theory, [DR] can be substituted by effect E, and the total receptor concentration $[R_T]$, which will bind with drug and form [DR], can be represented by the maximum response E_{max}. The steady-state free drug concentration at the biophase [D] is often assumed to be the same as the steady-state free drug concentration in plasma $[C_p]$. Taken together, Eq. 34.5 can be rewritten as follows:

$$E = \frac{E_{max} \times [C_p]}{K_D + [C_p]} \tag{34.6}$$

K_D is in units of concentration (mass/volume). EC_{50} may be defined as the drug concentration associated with the binding of 50% of the drug receptor, where effect is one-half of E_{max} $[E_{max}/2]$.

$$\frac{E_{max}}{2} = \frac{E_{max} \times [EC_{50}]}{K_D + [EC_{50}]} \tag{34.7}$$

By rearranging Eq. 34.7, K_D can be represented as the concentration that produces 50% of the maximum response:

$$K_D = EC_{50} \tag{34.8}$$

Equation 34.6 can be rewritten as follows:

$$E = \frac{E_{max} \times [C_p]}{EC_{50} + [C_p]} \tag{34.9}$$

This equation is often referred to as the *maximum effect* (E_{max}) *model.*

34.3.2 E_{max} Model

The E_{max} model predicts a hyperbolic relationship between concentration and response, where, at low concentrations, the relationship between concentration and response is linear but, as the dose increases, the response becomes saturated and reaches a plateau (Fig. 34.2). As indicated in the simple E_{max} model (Eq. 34.9), drug response will be zero when no drug is present. However, in many cases, the effects produced by endogenous ligands for the receptor may not be differentiated from drug effects, and it is necessary to consider a "baseline" level of response (E_0):

$$E = E_0 + \frac{E_{max} \times [C_p]}{EC_{50} + [C_p]} \tag{34.10}$$

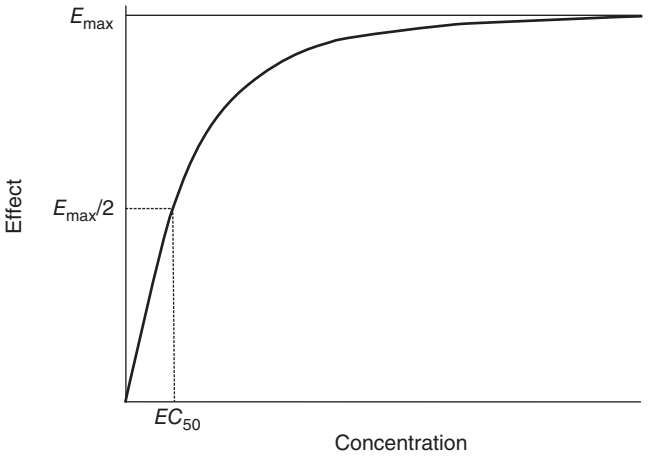


FIGURE 34.2 Typical effect versus concentration relationship predicted by the E_{max} model. At low concentrations, there is a linear relationship between drug concentration and response. As the concentration increases, the drug response pathways become saturated and eventually a plateau is achieved. E_{max} represents the maximal effect of the drug and EC_{50} represents the potency of the drug. EC_{50} is defined as the concentration of drug required to produce 50% of the maximum effect.

where E_0 represents the baseline effect measured in the absence of drug.

In cases where drug inhibits a physiological process, effect may be characterized by rearrangement of the E_{max} model as follows:

$$E = E_0 - \frac{I_{max} \times [C_p]}{IC_{50} + [C_p]} \tag{34.11}$$

In the inhibitory model, the maximum inhibitory response and the concentration that produces 50% of the maximum inhibitory response are regarded as I_{max} and IC_{50} instead of E_{max} and EC_{50}. In certain cases, response is represented as the percentage change of baseline value. Using the percentage change makes the baseline zero and thus a simple E_{max} model (Eq. 34.9) may be applied.

Efficacy, Potency, and Intrinsic Activity In Fig. 34.2, E_{max} represents the *efficacy* of the drug and EC_{50} represents the *potency* of the drug. The efficacy means the strength of response that is generated by a single receptor [4]. The potency is commonly represented by the EC_{50} value. A smaller EC_{50} value means a higher potency. Figure 34.3 presents effect versus concentration curves for drugs with differing efficacy and potency. In Fig. 34.3a, both drug A and drug B have the same E_{max} value, although drug A has a smaller EC_{50} value compared with drug B. Thus, to reach the same response, a higher concentration is needed for drug B as compared with drug A, indicating that drug A exhibits a higher potency than drug B. In Fig. 34.3b, drug A has a smaller EC_{50} value compared with drug B. However, the E_{max} value of drug B is higher than that of drug A. Thus, drug A has a higher potency but lower efficacy compared with drug B. Another important concept of the E_{max} model is the *intrinsic activity* (ε) introduced by Ariens and De Groot [3]. The intrinsic activity can be presented by a relationship between response and occupancy of receptor. Although biological response is directly proportional to receptor occupancy, drugs with different intrinsic activity will generate different levels of response at any given value of receptor occupancy (e.g., as seen with "full agonists" vs. "partial agonists").

$$\varepsilon = \frac{[DR]}{E} \tag{34.12}$$

Linear Model At low concentrations of drug, the relationship between concentration and response is assumed to be linear (Fig. 34.4a):

$$E = mC_p + E_0 \tag{34.13}$$

where m represents the slope, which is equivalent to E_{max}/EC_{50}. However, as the concentration increases, the drug receptors will become saturated and eventually the response reaches the E_{max}. Thus, this linearization of the E_{max} model is valid only at low concentrations ($C_p << EC_{50}$).

Log-Linear Model As indicated previously, when plotted on a linear scale, the E_{max} model predicts a hyperbolic relationship between drug concentration and

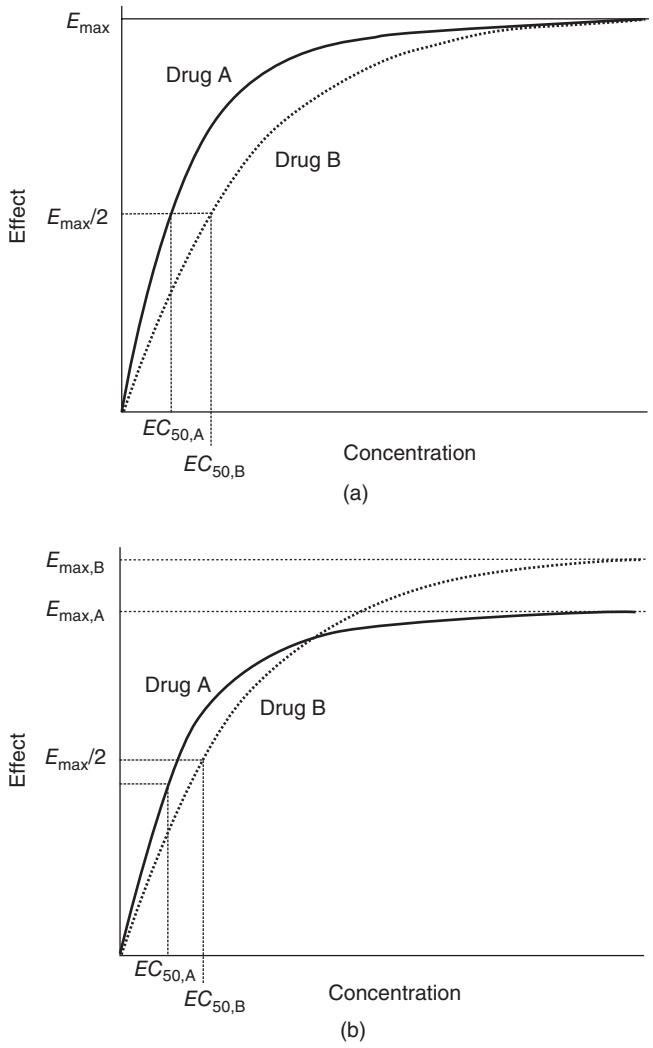


FIGURE 34.3 Influence of E_{max} and EC_{50} on effect versus concentration profiles predicted by the E_{max} model. (a) Drug A and drug B have the same efficacy (E_{max}) but drug A is more potent compared to drug B ($EC_{50,A} < EC_{50,B}$). Thus, to reach the same response, higher concentrations of drug B are needed compared to drug A. (b) Drug A and drug B show different efficacy and different potency. Drug A has a smaller EC_{50} value compared to drug B, and drug A has a smaller E_{max} value compared to drug B. Thus, drug A shows higher potency but less efficacy compared to drug B.

response. However, when plotted using a log scale for drug concentration, the plot becomes sigmoidal (Fig. 34.4b), and a log-linear relationship is found between concentration and response over the range of 20–80% of E_{max}. This relationship may be represented with the following equation:

$$E = m\log(C_p) + b \tag{34.14}$$

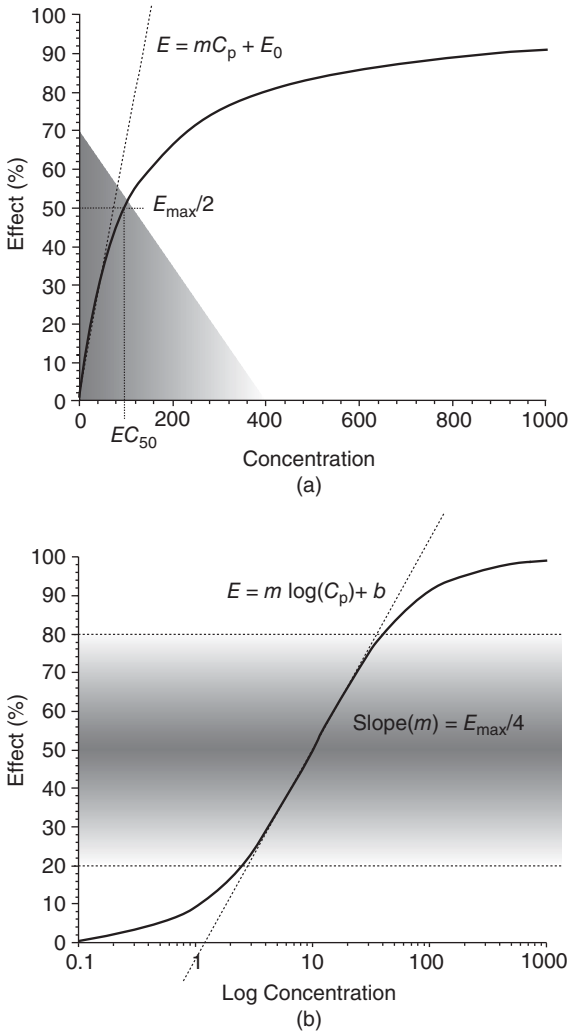


FIGURE 34.4 Comparison of rectilinear and semilog plots of effect versus concentration profiles predicted by the E_{max} model. (a) Plotting effect versus concentration profile on a linear scale provides a hyperbolic relationship between response and drug concentration. At very low concentrations of drug, the relationship between response and concentration can be described as linear and can be represented by the equation $E = mC_p + E_0$, where m is the slope and E_0 is the intercept. (b) Plotting the effect versus concentration profile on a semilog scale, the relationship between response and concentration becomes sigmoidal. Between 20% and 80% of the maximum response, the relationship between response and concentration is linear and may be described by the equation $E = m \log(C_p) + b$, where m is the slope and b is the intercept. The slope of this linear relationship (m) is equal to one-quarter of the maximum response ($E_{max}/4$).

where m and b represent the slope and the intercept, respectively. However, note that in contrast to the linear model, the intercept of the log-linear model does not represent the baseline effect.

The meaning of slope (m) may be derived as follows [5]:

$$\text{Slope} = m = \frac{dE}{d\ln C_p} \tag{34.15}$$

Since C_p can be written as

$$e^{\ln C_p} = C_p \tag{34.16}$$

Eq. 34.9 may be rewritten as

$$E = \frac{E_{max} \times [e^{\ln C_p}]}{EC_{50} + [e^{\ln C_p}]} \tag{34.17}$$

Solving for the slope, or the derivative of E with respect to $e^{\ln C_p}$, we find

$$\frac{dE}{d\ln C_p} = \frac{E_{max} C_p (EC_{50} + C_p) - E_{max} C_p^2}{(EC_{50} + C_p)^2} = \frac{E_{max} EC_{50} C_p}{(EC_{50} + C_p)^2} \tag{34.18}$$

Using Eq. 34.18, the slope at $C_p = EC_{50}$ can be derived as follows:

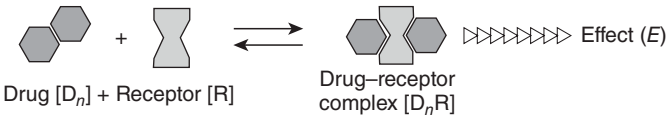
$$\frac{dE}{d\ln C_p} = \frac{E_{max} EC_{50}^2}{(2EC_{50})^2} = \frac{E_{max}}{4} \tag{34.19}$$

As shown in Eq. 34.19, the slope will increase as a function of E_{max}. Additionally, this derivation allows rapid estimation of E_{max} from the slope of the E versus. ln C_p relationship.

The major benefit of the linear and log-linear models is, of course, the linearization of the relationship. These linearizations allow characterization of pharmacodynamic relationships with the use of simple linear regression, thereby avoiding the need for more computationally intensive analyses (e.g., nonlinear regression) [6, 7]. Although increased availability of nonlinear regression software has minimized the need for application of linearized models for final analyses of datasets, the linear models remain useful for initial analyses and for estimation of initial parameter values (i.e., to facilitate subsequent nonlinear regression analyses).

34.3.3 Sigmoid E_{max} Model (Hill Equation)

The *sigmoid* E_{max} *model* was first introduced by Hill to explain the association of oxygen with hemoglobin [8]. Wagner applied this equation to pharmacodynamics in 1968 [9]. Mathematically, this equation is an extension of the E_{max} model by adding the Hill coefficient (n). In the sigmoid E_{max} model, the relationship between receptor and drug can be represented as



where R and D represent free receptor and drug, respectively. DR and E represent the drug–receptor complex and effect, and n represents the Hill coefficient. At equilibrium,

$$K_{\mathrm{D}} = \frac{[\mathrm{D}]^n[\mathrm{R}]}{[\mathrm{D}_n\mathrm{R}]} \tag{34.20}$$

Free receptor concentration can be described as

$$[\mathrm{R}] = [\mathrm{R}_{\mathrm{T}}] - [\mathrm{D}_n\mathrm{R}] \tag{34.21}$$

Substituting Eq. 34.21 into Eq. 34.20, we find

$$K_{\mathrm{D}} = \frac{[\mathrm{D}]^n[\mathrm{R}_{\mathrm{T}}] - [\mathrm{D}_n\mathrm{R}][\mathrm{D}]^n}{[\mathrm{D}_n\mathrm{R}]} \tag{34.22}$$

Rearranging Eq. 34.22 in terms of [D$_n$R], we have

$$[\mathrm{D}^n\mathrm{R}] = \frac{[\mathrm{R}_{\mathrm{T}}][\mathrm{D}]^n}{K_{\mathrm{D}} + [\mathrm{D}]^n} \tag{34.23}$$

Using a derivation similar to that employed for the $E_{\max}$ model (above), we have

$$E = \frac{E_{\max} \times [C_{\mathrm{p}}]^n}{EC_{50}^n + [C_{\mathrm{p}}]^n} \tag{34.24}$$

The Hill coefficient determines the "steepness" of the effect versus concentration curve. As with the $E_{\max}$ model, the response range between 20% and 80% of $E_{\max}$ is linear when plotted on semilog axes. If $n = 1$, the curve of the sigmoid $E_{\max}$ model is identical with the $E_{\max}$ model. When n is greater than 1 ($n > 1$), the linear portion of the curve becomes steeper. Conversely, if n is less than 1 ($n < 1$), the linear portion of the curve becomes more shallow. The value of n does not change EC_{50} and $E_{\max}$ values and all curves pass through the EC_{50} (Fig. 34.5).

The steepness of the curve can also be represented by the following equation [5]:

$$\frac{dE}{d\ln C_{\mathrm{p}}} = \frac{nE_{\max}}{4} \tag{34.25}$$

In this equation, the linear portion of the slope is directly proportional to the Hill coefficient. Theoretically, the n value reflects cooperativity in drug binding with

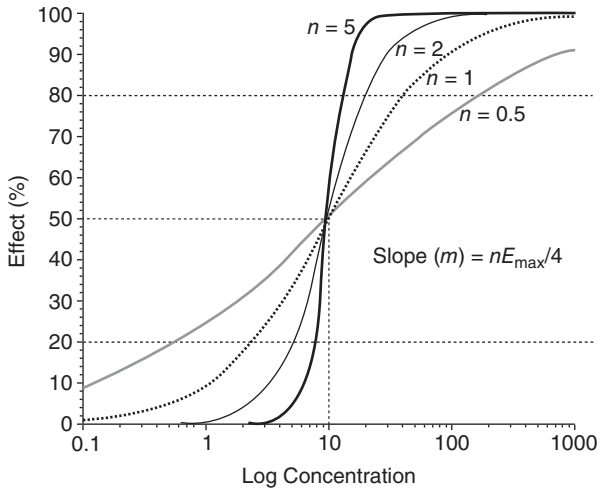


FIGURE 34.5 Effect versus concentration profiles predicted by the sigmoidal E_{max} model. If the Hill coefficient, n, is equal to 1, the curve is identical to that predicted by the E_{max} model. If $n > 1$, then the linear portion of the curve (between 20% and 80% of the maximum response) becomes steeper; and if $n < 1$, the linear portion becomes more shallow. The slope of the linear portion is equal to the Hill coefficient multiplied by one-quarter of the maximum response ($nE_{max}/4$).

specific receptors. In practical terms, the n value is determined by curve fitting and is typically considered as an empirical parameter with no defined physiological meaning. However, attempts have been made to explain the Hill coefficient pharmacologically and mechanistically. In 1994, Hoffman and Goldberg [10] suggested that the Hill coefficient reflected the extent of heterogeneity in drug receptors. They proposed that the statistical distribution of heterogeneity could affect the steepness of the effect versus concentration curve, where more homogeneous receptor populations would be associated with high values of n.

34.4 "KINETIC" MODELS OF PHARMACOLOGICAL RESPONSE

Static pharmacodynamic models are limited to consideration of equilibrium or steady-state conditions and, consequently, static models are unable to describe the time course of pharmacological effect following acute dosing. Evaluation of drug response following acute dosing, particularly where plasma concentrations change rapidly with time, often facilitates the identification of underlying mechanisms associated with drug effect. In this section, "kinetic" models are described that allow characterization of the time course of drug effect. When linked with an appropriate pharmacokinetic model, the combined pharmacokinetic–pharmacodynamic (PKPD) model allows description of the time course of drug effect as a function of the time course of drug administration.

34.4.1 Direct Effect Models

Some drug responses may be characterized as *direct effects*, where interaction of drug and the drug receptor leads to an observed response by direct action of the drug. In practical terms, a drug effect may be categorized as "direct" when all events associated with response proceed very rapidly relative to the kinetics of drug–receptor binding (e.g., consider the vasodilatory and antihypertensive effects of sodium nitroprusside, which appear to be directly and immediately related to the concentrations of sodium nitroprusside in blood). Models appropriate for direct effects are described next.

Levy's Direct Effect Model Following drug administration, the concentration of drug in the body changes with time. Thus, the drug response also changes as a function of time. The first PKPD models, introduced by Gerhard Levy [11, 12], described drugs with direct effects, where it may be assumed that there is no time delay between drug response and drug concentration. Additionally, Levy's initial model assumed rapid equilibration between the drug concentrations in plasma and at the site of action. This model consisted of a one-compartment pharmacokinetic model and log-linear pharmacodynamic model.

Equation 34.26 represents drug concentration as a function of time for a one-compartment model, where k represents a first-order elimination rate constant:

$$\ln C = \ln C_0 - kt \tag{34.26}$$

Equation 34.27 represents the log-linear model, which explains the linear relationship between response and log concentration in the response range between 20% and 80% of E_{max}:

$$E = m \ln C + e \tag{34.27}$$

Equation 34.27 may be rearranged as

$$\ln C = \frac{E - e}{m} \tag{34.28}$$

At the initial concentration, C_0, the effect can be represented by the initial effect, E_0. Thus, another equivalent equation may be derived:

$$\ln C_0 = \frac{E_0 - e}{m} \tag{34.29}$$

By substituting Eqs. 34.28 and 34.29 into Eq. 34.26, the following equation results:

$$\frac{E - e}{m} = \frac{E_0 - e}{m} - kt \tag{34.30}$$

Finally, multiplying each term by m and simplifying yields

$$E = E_0 - kmt \tag{34.31}$$

Interestingly, the model predicts that pharmacological effect will decline linearly with time, whereas drug concentrations decline exponentially with time (Fig. 34.6) [13]. Although this model only describes the region associated with 20–80% of maximal response, this region includes the entire therapeutic working range for many approved drugs (e.g., theophylline) and, consequently, this simple model has been shown to be extremely useful.

E_{max} *Model* Levy's direct response model only covers the linear range (20–80% of maximum response) of the time course of pharmacodynamic responses. Most time courses of pharmacodynamic profiles consist of linear and nonlinear curves. To obtain a complete profile of the time course of pharmacodynamic responses, the

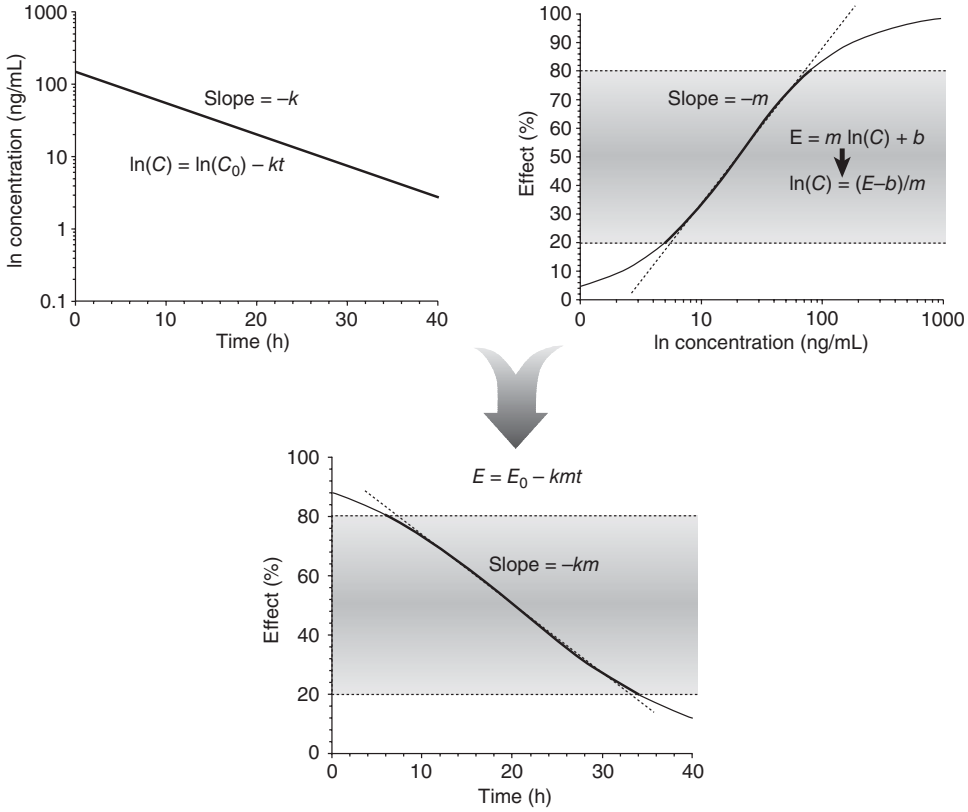


FIGURE 34.6 Levy's direct effect model. This model consists of two functions, one is pharmacokinetics (linear, one-compartment) and the other is pharmacodynamics (log-linear; E_{max} model). Note that the model predicts a linear decline in pharmacologic effect with time despite an exponential decline in drug concentration with time. Effect declines with the slope ($-km$), reflecting both pharmacokinetics (k) and pharmacodynamics (m).

E_{max} or sigmoid E_{max} model may be linked with appropriate pharmacokinetic models. In Fig. 34.7, the time course of drug concentration and pharmacological response are shown. This decline of drug concentration is predicted from a one-compartment model after intravenous bolus injection (Eq. 34.32) and the pharmacological response curve is predicted by the E_{max} model linked to the one-compartment pharmacokinetic model (Eq. 34.33).

$$C = C_0 e^{-kt} \tag{34.32}$$

$$E = \frac{E_{max} C_0 e^{-kt}}{E_{50} + C_0 e^{-kt}} \tag{34.33}$$

Immediately following intravenous (IV) bolus injection of a drug, the model predicts a small change in the drug response despite a large change in drug concentration. This prediction is due to the saturation of receptors at high drug concentrations. Within the range of 20–80% of the maximum response, the time course of pharmacological response declines linearly as a function of time, which is consistent with Levy's direct effect model. At low concentrations, below the EC_{50}, the drug response declines in parallel with drug concentration as predicted by the log-linear model. The direct effect E_{max} model was first introduced by Wagner in 1968. Using the E_{max} model linked with one-compartment IV bolus injection model, Wagner measured the total response of various dosing intervals by calculating the area under the response–time curve (AUC_E) [9]. He demonstrated that the total response was increased substantially by decreasing the dosing interval from 24 h to

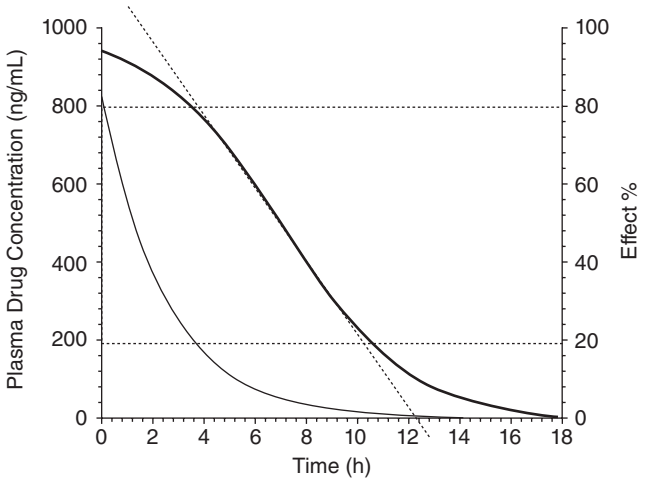


FIGURE 34.7 Predictions of a PKPD model defined with a one-compartment pharmacokinetic model and a direct effect E_{max} pharmacodynamic model. Initially, drug effect shows a plateau despite a large change of concentration, and this is due to the saturation of drug receptors at high drug concentrations. Within the range of 20–80% of maximum response, the time course of pharmacological response declines linearly as a function of time. At concentrations less than EC_{50}, drug response declines in parallel with drug concentration.

12 h (with simulated administration of the same total dose). With further decreases in the dosing interval (to 6 h or 3 h), the response continued to increase, but in smaller increments. As such, this simulation predicted that drug response could be changed by modulation of the dosing regimen, and high drug response may be achieved by dividing doses into smaller quantities given more frequently. This principle has been demonstrated in clinical studies [14, 15] and provides an early demonstration of the use of modeling and simulation to guide the selection of optimal dosing strategies.

Biophase Model In many cases, the time course of drug effect is delayed relative to the time course of plasma concentrations. This delay between drug effect and concentration may be recognized by comparing the time value associated with maximum plasma concentrations (T_{max}) and the time value associated with maximum effect. Additionally, plotting the effect data versus plasma concentration data will often show a nonunique relationship of effect and concentration, where the same value of drug concentration is associated with two different levels of effect (Fig. 34.8). The plot of effect versus concentration will form a counterclockwise hysteresis loop, where, at a given concentration, the effect value is lower prior to T_{max} relative to effect value observed following T_{max}. Delays in the relationship between drug effect and drug concentration may be explained by several mechanisms. Common causes for delays between effect and plasma concentration include (1) distribution delays between plasma and the site of drug action (i.e., the biophase), (2) indirect effect kinetics, where the delay is related to the time course of production or elimination of an endogenous mediator of effect, (3) delays associated with the formation of an active metabolite, and (4) delays associated with transduction mechanisms. Clockwise hysteresis may also be observed in effect versus plasma concentration plots, where effect at a given concentration decreases with time. Clockwise hysteresis occurs much less frequently than counterclockwise hysteresis, and it is typically associated with the development of pharmacological tolerance [16].

The concept of drug distribution to the biophase was first introduced by Furchgott in 1955 [17], and mathematically described by Segre in 1968. Several years later, Sheiner and co-workers [18] introduced a simple model consistent with first-order drug distribution to the biophase, and this *effect site model* rapidly gained wide use. Figure 34.9 shows a simple effect site PKPD model, where a one-compartment IV bolus injection model is linked with the hypothetical effect site compartment. The differential equations for the rate of change in drug concentration of central and hypothetical effect compartments are

$$\frac{dC_p}{dt} = -k_{el}C_p \tag{34.34}$$

$$\frac{dC_e}{dt} = k_{1e}C_e - k_{eo}C_e \tag{34.35}$$

Solving these two differential equations yields

$$C_p = C_0 e^{-kt} \tag{34.36}$$

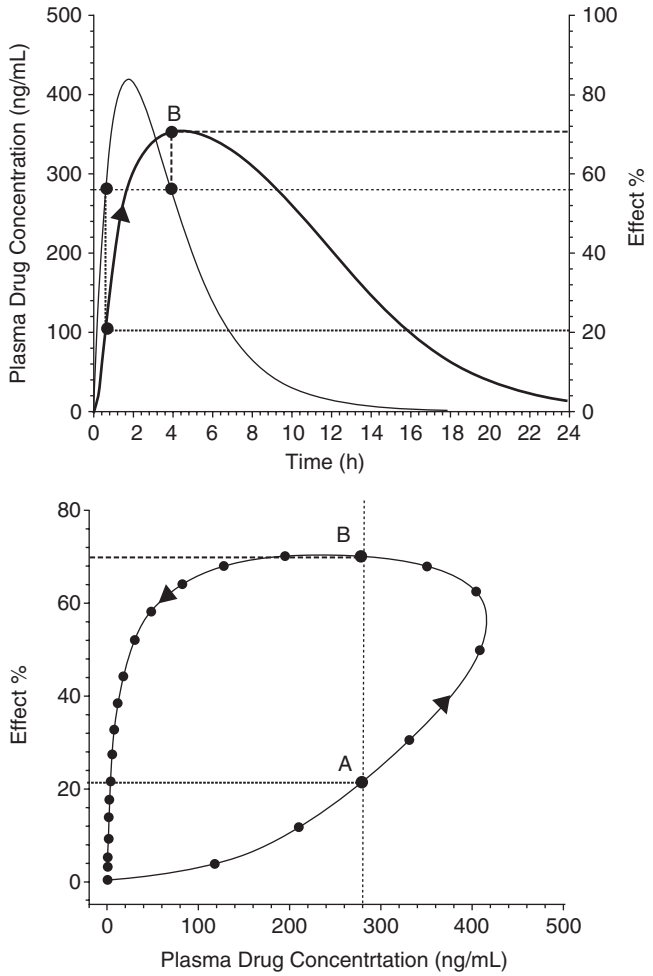


FIGURE 34.8 Counterclockwise hysteresis curve of effect versus plasma drug concentration. In case of delayed response (upper panel), plotting of effect versus plasma concentration will show a counterclockwise hysteresis loop (lower panel). Counterclockwise hysteresis loops show a nonunique relationship of effect and concentration, where a given concentration value is associated with two values of drug effect (note ascending (A) and descending (B) concentrations).

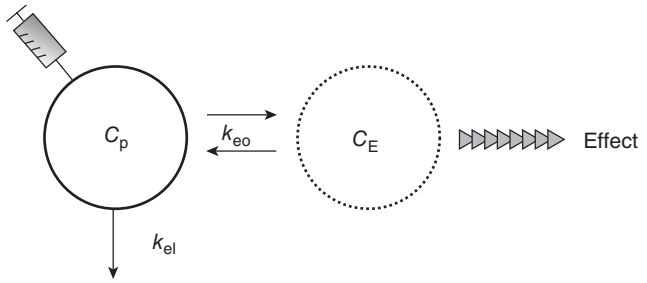


FIGURE 34.9 Biophase model. k_{el} represents the elimination rate constant of drug from the central compartment and k_{eo} represents the rate constant for drug distribution between the central and biophase compartments. (Adapted from Ref. 18.)

$$C_e = \frac{k_{1e}C_0}{k_{eo} - k_{el}}(e^{-kt} - e^{-k_{eo}t}) \tag{34.37}$$

Of note, the effect site model assumes that an insignificant quantity of drug distributes to the biophase and, consequently, the effect site compartment does not influence the plasma pharmacokinetics of the drug. The rate constants k_{1e} and k_{eo} are typically assumed to be identical for model simplification and, with this simplification, Eq. 34.37 may be rewritten as

$$C_e = \frac{k_{eo}C_0}{k_{eo} - k_{el}}(e^{-kt} - e^{-k_{eo}t}) \tag{34.38}$$

In most applications of the effect site model, the drug is assumed to produce a direct effect, which is described through the relationship of the effect site concentration, C_e, and the pharmacological response with an E_{max} or sigmoid E_{max} model.

$$E = \frac{E_{max}C_e}{E_{50} + C_e} \tag{34.39}$$

Distribution delays have also been described in PKPD models by the assumption that the biophase is within a peripheral compartment of a mammillary compartmental pharmacokinetic model [19, 20]. Although these models are quite similar to Sheiner's effect site model, some important differences exist. First, the hypothetical effect site compartment of Sheiner's model is not an actual compartment, and a negligible amount of drug is assumed to distribute to the hypothetical effect compartment. This independency between the hypothetical effect compartment and the pharmacokinetic model provides tremendous flexibility and, consequently, Sheiner's model is much more robust than models assuming that effect occurs in a peripheral pharmacokinetic compartment. Second, mammillary, multicompartment pharmacokinetic models predict that drug concentrations in the central and peripheral compartments decline in parallel; however, the biophase model allows values of k_{eo} that may be much smaller than any of the pharmacokinetic rate constants. This facilitates characterization of the time course of effects that dissipate at a rate much slower than predicted by the plasma clearance of drug (Fig. 34.10). The value of k_{eo} dictates the shape of the hysteresis curve, as shown in Fig. 34.11, and also influences the magnitude of the response, as shown in Fig. 34.12. Due to the assumption of first-order kinetics for entry and loss of drug from the biophase, the effect site model predicts that peak concentrations in the effect compartment will occur at the same time for all doses (i.e., from a given dosage regimen), and the effect site model predicts that all doses will lead to peak effects at the same time (relative to drug administration). Following large doses of drug, the effect will plateau at E_{max} and the effect versus time curve will decline linearly over the range of 20–80% of maximum effect. The biophase model is very robust, and the model has been applied successfully to characterize the delayed pharmacological responses of many drugs [21–24].

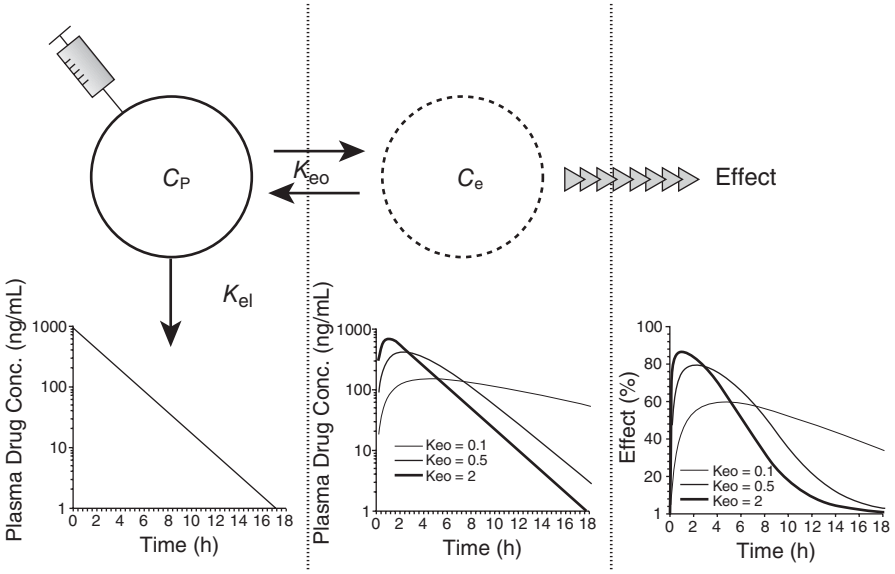


FIGURE 34.10 Simulated time course profile of effect site drug concentration and drug effect as a function of k_{eo}. Higher values of k_{eo} provide a more rapid rise and fall in effect compartment concentrations and responses that are less delayed. Small values of k_{eo}, where $k_{eo} << k_{el}$, leads to a "flip-flop" phenomenon where the time course of effect is very protracted relative to the time course of drug concentrations in plasma.

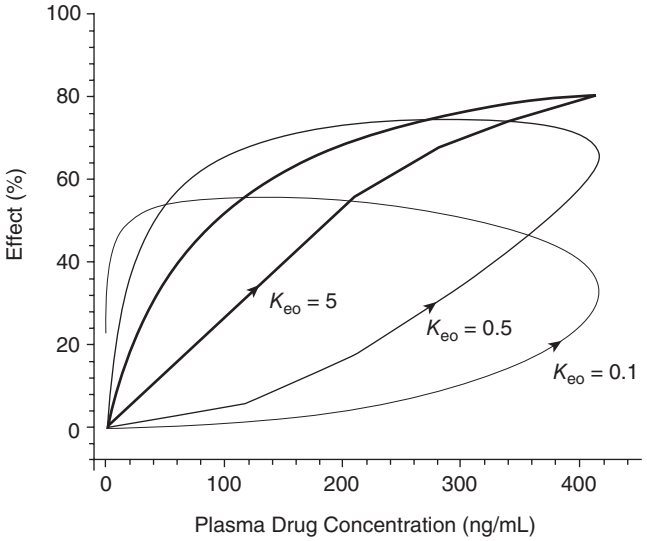


FIGURE 34.11 The impact of k_{eo} on the shape of the hysteresis loop. At high values of k_{eo}, there is rapid equilibration between plasma and effect compartment drug concentrations, and this leads to little delay in the time course of drug effect relative to drug concentration. As k_{eo} approaches infinity, the hysteresis loop collapses.

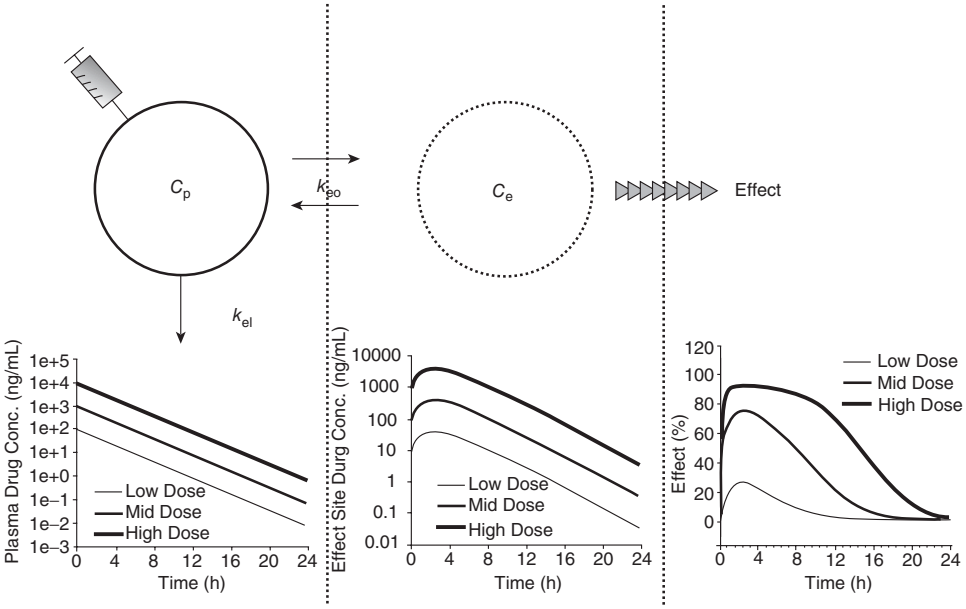


FIGURE 34.12 Biophase model simulations: effect of dose. Drug concentration versus time profiles within the hypothetical effect compartment are delayed relative to plasma concentrations; however, the time associated with peak concentrations in the effect compartment are identical for all doses. At large doses, the plateau in the response profile represents E_{max}, and the magnitude of effect declines linearly in the range of 20–80% of the maximum response.

34.4.2 Indirect Response Models

Following the introduction of the biophase model [18], many investigators used the biophase model to explain time delays in drug response with little thought as to whether the biophase model was mechanistically appropriate for the given application. Given the simple, robust nature of the biophase model, the model provided good characterization of a wide variety of response data; however, in many cases, the model did not allow simultaneous characterization of data from different doses, and the model did not allow accurate, prospective predictions of drug response. One main reason for these difficulties was the application of the biophase model to drugs that achieve effects indirectly, where the measured drug response occurs not as a direct effect, but due to the effect of drug on the production or elimination of endogenous substances associated with the measured response (Fig. 34.13).

Areins introduced the concept of indirect effects in 1964 [25], while Nagashima et al. [7] first applied an indirect effect model for PKPD to explain the effect of warfarin on the time course of prothrombin complex activity. Warfarin is an inhibitor of vitamin K epoxidase, which reduces the vitamin K epoxide to vitamin K. Vitamin K is needed for blood coagulation as a cofactor for carboxylation of clotting factors; thus, inhibition of vitamin K production results in the inhibition of coagulation [26]. Due to the indirect nature of the effect of warfarin on the measured response (coagulation), and due to the time delays associated with the elimination

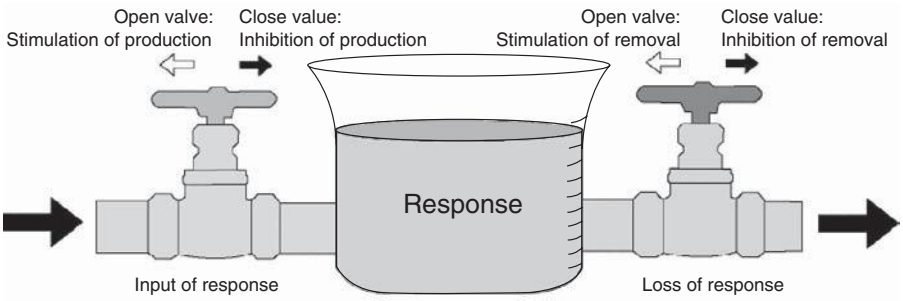


FIGURE 34.13 Indirect effects: impact of changes in the production or elimination of response mediators on the measured response. Stimulation of the production or inhibition of the elimination of response mediators will lead to an increase in the measured response. However, inhibition of input or stimulation of the elimination of response mediators will lead to a decrease in the measured response.

of vitamin K and clotting factors, the time course of warfarin effect is dramatically delayed relative to the time course of warfarin exposure, and this delay was well captured by the indirect effect model of Nagashima et al. [7] Jusko and Ko [27] subsequently developed and elaborated a family of models to allow mechanistically appropriate characterization of four common types of indirect effects.

The conceptual basis for indirect response models is provided in the differential equation

$$\frac{dR}{dt} = k_{\text{in}} - k_{\text{out}}R \tag{34.40}$$

where R refers to the measured response, k_{in} is the zero-order rate constant for the production of the response, and k_{out} is the first-order rate constant for loss of the response. Under steady-state conditions, the change of response over time becomes zero; thus, the initial response can be represented as follows:

$$R_0 = \frac{k_{\text{in}}}{k_{\text{out}}} \tag{34.41}$$

After administration of drug, the measured response (R) is changed from the effect of drug (inhibition or stimulation) on the production or dissipation of response, as a function of drug concentration. Four general submodels have been deduced (Fig. 34.14). Models I and II describe the time course of drug response by inhibition of the rate constant associated with production (k_{in}) or dissipation (k_{out}). The inhibitory function includes a parameter, $I_{\max}$, which describes the maximal extent of inhibition; $I_{\max}$ is always greater than zero and less than or equal to one ($0 < I_{\max} \leq 1$).

$$I(t) = 1 - \frac{I_{\max}C_{\text{p}}}{IC_{50} + C_{\text{p}}} \tag{34.42}$$

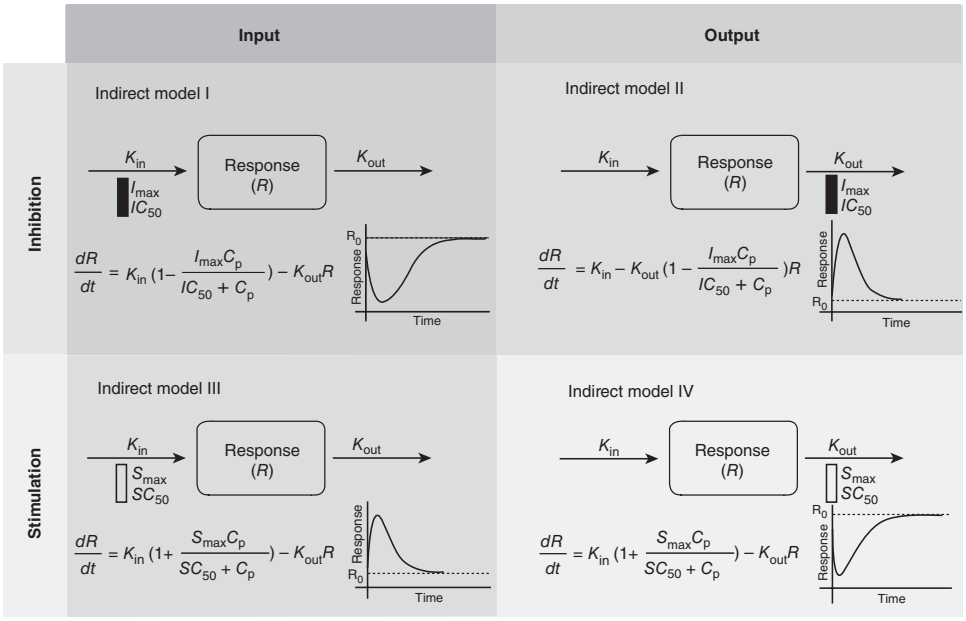


FIGURE 34.14 Basic indirect effect models. Shown are the four basic indirect response submodels (I, II, III and IV), and typical response patterns.

C_p represents the plasma concentration and IC_{50} represents the drug concentration needed to produce 50% of the maximum inhibitory response.

Models III and IV include a stimulation function $S(t)$, which affects the production or dissipation of response.

$$S(t) = 1 + \frac{S_{max} C_p}{SC_{50} + C_p} \tag{34.43}$$

C_p represents the plasma concentration, SC_{50} represents the drug concentration that produces 50% of the maximum stimulation response, and S_{max} represents the maximum stimulation response. Unlike the inhibitory function $I(t)$, the value of S_{max} is any value greater than zero.

In model I, the rate of change in response over time may be represented by Eq. 29.43, and the results of simulation of drug response after intravenous injection of four different doses are shown in Fig. 34.15.

$$\frac{dR}{dt} = k_{in}\left(1 - \frac{I_{max} C_p}{IC_{50} + C_p}\right) - k_{out} R \tag{34.44}$$

The "baseline" response, in the absence of drug, is assumed to be equivalent to the steady-state solution provided in Eq. 34.41. Immediately after dosing, plasma drug concentrations are high ($C_p >> IC_{50}$), and inhibitory function $I(t)$ becomes $(1 - I_{max})$. If $I_{max} = 1$, then the term k_{in} is eliminated, and the decline of the drug response is

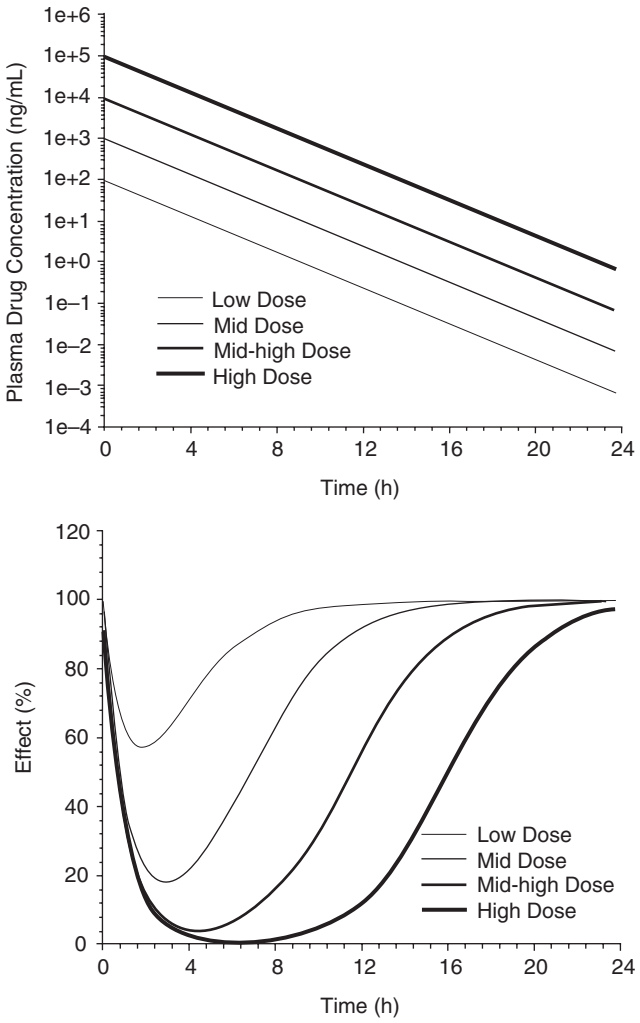


FIGURE 34.15 Simulated profile of the indirect response model I, with four different doses. As the amount of dose increases, indirect response model I predicts an increase an response and an increase in the time associated with maximum effect.

governed solely by the first-order rate of k_{out}. Thus, initial decline in the slope of the ln response versus time profile becomes $-k_{out}$. As plasma concentrations decrease, the inhibitory effect of drug decreases and, eventually, response begins to increase back to the baseline value. The minimum response value may be defined as the peak effect of drug, R_{max}. At R_{max}, the change of drug response with time will equal zero, and Eq. 34.44 may be rearranged to solve for R_{max} as follows:

$$R_{max} = \frac{k_{in}}{k_{out}}\left(1 - \frac{I_{max}C_p}{IC_{50} - C_p}\right) = R_0\left(1 - \frac{I_{max}C_p}{IC_{50} - C_p}\right) \tag{34.45}$$

When $C_p >> IC_{50}$, the inhibitory function $I(t)$ becomes $(1 - I_{max})$, and Eq. 34.45 can be rewritten as

$$R_{max} = R_0(1 - I_{max}) \quad \text{model I} \tag{34.46}$$

In a similar manner, R_{max} for models II, III, and IV can be shown as follows:

$$R_{max} = R_0/(1 - I_{max}) \quad \text{model II} \tag{34.47}$$

$$R_{max} = R_0(1 + S_{max}) \quad \text{model III} \tag{34.48}$$

$$R_{max} = R_0/(1 + S_{max}) \quad \text{model IV} \tag{34.49}$$

After R_{max} has been reached, the response starts to go back to baseline. However, even if the plasma drug concentration is below the IC_{50}, time is needed for reequilibration and to return back to baseline. This is the primary difference from the biophase model. In the biophase model, the delayed response is governed by the rate constant from plasma to biophase, k_{eo}; thus, the time of maximum effect is not affected by dose. However, in indirect response models, higher doses will result in a longer plateau and increase in the time of maximum effect.

Concerning the shape of the time course of the response profile, four subgroup indirect response models can be divided into two groups, with either a downward trend in response (for models I and IV) or an upward trend in response (for models II and III). In assigning an appropriate model, it is reasonable to start with consideration of the shape of the response profile. Additionally, Sharma and Jusko [28] proposed an infusion study, using multiple dosing rates to allow collection of data to assist with model selection. In many ways, the kinetics represented by the indirect response model equation are similar to those associated with IV infusion in a one-compartment pharmacokinetic model. The zero-order rate constant for the production (k_{in}) corresponds to the zero-order infusion rate (K_o), and the first-order rate constant (k_{out}) for loss of the response corresponds to the elimination rate constant of plasma compartment (k_{el}). In the case of infusion, the time to reach steady state ($t_{R_{max}}$) is governed by the elimination rate constant, not the infusion rate. Similarly, in indirect response, the time to reach maximum response is governed by k_{out}. In models I and III, $t_{R_{max}}$ is constant (for all drug infusion rates), since k_{out} is not affected by changes in "input." However, in models II and IV, $t_{R_{max}}$ would change as a function of drug infusion rate, because k_{out} is affected by the administration of drug. As such, appropriate selection of indirect models is facilitated by administration of drug over a range of infusion rates.

34.4.3 Transduction Models

The starting point for a pharmacological response is drug–receptor binding. However, in many cases, generation of pharmacological responses requires subsequent signal transduction events. For example, prednisone, a glucocorticoid hormone, binds to cytosolic receptors. The prednisone–receptor complex is then tranlocated to the nucleus, where the complex binds with DNA, modulating the rate of RNA transcription, protein production, and, finally, protein expression [29]. Such cascading steps for signal transduction require time and lead to delayed responses. Ideally, receptor

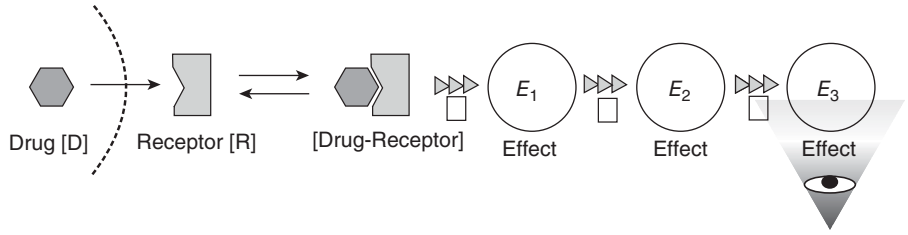


FIGURE 34.16 Transit compartment model for signal transduction. Response starts by drug–receptor binding, but the measured effect is achieved via a signal transduction process. τ represents transit time required for the signal to move from compartment to compartment in the transduction cascade. (Adapted from Ref. 30.)

and gene mediated processes should be included in a PKPD model to explain the delayed responses. However, data associated with each step in the signal transduction cascade is difficult to obtain due to limitations of technical feasibility. Although the delayed response may be due to complicated signal transduction pathways, relatively simple transit compartment models have been applied to successfully describe the time course of associated responses *in vivo* [30]. A representative transit compartment model for the signal transduction process is shown in Fig. 34.16.

As proposed by Ariens and Stephenson, the drug effects may be directly proportional to the concentration of drug–receptor complexes. The initial effective signal in a signal transduction cascade, E^*, may be defined as a function of drug–receptor complexes and the intrinsic efficacy of the drug:

$$E^* = \varepsilon \cdot [\mathrm{DR}] \tag{34.50}$$

where ε represents the efficacy of the drug.

The E^* term may be included within any of the direct or indirect effect models described previously. For example, within the E_{max} model,

$$E^* = \frac{E_{\max} C_e}{EC_{50} + C_e} \tag{34.51}$$

where C_e represents the free drug concentration at the effect site.

To characterize signal transduction, a cascade of transit compartments is employed:

$$\frac{dE}{dt} = \frac{1}{\tau}(E^* - E) = \frac{1}{\tau}\left(\frac{E_{\max} C_e}{EC_{50} + C_e} - E\right) \tag{34.52}$$

where τ represents the transit time.

Additional transit compartments may be employed to allow greater delay and flexibility in the response versus time profile. If the signal transduction process involves three transit compartments, the signal transit step of each transit compartment can be represented by the following series of equations:

$$\frac{dE_1}{dt} = \frac{1}{\tau}(E^* - E_1) = \frac{1}{\tau}\left(\frac{E_{\max}C_e}{EC_{50} + C_e} - E_1\right) \tag{34.53}$$

$$\frac{dE_2}{dt} = \frac{1}{\tau}(E_1 - E_2) \tag{34.54}$$

$$\frac{dE_3}{dt} = \frac{1}{\tau}(E_2 - E_3) \tag{34.55}$$

The transit time between each compartment is often assumed to be equal ($\tau = \tau_1 = \tau_2 = \tau_3$). Simulated profiles for each transit compartment, with different transit time values, are shown in Fig. 34.17. As shown in this figure, the response associated with the final transit compartment (E_3) is more delayed compared with the initial transit compartment (E_1). Also, as the transit time (τ) increases, responses become more delayed, and the maximum peak effect is decreased.

Within signal transduction processes, there is opportunity for the amplification or dampening of the signal. Power coefficients may easily be incorporated with transit compartments to account for these effects.

$$\frac{dE_3}{dt} = \frac{1}{\tau}(E_2^{\gamma} - E_3) \tag{34.56}$$

Simulated data associated with a range of power coefficients are shown in Fig. 34.18 in terms of simulation. For example, if the power coefficient of the last transit compartment is less than 1, the effect is lower than the unity condition. This indicates that effect is suspended between transit compartments E_2 and E_3. Conversely, if the power coefficient of the last transit compartment is greater than 1, the effect is higher than the unity condition. This indicates that effect is amplified between transit compartments E_2 and E_3 [31].

Transit compartment models are typically employed in an empirical manner to allow curve fitting with a minimal number of parameters. However, when detailed mechanistic data are available, this information may easily be added to the structure of the transit compartments to enhance the mechanistic reality of the model [33–35].

34.4.4 Irreversible Effects

Drug effects may be categorized as reversible or irreversible. Examples of irreversible effects include cell killing by action of anticancer or antimicrobial agents, irreversible enzyme inhibition, and formation of covalent drug adducts (e.g., via formation of reactive drug metabolites [1]). PKPD modeling of irreversible effects was introduced by Jusko [36] to explain chemotherapeutic effects.

A typical cell proliferation model of a chemotherapeutic agent is shown in Fig. 34.19a. The representative equation for the growth and death of cells by the action of a drug is

$$\frac{dR}{dt} = k_s \cdot R - k \cdot C \cdot R \tag{34.57}$$

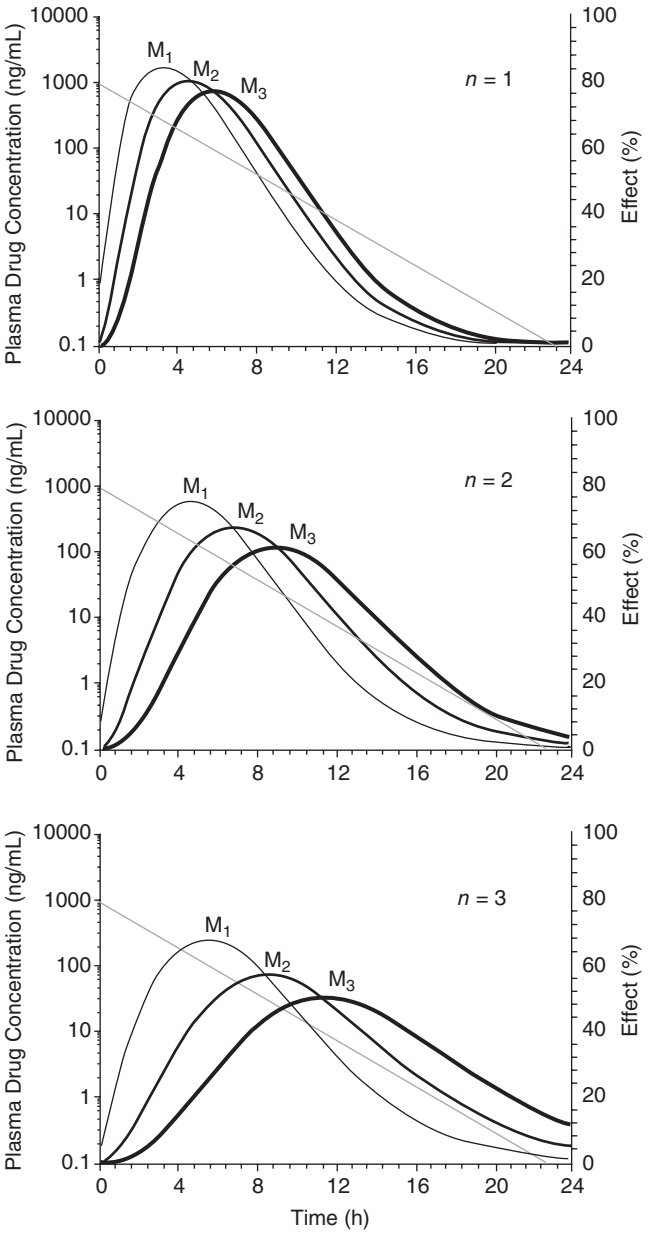


FIGURE 34.17 Transit compartment model: effect of transit time. Response in the final compartment (M_3) is delayed compared to the first effect compartment (M_1). As transit time increases, the response becomes more delayed for all three compartments, and the maximum effect decreases (upper, middle, and lower panels).

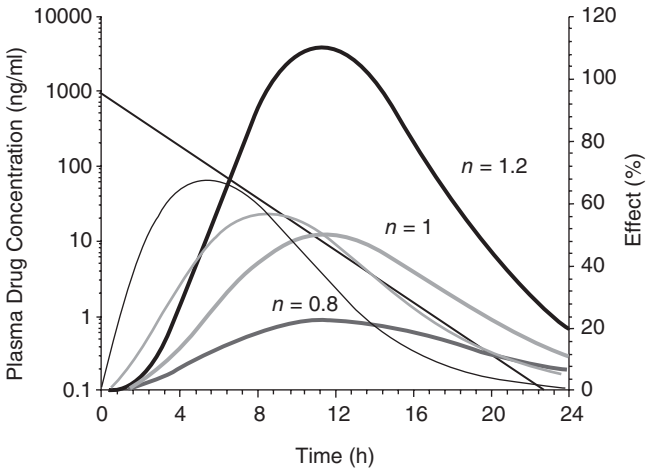


FIGURE 34.18 Transit compartment model: effect of the power coefficient. Higher values of the power coefficient ($\gamma > 1$) will amplify response; conversely, power coefficients below 1 will lead to a dampened response.

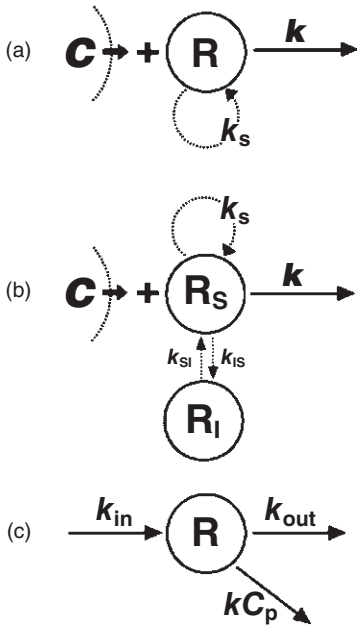


FIGURE 34.19 Representative irreversible effect model for chemotherapeutic agents. **(a)** Cell killing model for the effect of a chemotherapeutic agent. (Adapted from Ref. 36.) **(b)** Phase-specific model of cell killing. k_{SI} and k_{IS} are the rate constants for cell movement between compartments associated with sensitivity to drug and with insensitivity to drug. (Adapted from Ref. 38.) **(c)** Application of an indirect response model within a model for irreversible cell killing. (Adapted from Ref. 40.)

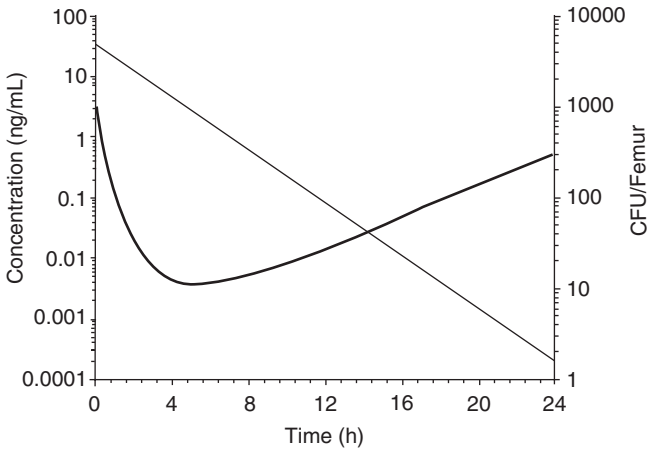


FIGURE 34.20 A typical simulated profile for the effect of a chemotherapeutic agent on cell number. The biphasic profile results from the processes of cell proliferation and drug-induced cell killing.

R represents the number of cells, k_s represents the first-order rate constant for growth rate in the natural condition, and k represents the second-order rate constant for cell killing by the action of drug. This equation includes terms for the natural growth and death of cells by the drug effect; thus, the change in the number of cells as a function of time is represented as a biphasic profile that consists of killing and regrowing phases (Fig. 34.20). The linear term for death of a cell by the drug effect (kC) can be substituted by the E_{max} model as

$$\frac{dR}{dt} = k_s \cdot R - \frac{K_{max} C}{KC_{50} + C} \cdot R \tag{34.58}$$

Using this model, Zhi et al. [37] characterized the effect of piperacillin on the killing and growth kinetic of *Pseudomonas aeruginosa*.

Some chemotherapeutic agents show cell cycle phase-specific effects. To characterize this property, Jusko [38] proposed extension of the cell proliferation model by adding an insensitive cell compartment (Fig. 34.19b):

$$\frac{dR_S}{dt} = k_S \cdot R_S - k \cdot C_S \cdot R_S - k_{SI} R_S + k_{IS} R_I \tag{34.59}$$

$$\frac{dR_I}{dt} = k_{SI} R_S - k_{IS} R_I \tag{34.60}$$

R_I represents the number of insensitive cells and k_{SI} and k_{IS} represent the rate constants for conversion into each cell compartment. The interconversion rate between sensitive and insensitive cells is governed by the rate constants k_{SI} and k_{IS}. Another modified form of this model was successfully applied to describe the pharmacodynamic effect of β-lactam antibiotics in *in vitro* bactericidal kinetics [39].

The modeling of irreversible effect can be extended to the indirect response model (Fig. 34.19c). The typical equation of an indirect response model modified for characterization of an irreversible effect is as follows:

$$\frac{dR}{dt} = k_{in} - k_{out} \cdot R - k \cdot C_p \cdot R \tag{34.61}$$

Acetyl salicylic acid irreversibly inhibits platelet aggregation, and the turnover time of platelets is 7–10 days; thus, a small amount of aspirin shows a long duration of the antiplatelet effect. Using an irreversible effect model, Yamamoto et al. [40] explained the long duration of the antiplatelet effect of acetyl salicylic acid. The extension of this model with addition of precursor compartment was used to explain the prolonged duration of the effect of omeprazole [41].

34.4.5 Tolerance Models

Repeated or continuous exposure to several drugs such as glyceryl trinitrate, morphine, dobutamine, nicotine, cocaine, and benzodiazepines leads to clockwise hysteresis due to pharmacological tolerance [42]. Tolerance may occur due to desensitization, downregulation of receptor, or depletion of precursor. In the E_{max} model, desensitization and downregulation of drug receptors may be characterized by increasing EC_{50} and decreasing E_{max} as functions of time ($EC_{50} \cdot e^{kt}$, $E_{max} \cdot e^{-kt}$) [43]. In another mathematical model of tolerance, Porchet et al. [44] proposed the time-dependent development of a hypothetical antagonist to the effects of nicotine (Fig. 34.21a). Wakelkamp et al. [45] employed an indirect response model to describe acute tolerance to furosemide. In this model, the observed response was used to drive the production of a "modulator," which antagonized the effect of the drug (Fig. 34.21b). Equations describing this model are

$$\frac{dR}{dt} = k_{in} - k_{out} \cdot \left(1 - \frac{I_{max} \cdot ER}{IC_{50} + ER}\right) \cdot R \cdot (1 + M) \tag{34.62}$$

$$\frac{dM}{dt} = k_{tol} \cdot R - k_{tol} \cdot M \tag{34.63}$$

where M represents the modulator response and k_{tol} represents the first-order rate constant of loss and production of modulator responses. Among other models of tolerance is an adaptive pool model presented by Gardmark et al. [46] to describe morphine tolerance.

34.5 CONCLUSION

The relationship between the magnitude and time course of pharmacological response and the time course of drug concentrations is often complex and may be impacted by the time course of drug diffusion to the biophase, the interaction of

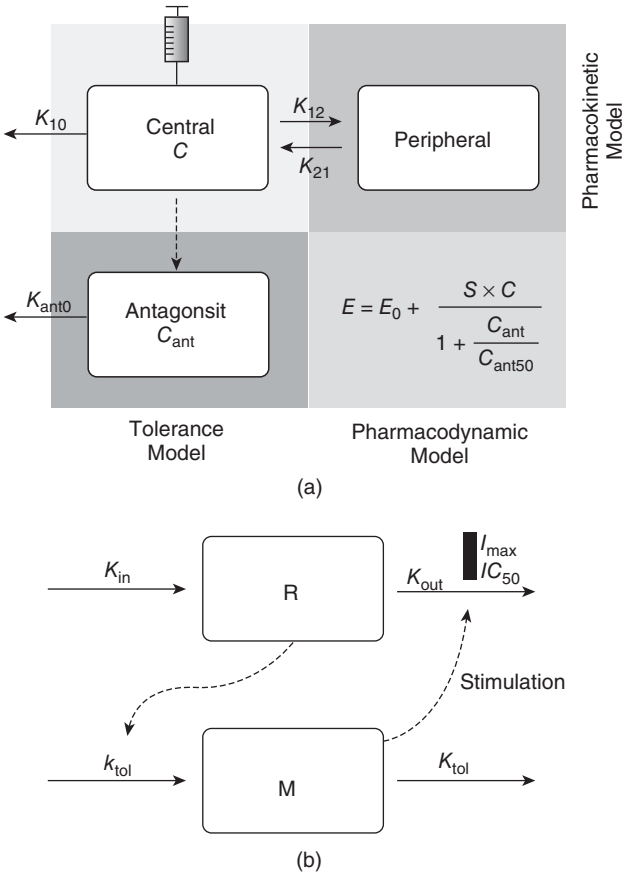


FIGURE 34.21 Representative tolerance models. **(a)** Model for acute tolerance to nicotine effect. Tolerance is generated due to the generation of a hypothetical agent that antagonizes drug effect. (Adapted from Ref. 44.) **(b)** Application of an indirect response model to describe tolerance to furosemide. Tolerance results from generation of a modulator that counteracts the effect of furosemide. (Adapted from Ref. 45.)

drug with endogenous mediators of effect, transduction or signaling events, and the development of pharmacological tolerance or sensitization. The main sequences of drug response are summarized in Fig. 34.22 [47]. As the field of PKPD modeling has progressed, there has been movement from empirical models to models that may be deemed to be more mechanistically appropriate. There is promise that mechanism-based PKPD modeling may accelerate efforts to enhance the therapeutic efficacy and safety of drug therapy, lead to rapid identification of optimal dosing strategies, and assist in testing hypotheses related to the mechanisms responsible for drug action. The catalog of models presented in this chapter offers a starting point for readers interested in using pharmacodynamic analyses to achieve these goals.

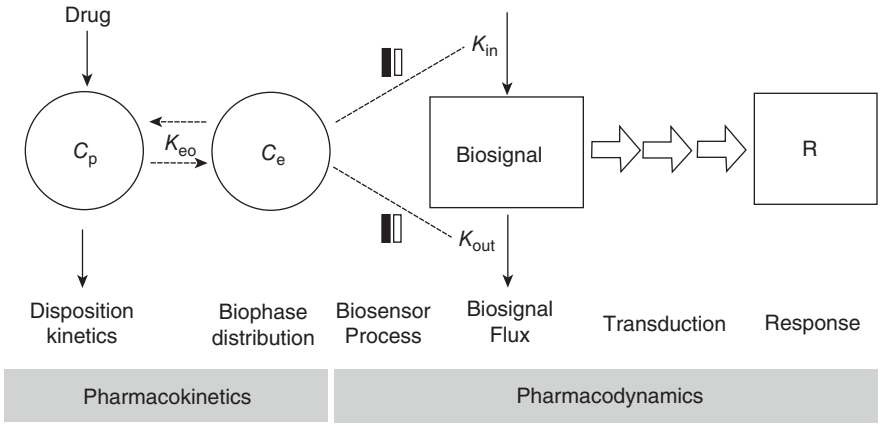


FIGURE 34.22 Pharmacokinetics and pharmacodynamics. This scheme summarizes many of the processes associated with the relationship between the time course of drug administration and the time course of drug response. The time course of response is potentially impacted by drug disposition, drug diffusion to the biophase, interaction of drug with processes associated with the production and elimination of endogenous mediators of response, and signaling pathways associated with the measured drug response. (Adapted from Ref. 47.)

ACKNOWLEDGMENTS

Work on this chapter was supported by Grants AI60687 and CA118213 from the National Institutes of Health. Dr. Beom Soo Shin is supported by a fellowship provided by Pfizer, Inc.

REFERENCES

1. Jusko WJ. In *Course on Pharmacokinetic–Pharmacodynamic Modeling Concepts and Applications*. Buffalo, NY: The State University of New York; 2006.
2. Clark AJ. The reaction between acetyl choline and muscle cells. *J Physiol* 1926;61: 530–546.
3. Ariens EJ, De Groot WM. Affinity and intrinsic-activity in the theory of competitive inhibition. III. Homologous decamethonium-derivatives and succinyl-choline-esters. *Arch Int Pharmacodyn Ther* 1954;99:193–205.
4. Stephenson RP. A modification of receptor theory. *Br J Pharmacol Chemother* 1956;11: 379–393.
5. Levy G. In *Course of Pharmacokinetic–Pharmacodynamic Modeling: Concepts and Applications*. Buffalo, NY: The State University of New York; 1995.
6. McDevitt DG, Shand DG. Plasma concentrations and the time-course of beta blockade due to propranolol. *Clin Pharmacol Ther* 1975;18:708–713.
7. Nagashima R, O'Reilly RA, Levy G. Kinetics of pharmacologic effects in man: the anticoagulant action of warfarin. *Clin Pharmacol Ther* 1969;10:22–35.
8. Hill AV. The possible effects of the aggregation of the molecules of hemoglobin on its dissociation curves. *J Physiol (London)* 1910;61:530–546.

9. Wagner JG. Kinetics of pharmacologic response. I. Proposed relationships between response and drug concentration in the intact animal and man. *J Theor Biol* 1968;20: 173–201.
10. Hoffman A, Goldberg A. The relationship between receptor–effector unit heterogeneity and the shape of the concentration–effect profile: pharmacodynamic implications. *J Pharmacokinet Biopharm* 1994;22:449–468.
11. Levy G. Relationship between elimination rate of drugs and rate of decline of their pharmacologic effects. *J Pharm Sci* 1964;53:342–343.
12. Levy G. Kinetics of pharmacologic effects. *Clin Pharmacol Ther* 1966;7:362–372.
13. Levy G. Pharmacokinetics of succinylcholine in newborns. *Anesthesiology* 1970;32: 551–552.
14. Alvan G, Paintaud G, Wakelkamp M. The efficiency concept in pharmacodynamics. *Clin Pharmacokinet* 1999;36:375–389.
15. Lalonde RL, Pieper JA, Straka RJ, Bottorff MB, Mirvis DM. Propranolol pharmacokinetics and pharmacodynamics after single doses and at steady-state. *Eur J Clin Pharmacol* 1987;33:315–318.
16. Girard P, Boissel JP. Clockwise hysteresis or proteresis. *J Pharmacokinet Biopharm* 1989;17:401–402.
17. Furchgott RF. The pharmacology of vascular smooth muscle. *Pharmacol Rev* 1955;7: 183–265.
18. Sheiner LB, Stanski DR, Vozeh S, Miller RD, Ham J. Simultaneous modeling of pharmacokinetics and pharmacodynamics: application to *d*-tubocurarine. *Clin Pharmacol Ther* 1979;25:358–371.
19. Kramer WG, Kolibash AJ, Lewis RP, Bathala MS, Visconti JA, Reuning RH. Pharmacokinetics of digoxin: relationship between response intensity and predicted compartmental drug levels in man. *J Pharmacokinet Biopharm* 1979;7:47–61.
20. Wagner JG, Aghajanian GK, Bing OH. Correlation of performance test scores with "tissue concentration" of lysergic acid diethylamide in human subjects. *Clin Pharmacol Ther* 1968;9:635–638.
21. Hammarlund-Udenaes M, Paalzow LK, De Lange EC. Drug equilibration across the blood–brain barrier—pharmacokinetic considerations based on the microdialysis method. *Pharm Res* 1997;14:128–134.
22. Collins JM, Dedrick RL. Distributed model for drug delivery to CSF and brain tissue. *Am J Physiol* 1983;245:R303–R310.
23. Wang Y, Welty DF. The simultaneous estimation of the influx and efflux blood–brain barrier permeabilities of gabapentin using a microdialysis-pharmacokinetic approach. *Pharm Res* 1996;13:398–403.
24. Gupta SK, Ellinwood EH, Nikaido AM, Heatherly DG. Simultaneous modeling of the pharmacokinetic and pharmacodynamic properties of benzodiazepines. I: Lorazepam. *J Pharmacokinet Biopharm* 1990;18:89–102.
25. Ariens EJ. *Molecular Pharmacology*. New York: Academic Press; 1964.
26. Whitlon DS, Sadowski JA, Suttie JW. Mechanism of coumarin action: significance of vitamin K epoxide reductase inhibition. *Biochemistry* 1978;17:1371–1377.
27. Jusko WJ, Ko HC. Physiologic indirect response models characterize diverse types of pharmacodynamic effects. *Clin Pharmacol Ther* 1994;56:406–419.
28. Sharma A, Jusko WJ. Characteristics of indirect pharmacodynamic models and applications to clinical drug responses. *Br J Clin Pharmacol* 1998;45:229–239.
29. Boudinot FD, D'Ambrosio R, Jusko WJ. Receptor-mediated pharmacodynamics of prednisolone in the rat. *J Pharmacokinet Biopharm* 1986;14:469–493.

30. Mager DE, Jusko WJ. Pharmacodynamic modeling of time-dependent transduction systems. *Clin Pharmacol Ther* 2001;70:210–216.
31. Sun YN, Jusko WJ. Transit compartments versus gamma distribution function to model signal transduction processes in pharmacodynamics. *J Pharm Sci* 1998;87:732–737.
32. Oosterhuis B, Braat MC, Roos CM, Wemer J, Van Boxtel CJ. Pharmacokinetic–pharmacodynamic Modeling of Terbutaline bronchodilation in asthma. *Clin Pharmacol Ther* 1986;40:469–475.
33. Nichols AI, Boudinot FD, Jusko WJ. Second generation model for prednisolone pharmacodynamics in the rat. *J Pharmacokinet Biopharm* 1989;17:209–227.
34. Sun YN, DuBois DC, Almon RR, Jusko WJ. Fourth-generation model for corticosteroid pharmacodynamics: a model for methylprednisolone effects on receptor/gene-mediated glucocorticoid receptor down-regulation and tyrosine aminotransferase induction in rat liver. *J Pharmacokinet Biopharm* 1998;26:289–317.
35. Xu ZX, Sun YN, DuBois DC, Almon RR, Jusko WJ. Third-generation model for corticosteroid pharmacodynamics: roles of glucocorticoid receptor mRNA and tyrosine aminotransferase mRNA in rat liver. *J Pharmacokinet Biopharm* 1995;23:163–181.
36. Jusko WJ. Pharmacodynamics of chemotherapeutic effects: dose–time-response relationships for phase-nonspecific agents. *J Pharm Sci* 1971;60:892–895.
37. Zhi JG, Nightingale CH, Quintiliani R. Microbial pharmacodynamics of piperacillin in neutropenic mice of systematic infection due to *Pseudomonas aeruginosa*. *J Pharmacokinet Biopharm* 1988;16:355–375.
38. Jusko WJ. A pharmacodynamic model for cell-cycle-specific chemotherapeutic agents *J Pharmacokinet Biopharm* 1973;1:175–200.
39. Yano Y, Oguma T, Nagata H, Sasaki S. Application of logistic growth model to pharmacodynamic analysis of *in vitro* bactericidal kinetics. *J Pharm Sci* 1988;87:1177–1183.
40. Yamamoto K, Abe M, Katashima M, Sawada Y. Pharmacodynamic analysis of antiplatelet effect of aspirin in literature—modeling based on inhibition of cyclooxygenase in the platelet and the vessel wall endothelium. *Jpn J Hosp Pharm* 1996;22:113–141.
41. Abelo A, Eriksson UG, Karlsson MO, Larsson H, Gabrielsson J. A turnover model of irreversible inhibition of gastric acid secretion by omeprazole in the dog. *J Pharmacol Exp Ther* 2000;295:662–669.
42. Gardmark M, Brynne L, Hammarlund-Udenaes M, Karlsson MO. Interchangeability and predictive performance of empirical tolerance models. *Clin Pharmacokinet* 1999;36:145–167.
43. Lalonde RL. In Burton ME, Shaw LM, Schentag JJ, Evans WE, Eds. *Applied Pharmacokinetics & Pharmacodynamics*. Baltimore: Lippincott Williams & Wilkins; 2006, pp 60–81.
44. Porchet HC, Benowitz NL, Sheiner LB. Pharmacodynamic model of tolerance: application to nicotine. *J Pharmacol Exp Ther* 1988;244:231–236.
45. Wakelkamp M, Alvan G, Gabrielsson J, Paintaud G. Pharmacodynamic modeling of furosemide tolerance after multiple intravenous administration. *Clin Pharmacol Ther* 1996;60:75–88.
46. Gardmark M, Karlsson MO, Jonsson F, Hammarlund-Udenaes M. Morphine-3-glucuronide has a minor effect on morphine antinociception. Pharmacodynamic modeling. *J Pharm Sci* 1998;87:813–820.
47. Jusko WJ, Ko HC, Ebling WF. Convergence of direct and indirect pharmacodynamic response models. *J Pharmacokinet Biopharm* 1995;23:5–8.

35

PHYSIOLOGICALLY BASED PHARMACOKINETIC MODELING

HARVEY J. CLEWELL III,[1] MICAELA B. REDDY,[2] THIERRY LAVE,[3] AND MELVIN E. ANDERSEN[1]

[1]*The Hamner Institutes for Health Sciences, Research Triangle Park, North Carolina*
[2]*Roche Palo Alto LLC, Palo Alto, California*
[3]*F. Hoffmann-La Roche Ltd., Basel, Switzerland*

Contents

35.1 Introduction
- 35.1.1 Noncompartmental, Compartmental, and PBPK Modeling
- 35.1.2 Modeling and Simulation Considerations in the Generation of Drug Metabolism and Pharmacokinetic (DMPK) Data

35.2 PBPK Modeling Fundamentals
- 35.2.1 Elements of PBPK Model Development
- 35.2.2 Elements of Model Structure

35.3 PBPK Model Implementation
- 35.3.1 Model Parameterization
- 35.3.2 Numerical Solution of Model Equations
- 35.3.3 Model Evaluation
- 35.3.4 Model Validation

35.4 Generic PBPK Models
- 35.4.1 User-Friendly Software Packages Bringing PBPK Modeling to the Nonexpert
- 35.4.2 Recent Advances in Generic PBPK Modeling Tools

35.5 Integrating Preclinical Data Using the PBPK Model
- 35.5.1 Preclinical Data Useful for PBPK Modeling
- 35.5.2 Lead Identification and Optimization Stages
- 35.5.3 Clinical Candidate Selection
- 35.5.4 Supporting Entry into Humans

Preclinical Development Handbook: ADME and Biopharmaceutical Properties,
edited by Shayne Cox Gad
Copyright © 2008 John Wiley & Sons, Inc.

35.6 Examples of the Use of PBPK Modeling in Drug Development
35.6.1 Methotrexate
35.6.2 All-*trans*-Retinoic Acid
35.6.3 Future Directions
35.7 Conclusions and Future Perspectives
Acknowledgments
References

35.1 INTRODUCTION

Pharmacokinetics is the quantitative study of factors that control the time course for absorption, distribution, metabolism, and excretion (ADME) of compounds within the body. Pharmacokinetic (PK) models provide sets of equations that simulate the time courses of compounds and their metabolites in various tissues throughout the body. The interest in PK modeling in pharmacology and toxicology arose from the need to relate internal concentrations of active compounds at their target sites with the doses of the compound given to an animal or human subject. The reason, of course, is a fundamental tenet in pharmacology or toxicology that both beneficial and adverse responses to compounds are related to the free concentrations of active compounds reaching target tissues rather than the amounts of compound at the site of absorption. The relationships between tissue dose and administered dose can be complex, especially in high dose toxicity testing studies, with multiple, repeated daily dosing, or when metabolism or toxicity at routes of entry alter uptake processes for various routes of exposure. PK models of all kinds are primarily a tool to assess internal dosimetry at target tissues for a wide range of exposure situations.

In the 1930s, Teorell [1, 2] provided a set of equations for uptake, distribution, and elimination of drugs from the body. These papers are rightly regarded as providing the first physiological model for drug distribution. However, computational methods were not available to solve the sets of equations at that time. Exact mathematical solutions for distribution of compounds in the body could only be obtained for simplified models in which the body was reduced to a small number of compartments that did not correspond directly with specific physiological compartments. Over the next thirty years, PK modeling focused on these simpler descriptions with exact solutions rather than on developing models more concordant with the structure and content of the biological system itself. These approaches are sometimes referred to as *data-based* compartmental modeling, since the work generally took the form of a detailed collection of time-course blood/excreta concentrations at various doses. Time-course curves were analyzed by assuming particular model structures and estimating a small number of model parameters by curve-fitting. In the earliest of these models, all processes for metabolism, distribution, and elimination were treated as first order (i.e., rates changed in direct proportion to the concentration of the chemical species). Two areas of concern that particularly

affected data-based compartmental PK modeling arose in the 1960s and early 1970s: (1) the saturation of elimination pathways and (2) the possibility that blood flow rather than metabolic capacity of an organ might limit clearance. Saturation led to models that were not first order, making it difficult to derive exact solutions to the sets of equations, while blood-flow-limited metabolism in an organ meant that the removal rate constant from a central compartment could not increase indefinitely as the metabolic capacity increased [3].

Scientists trained in chemical engineering and computational methods developed physiologically based pharmacokinetic (PBPK) models for chemotherapeutic compounds [4]. Many of these compounds are highly toxic and have therapeutic efficacy by being slightly more toxic to rapidly growing cells (the cancer cells) than to normal tissues. Initial successes with methotrexate [5] led to PBPK models for other compounds, including 5-fluorouracil [6] and cisplatin [7]. These seminal contributions showed the ease with which realistic descriptions of physiology and relevant pathways of metabolism could be incorporated into PBPK models and paved the way for their more extensive use.

Although PBPK modeling was initially developed in the pharmaceutical industry [8–10], its recent use has primarily been in the area of environmental risk assessment. In the pharmaceutical area, the use of PBPK models was limited in drug development mainly due to the perceived mathematical complexity of the models and the labor-intensive input data required. However, advances in the prediction of hepatic metabolism and tissue distribution from *in vitro* and *in silico* data have made the use of these models more attractive, providing the opportunity to integrate key input data from different sources to not only estimate PK parameters and predict plasma and tissue concentration–time profiles, but also to gain mechanistic insight into the compound's properties. Thus, there is recent evidence of growing interest in applying PBPK models for the discovery and development of drugs [11, 12]. Strategies for PBPK application in drug research are being published [13, 14] and several commercial PBPK simulation tools have recently become available (e.g., GastroPlus™ and PK-Sim®, to name a few).

Some of the inertia to developing PBPK models was also due to the idea that extrapolations were unnecessary since human PK data would eventually be developed in clinical studies. This viewpoint neglects other attributes inherent in PBPK approaches. Some of the capabilities offered by PBPK approaches that have driven their extensive use in environmental risk assessment are: (1) creating models from physiological, biochemical, and anatomical information, entirely separate from collection of detailed concentration time-course curves; (2) evaluating mechanisms by which biological processes govern disposition of a wide range of compounds by comparison of PK results with model predictions; (3) using compounds as probes of the biological processes to gain more general information on the way biochemical characteristics govern the importance of various transport pathways in the body; (4) applying the models in safety assessments; and (5) using annotation of a modeling database as a repository of information on toxicity and kinetics of specific compounds [8]. Due to these perceived advantages, PBPK modeling was adopted as a tool for toxicological investigations and risk assessment in the early 1980s and many advances were made in this area. Recently, PBPK modeling has received new attention from the pharmaceutical industry. Lupfert and Reichel [11] recently wrote:

"The stage is set for a wide penetration of PBPK modeling and simulations to form an intrinsic part of a project starting from lead discovery, to lead optimization and candidate selection, to preclinical profiling and clinical trials."

Here, we present fundamental information necessary to understanding the application of PBPK models in preclinical drug development. Next, we describe the emerging role of PBPK modeling in the pharmaceutical industry in terms of advances in the available tools and increasingly used applications. Additionally, we provide our thoughts on potential applications that have not yet been widely explored. Although some advances have been made in applying PBPK modeling in the development of biotherapeutics (e.g., PBPK modeling for monoclonal antibodies in the mouse [15] and human [16]), this chapter is primarily geared toward small molecules.

35.1.1 Noncompartmental, Compartmental, and PBPK Modeling

Noncompartmental analysis (NCA) is widely used in the pharmaceutical industry for the analysis of single-dose PK (SDPK) data and PK data generated during safety studies. NCA, which involves calculating parameters such as steady-state volume of distribution (V_{ss}), clearance (CL), area under the plasma concentration curve (AUC), and peak plasma concentration (C_{max}) based solely on experimental data (i.e., these calculations are model independent), is a convenient way to understand, tabulate, and compare the PK properties of compounds. NCA results are easy to understand and a standard analysis technique. However, NCA results cannot be used to perform simulations or extrapolate to other exposure conditions. Although it is possible to use NCA parameters in a one-compartment model for performing simulations, this method is not likely to result in accurate predictions of pharmacokinetics.

Classical PK models are less commonly used than NCA calculations, but are used to perform simulations (e.g., use data generated for one experimental design to simulate a different experimental design). For example, a compartment model parameterized with intravenous (IV) SDPK data can be used to simulate an IV infusion study, and compartment modeling can be used to predict steady-state pharmacokinetics from SDPK data. Standard software packages often provide flexible tools for developing one-, two-, and three-compartment models from time-course plasma concentrations and provide statistical tools for discriminating between models. Compartment models require more mathematical skill than NCA but are still easy to use. However, the parameters and compartments in compartment models have no physiological meaning and provide no basis for extrapolating from the conditions of the experimental data used to develop the model.

PBPK models differ from classical PK models in that they include specific compartments for tissues involved in exposure, toxicity, biotransformation, and clearance processes connected by blood flow; compartments and blood flows are described using physiologically meaningful parameters, which allows for interspecies extrapolation by altering the physiological parameters appropriately. As with compartment models, PBPK models can be used to simulate a variety of conditions. Because the models have a mechanistic basis, extrapolation to situations differing from the conditions of the data used to calibrate the model is justifiable [17]. PBPK modeling has been used to great effect for interspecies extrapolation, both among animal

models [18] and for predicting human pharmacokinetics based on animal data [13, 19]. The mechanistic basis of PBPK models allows for applications such as understanding species differences in pharmacokinetics, determining if results from different experimental designs are consistent, and exploring possible mechanisms responsible for unexpected or unusual data. These attributes have led to widespread development of PBPK models in recent years [20].

Possibly the primary reason that PBPK models fell out of favor in the pharmaceutical industry is that PBPK models require more than the plasma time-course concentrations that are required by NCA and compartment models. PBPK models require physiological, physicochemical, and biochemical parameters. The physiological, mechanistic basis of the models is both their strength (the mechanistic basis provides exception utility) and their weakness (PBPK models can be expensive and time consuming to construct). However, recent contributions to the literature have demonstrated the effective application of PBPK models using the data normally generated during preclinical development [13, 14, 21, 22]. While NCA and compartment models will always be useful for many routine applications, PBPK modeling can be used for many situations when NCA and compartmental modeling simply cannot be used.

35.1.2 Modeling and Simulation Considerations in the Generation of Drug Metabolism and Pharmacokinetic (DMPK) Data

In preclinical drug development, an array of data is generated to investigate the potential of prospective drug candidates to have drug-like ADME properties in humans (Table 35.1). Preliminary screens tend to have high throughput and quick turnaround times, but less physiological relevance. As increasingly promising compounds are identified, ADME assays with more physiological relevance, but lower throughput and higher cost, are utilized. In the past, the conceptual model underlying preclinical development could be described as a filtering approach. The medicinal chemists would generate many candidates, and as compounds went through an array of screens for pharmacological, DMPK, and toxicological properties, compounds would be slowly eliminated from consideration until only the best compounds (clinical candidates) remained.

More recently, a different paradigm analogous to a cycle has been adopted. Medicinal chemists generate compounds that are tested for pharmacological activity. In parallel or in series, key ADME screening assays are employed to test for known liabilities of a class of compounds. For example, typical primary screens might be for permeability or metabolic stability, but should drug–drug interactions (DDIs) be a key liability for a given chemical class, then the appropriate DDI screen might be chosen as a primary screen, for example, to avoid the key liability of inhibition and/or induction of CYP3A4 by protease inhibitors for HIV [23]. Screening data is fed back to chemists, who go on to design better molecules based on assay results. The best compounds make it through the screening process to undergo more physiologically relevant, more expensive screens. Regardless of the screening cascade determined to be the best choice for a specific pharmacological target, much of the data generated is useful input for PBPK models. However, to ensure that PBPK modeling can be used to best advantage, a modeling strategy should be considered when making data generation choices.

TABLE 35.1 Common Screening Tools Used to Understand ADME Properties in Preclinical Development

Absorption	Distribution	Metabolism	Excretion
Physicochemical properties (calculated and measured) Solubility Log *P* Log *D* pK_a Polar surface area Permeability Artificial membrane PAMPA *In vitro* models Caco-2 cell line MDCK cell line P_{eff} with P-gp inhibited *In vivo* models Bioavailability Portal vein cannulated animals Transporter assays Cell lines Oocytes	Protein binding Equilibrium dialysis Ultracentrifugation Ultrafiltration Distribution in blood Blood-to-plasma ratio CNS penetration Permeability assays *In vitro* Caco-2 Transporter assays *In vivo* time-course tissue concentrations, microdialysis, mdr1a +/+, –/– mice *In vivo* PK Volume of distribution	Stability in biological fluids Plasma, blood stability Gut metabolism Caco-2 stability Intestinal microsomes Bile, gut fluids Hepatic metabolism Liver microsomes Hepatocytes Liver S-9, cytosol, slices Metabolic pathway Metabolite ID *in vitro, in vivo*, and *in situ* Reaction phenotyping Recombinant CYPs Liver microsomes with P450 inhibitor Inhibition CYP, UGT Induction PXR Hepatocyte RNA, activity	Urinary excretion *In vitro* MDCK and HEK *In situ* isolated, perfused rat kidney *In vivo* urine measurement Biliary excretion *In vitro* hepatocytes *In situ* isolated, perfused rat liver *In vivo* bile duct cannulated rats or dogs Transporter assays

The integration of preclinical data is a key to selecting good compounds for clinical development. The most common method for selecting compounds is by eliminating the compounds that fail to meet criteria for DMPK screens, and then picking the best candidate from the remaining compounds based on efficacy and other concerns. But take, for example, a choice between the following compounds: compound A has excellent efficacy in a rat pharmacology bioassay and good bioavailability, but has much higher protein binding in humans than rats, while compound B has good efficacy and good bioavailability, but has protein binding in humans similar to that of rats. Which compound should be chosen to move forward? We suggest integrating all available preclinical data using PBPK modeling, and whenever feasible integrating pharmacology data to develop the PK/PD (PK/pharmacodynamic) relationship, to come up with the most accurate, quantitative interpretation of the dataset and, therefore, the most science-driven selection of the clinical candidate.

35.2 PBPK MODELING FUNDAMENTALS

The basic approach for the development of a PBPK description is illustrated in Fig. 35.1. The process of model development begins with the identification of the compound and effect of concern. Literature evaluation involves the integration of available information about mechanisms of efficacy and/or toxicity, pathways of biochemical metabolism, the nature of the active compound processes involved in absorption, transport, and excretion, tissue partitioning and binding characteristics, and physiological parameters (e.g., tissue weights and blood flow rates) for the species of interest. Using this information, the investigator develops a PBPK model that expresses mathematically a conception of the animal/chemical system. In the

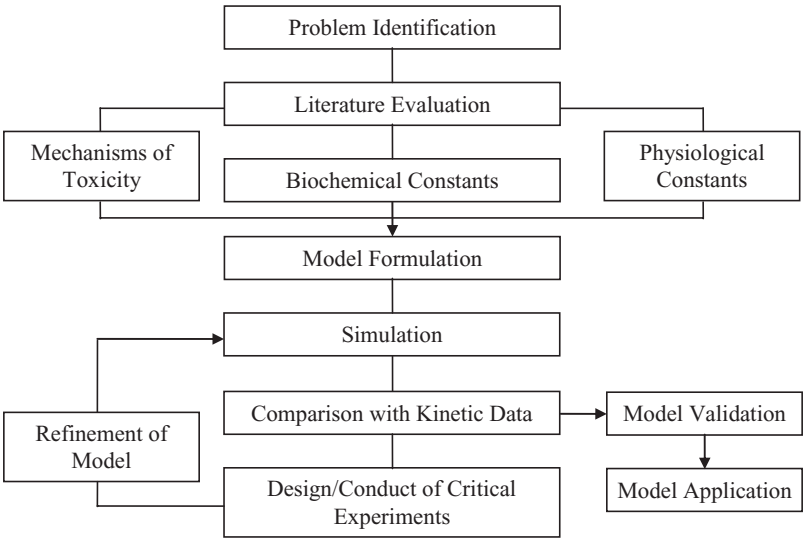


FIGURE 35.1 Flowchart of the PBPK modeling process.

model, the various time-dependent biological processes are described as a system of simultaneous differential equations. A mathematical model of this form can easily be written and exercised using commonly available computer software. The specific structure of the model is driven by the need to estimate the appropriate measure of tissue dose under the various exposure conditions of concern in both the experimental animal and the human. Before the model can be used with confidence, it has to be validated against kinetic information and, in many cases, refined based on comparison with the experimental results. The model itself can frequently be used to help design critical experiments to collect data needed for its own validation.

The chief advantage of a PBPK model over an empirical description is its greater predictive power. Since known physiological parameters are used, a different species can be modeled by simply replacing the appropriate constants with those for the species of interest, or by allometric scaling [18, 24, 25]. Similarly, the behavior for a different route of administration can be determined by adding equations that describe the nature of the new input function.

Since measured physicochemical and biochemical parameters are used, the behavior for a different compound can quickly be estimated by determining the appropriate constants. An important result is the ability to reduce the need for extensive experiments with new compounds. The process of selecting the most informative experimental data is also facilitated by the availability of a predictive PK model. Perhaps the most desirable feature of a physiologically based model is that it provides a conceptual framework for employing the scientific method in which the hypothesis can be described in terms of biological processes, predictions can be made on the basis of the description, and the hypothesis can be revised on the basis of comparison with experimental data.

The trade-off against the greater predictive capability of physiologically based models is the requirement for an increased number of parameters and equations. However, values for many of the parameters, particularly the physiological ones, are already available in the literature [4, 26–30], and *in vitro* techniques have been developed for rapidly determining the compound-specific parameters [31]. An important advantage of PBPK models is that they provide a biologically meaningful quantitative framework within which *in vitro* data can be more effectively utilized [32]. There is even a prospect that predictive PBPK models can someday be developed based almost entirely on data obtained from *in vitro* studies.

35.2.1 Elements of PBPK Model Development

This section explores some of the key issues associated with the development of PBPK models. It is meant to provide a general understanding of the basic design concepts and mathematical forms underlying the PBPK modeling process and is not meant to be a complete exposition of the PBPK modeling approach for all possible cases. It must be understood that the specifics of the approach can vary greatly for different types of compounds and for different applications.

Model building is an art and is best understood as an iterative process in the spirit of the scientific method [33–35]. A number of excellent reviews have been written on the subject of PBPK modeling [20, 36, 37], and the literature includes examples of successful PBPK models for a wide variety of compounds that provide a wealth of insight into various aspects of the PBPK modeling process [20]. These

sources should be consulted for further detail on the approach for applying the PBPK methodology in specific cases.

Tissue Grouping The first aspect of PBPK model development that will be discussed is determining the extent to which the various tissues in the body may be grouped together. Although tissue grouping is really just one aspect of model design, which is discussed in the next section, it provides a simple context for introducing the two alternative approaches to PBPK model development: *lumping* and *splitting*. In the context of tissue grouping, the guiding philosophy in the lumping approach can be stated as: "Tissues that are pharmacokinetically and toxicologically indistinguishable may be grouped together." In this approach, model development begins with information at the greatest level of detail that is practical, and decisions are made to combine physiological elements (tissues and blood flows) to the extent justified by their similarity [38]. The common grouping of tissues into richly (or rapidly) perfused and poorly (or slowly) perfused on the basis of their perfusion rate (ratio of blood flow to tissue volume) is an example of the lumping approach. The contrasting philosophy of splitting can be stated as: "Tissues that are pharmacokinetically or toxicologically distinct must be separated." This approach starts with the simplest reasonable model structure and increases the model's complexity only to the extent required to reproduce data on the compound of concern for the application of interest. Lumping (starting with a large number of compartments and then testing whether they can be combined) requires the greater initial investment in data collection and, if taken to the extreme, could paralyze model development. On the other hand, splitting (starting with a small number of compartments and only increasing complexity if the simple model fails) is more efficient but runs a greater risk of overlooking compound-specific determinants of disposition.

There are two alternative approaches for determining whether tissues are kinetically distinct or can be lumped together. In the first approach, the tissue rate constants are compared. The rate constant (k_T) for a tissue is similar to the perfusion rate except that the partitioning characteristics of the tissue are also considered:

$$k_T = Q_T/(P_T \cdot V_T)$$

where Q_T is the blood flow to the tissue (L/h), P_T is the tissue : blood partition coefficient for the compound, and V_T is the volume of the tissue (L). Thus, the units of the tissue rate constant are the same as for the perfusion rate, L/h, but the rate constant more accurately reflects the kinetic characteristics of a tissue for a particular compound.

The second, less rigorous, approach for determining whether tissues should be lumped together is simply to compare the performance of the model with the tissues combined and separated. The reliability of this approach depends on the availability of data under conditions where the tissues being evaluated would be expected to have an observable impact on the kinetics of the compound. Sensitivity analysis can sometimes be used to determine the appropriate conditions for such a comparison [39].

Model Design Criteria The alternative approaches to tissue grouping discussed previously are actually reflections of two competing criteria that must be balanced

during model design: *parsimony* and *plausibility*. The principle of parsimony simply states that a model should be as simple as possible for the intended application (but no simpler). This "splitting" philosophy is related to that of Occam's razor: "Entities should not be multiplied unnecessarily." That is, structures and parameters should not be included in the model unless they are needed to support the application for which the model is being designed.

There is no easy rule for determining the structure and level of complexity needed in a particular modeling application. The decision of which elements to include in the model structure for a specific compound and application draws on all of the modeler's experience and knowledge of the animal–chemical system. The wide variability of PBPK model design for different compounds can be seen by comparing the diagram of the PBPK model for methotrexate [5], shown in Fig. 35.2, with the diagram for the retinoic acid PBPK model [19], shown in Fig. 35.3.

The desire for parsimony in model development is driven not only by the desire to minimize the number of parameters whose values must be identified, but also by the recognition that as the number of parameters increases, the potential for unintended interactions between parameters also increases. A generally accepted rule of software engineering warns that it is relatively easy to design a computer program that is too complicated to be completely comprehended by the human mind. As a model becomes more complex, it becomes increasingly difficult to validate, even as the level of concern for the trustworthiness of the model should increase.

Countering the desire for model parsimony is the need for plausibility of the model structure. As discussed in Section 35.1, it is the physiological and biochemical realism of PBPK models that gives them an advantage for extrapolation. The

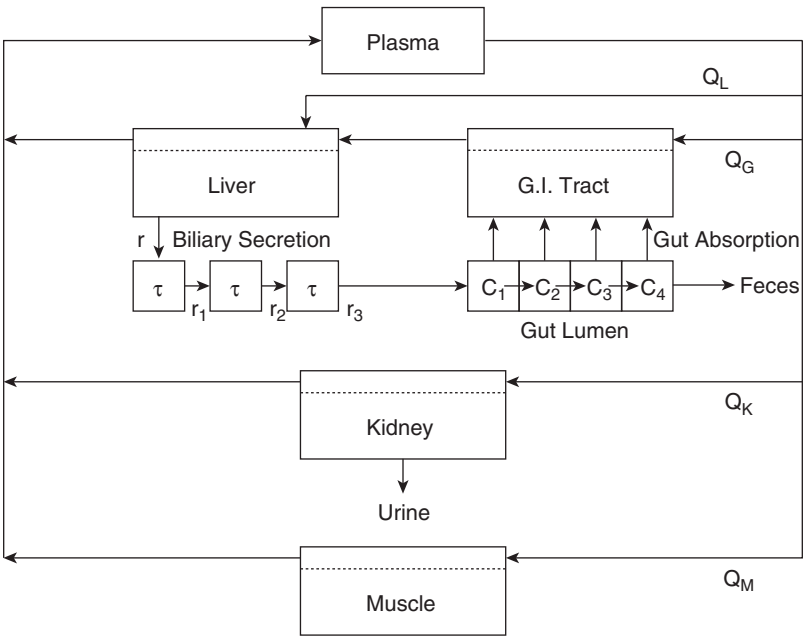


FIGURE 35.2 PBPK model for methotrexate [5].

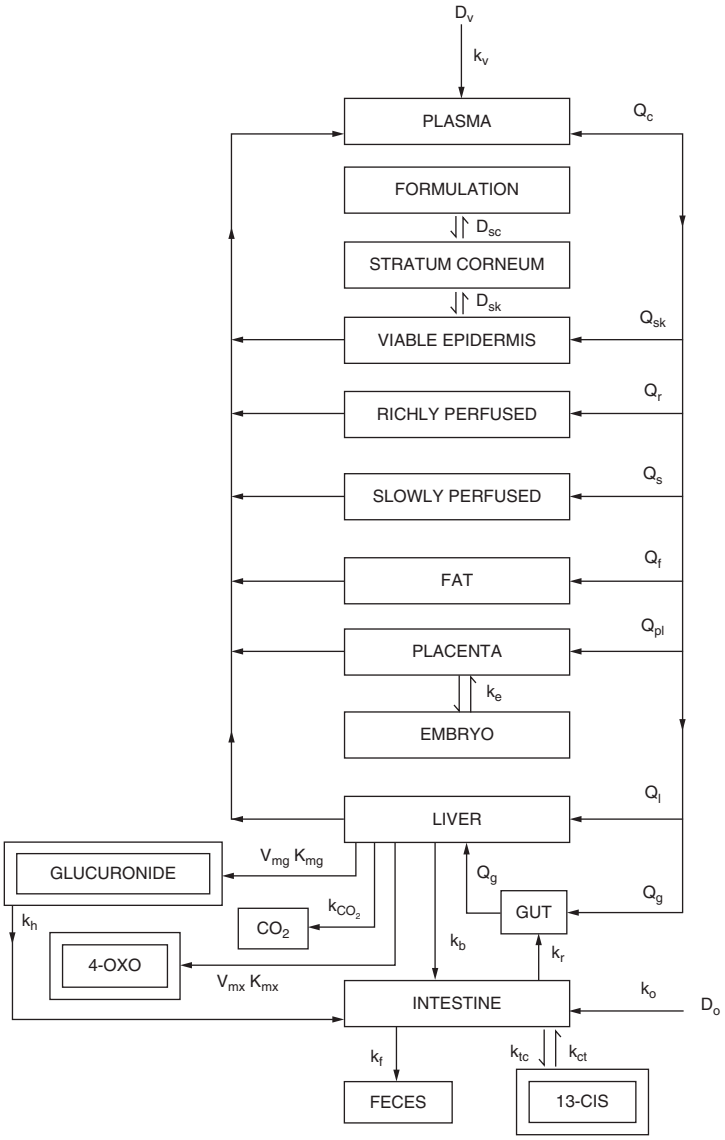


FIGURE 35.3 PBPK model for all-*trans*-retinoic acid [19].

credibility of a PBPK model's predictions of kinetic behavior under conditions different from those under which the model was validated rests to a large extent on the correspondence of the model design to known physiological and biochemical structures. In general, the ability of a model to adequately simulate the behavior of a physical system depends on the extent to which the model structure is homomorphic (having a one-to-one correspondence) with the essential features determining the behavior of that system.

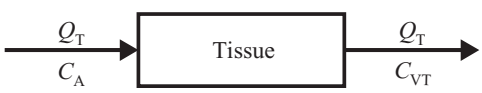
Model Identification The process of model identification begins with the selection of those model elements that the modeler considers to be minimum essential determinants of the behavior of the particular animal–chemical system under study, from the viewpoint of the intended application of the model. Comparison with appropriate data, relevant to the intended purpose of the model, can then provide insights into defects in the model that must be corrected either by reparameterization or by changes to the model structure. Unfortunately, it is not always possible to separate these two elements. In models of biological systems, estimates of the values of model parameters will always be uncertain, due both to biological variation and experimental error. At the same time, the need for biological realism unavoidably results in models that are "overparameterized"; that is, they contain more parameters than can be identified from the kinetic data the model is used to describe.

Model identification is the selection of a specific model structure from several alternatives, based on conformity of the models' predictions to experimental observations. The practical reality of model identification in the case of biological systems is that regardless of the complexity of the model there will always be some level of "model error" (lack of homomorphism), which will result in systematic discrepancies between the model and experimental data. This model structural deficiency interacts with deficiencies in the identifiability of the model parameters, potentially leading to misidentification of the parameters or misspecification of structures. This most dangerous aspect of model identification is exacerbated by the fact that, in general, adding equations and parameters to a model increases the model's degrees of freedom, improving its ability to reproduce data, regardless of the validity of the underlying structure. Therefore, when a particular model structure improves the agreement of the model with kinetic data, it can only be said that the model structure is "consistent" with the kinetic data; it cannot be said that the model structure has been "proved" by its consistency with the data. In such circumstances, it is imperative that the physiological or biochemical hypothesis underlying the model structure is tested using nonkinetic data.

35.2.2 Elements of Model Structure

The process of selecting a model structure can be broken down into a number of elements associated with the different aspects of uptake, distribution, metabolism, and elimination. This section treats each of these elements in turn.

Storage Compartments Naturally, any tissues that are expected to accumulate significant quantities of the compound or its metabolites need to be included in the model structure. As discussed earlier, these storage tissues can be grouped together to the extent that they have similar time constants. The muscle tissue in the methotrexate model (Fig. 35.2) is an example of a storage compartment. The generic mass balance equation for storage compartments such as these is



$$dA_T/dt = Q_T \cdot C_A - Q_T \cdot C_{VT}$$

where A_T is the mass of compound in the tissue (mg), C_A is the concentration of compound in the arterial blood reaching the tissue (mg/L), and C_{VT} is the concentration of compound in the venous blood leaving the tissue (mg/L). Thus, this mass balance equation simply states that the rate of change in the amount of compound in the tissue with respect to time (dA_T/dt) is equal to the difference between the rate at which compound enters the tissue and the rate at which compound leaves the tissue. We can then calculate the concentration of the compound in the storage tissue (C_T) from the amount in the tissue and the tissue volume (V_T):

$$C_T = A_T/V_T$$

In PBPK models, it is common to assume *venous equilibration*; that is, that in the time that it takes for the blood to perfuse the tissue, the compound is able to achieve its equilibrium distribution between the tissue and blood. Therefore, the concentration of the compound in the venous blood can be related to the concentration in the tissue by the equilibrium tissue:blood partition coefficient, P_T:

$$C_{VT} = C_T/P_T$$

Therefore, we obtain a differential equation in A_T:

$$dA_T/dt = Q_T \cdot C_A - Q_T \cdot A_T/(P_T \cdot V_T)$$

If desired, we can reformulate this mass balance equation in terms of concentration:

$$dA_T/dt = d(C_T \cdot V_T)/dt = C_T \cdot dV_T/dt + V_T \cdot dC_T/dt$$

If (and only if) V_T is constant (i.e., the tissue does not grow during the simulation), $dV_T/dt = 0$, and

$$dA_T/dt = V_T \cdot dC_T/dt$$

so we have the alternative differential equation:

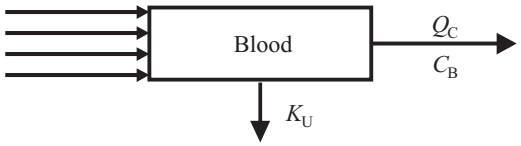
$$dC_T/dt = Q_T \cdot (C_A - C_T/P_T)/V_T$$

This alternative mass balance formulation, in terms of concentration rather than amount, is popular in the PK literature. However, in the case of models with compartments that change volume over time (e.g., in a model incorporating growth of a single or multiple tissues) it is preferable to use the formulation in terms of amounts in order to avoid the need for the additional term reflecting the change in volume ($C_T \cdot dV_T/dt$).

Depending on the compound, many different tissues can potentially serve as important storage compartments. The use of a fat storage compartment is typically required for lipophilic compounds. The gut lumen can also serve as a storage site for compounds subject to enterohepatic recirculation, as in the case of methotrexate. Important storage sites for metals, on the other hand, can include the kidney,

red blood cells, intestinal epithelial cells, skin, bone, and hair [40]. Transport to and from a storage compartment does not always occur via the blood, as was described previously; for example, in some cases the storage is an intermediate step in an excretion process (e.g., hair, intestinal epithelial cells). As with methotrexate, it may also be necessary to use multiple compartments in series, or other mathematical devices, to model plug flow (i.e., a time delay between entry and exit from storage).

Blood Compartment The description of the blood compartment can vary considerably from one PBPK model to another depending on the role the blood plays in the kinetics of the compound being modeled. In some cases the blood may be treated as a simple storage compartment, with a mass balance equation describing the summation (Σ) of the venous blood flows from the various tissues and the return of the total arterial blood flow (Q_C) to the tissues, as well as any urinary clearance (if, as in the case of glomerular filtration, clearance is described as occurring from the blood compartment):



$$dA_B/dt = \sum(Q_T \cdot C_{VT}) - Q_C \cdot C_B - K_U \cdot C_B$$

where A_B is the amount of compound in the blood (mg), Q_C is the total cardiac output (L/h), C_B is the concentration of compound in the blood (mg/L), and K_U is the urinary clearance (L/h). The value for K_U can often be estimated from the unbound fraction in plasma (f_{ub}) and the glomerular filtration rate (GFR), unless active transport processes contribute to renal elimination. An alternative method for estimating human renal clearance based on rat renal clearance and incorporating species-specific physiological differences in GFR has been proposed [13, 41].

Most often, drug concentrations are measured in plasma or serum and not in whole blood; hence, plasma or serum is the reference fluid for the derived PK parameters such as clearances and volumes of distribution. However, whole blood, not plasma or serum, is flowing through the vessels of the human body. Therefore, provided that there is evidence in support of fast equilibration of drug between red blood cells and plasma [42], whole blood rather than plasma is the more appropriate reference fluid for calculating and interpreting clearances and volumes of distribution. For this reason, parameterization of the PBPK model is often performed in terms of blood flows. To compare calculated plasma concentrations to experimental data, the calculated blood concentration must then be divided by the blood-to-plasma ratio (BPR), which is often measured experimentally.

In cases where a compound is not taken up by the red blood cells, plasma flow can be used in place of blood flow in the model [5]. For some compounds, where exchange between plasma and red blood cells is slow compared to tissue perfusion,

it may be necessary to model the red blood cells as a storage compartment in communication with the plasma via diffusion-limited transport. Typically, however, exchange between red blood cells and plasma is fast compared to tissue distribution, and the blood can be treated as a single compartment.

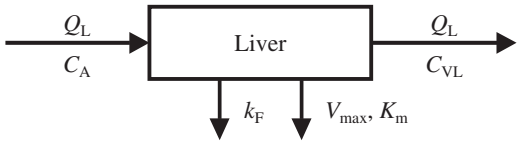
If the blood is an important storage compartment for a compound, it may be necessary to carefully evaluate data on tissue concentrations, particularly the richly perfused tissues, to determine whether compound in the blood perfusing the tissue could be contributing to the measured tissue concentration. For other compounds, the amount of compound actually in the blood may be relatively small, in which case only the concentration may be of interest. In this case, instead of having a true blood compartment, a steady-state approximation can be used to estimate the concentration in the blood at any time. Assuming the blood is at steady state with respect to the tissues,

$$dA_B/dt = 0$$

Therefore, solving the blood equation for the concentration:

$$C_B = \sum_T (Q_T \cdot C_{VT})/Q_C$$

Metabolism/Elimination The liver is frequently the primary site of metabolism for a compound. The following equation is an example of the mass balance equation for the liver in the case of a compound that is metabolized through both saturable and nonsaturable components:



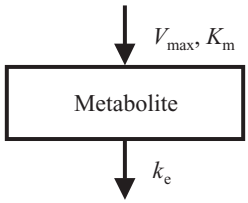
$$dA_L/dt = Q_L \cdot (C_A - C_{VL}) - k_F \cdot C_{Lfree} \cdot V_L - V_{max} \cdot C_{Lfree}/(K_m + C_{Lfree})$$

where Q_L is the total blood flow (arterial and portal) to the liver and C_{Lfree} is the free (unbound) concentration in the liver.

In the equation above, the first term on the right-hand side of the equation represents the mass flux associated with transport in the blood and is essentially identical to the case of the storage compartment described previously. In the case of the liver, however, it should be noted that there are two sources of blood flow: the arterial flow directly to the liver and the portal flow that first perfuses the intestines. When appropriate, these two blood flows can be differentiated in the model (Fig. 35.2 and 35.3).

The second term in the equation above describes metabolism by a linear (first-order) pathway with rate constant k_F (h^{-1}) and the third term represents metabolism by a saturable (Michaelis–Menten) pathway with capacity V_{max} (mg/h) and affinity K_m (mg/L). If it were desired to model a water-soluble metabolite produced by this

saturable pathway, an equation for its formation and elimination could also be added to the model:



$$dA_M/dt = R_{stoch} \cdot V_{max} \cdot C_{Lfree}/(K_m + C_{LFree}) - k_e \cdot A_M$$

$$C_M = A_M/V_D$$

where A_M is the amount of metabolite in the body (mg), R_{stoch} is the stoichiometric fractional yield of the metabolite (unitless) (times the ratio of its molecular weight to that of the parent compound), k_e is the rate constant for the clearance of the metabolite from the body (h^{-1}), C_M is the concentration of the metabolite in the plasma (mg/L), and V_D is the apparent volume of distribution for the metabolite (L).

The definition of free concentration in the liver (C_{Lfree}) in these equations is not as straightforward as it may at first appear. In cases where hepatic clearance is relatively low, the free concentration in the liver is often assumed to be equal to the free (unbound) concentration in the blood; that is, $C_{Lfree} = f_u \cdot C_B$. However, when hepatic clearance is high, the free concentration in the liver can be drawn well below the free concentration in the blood, and such an assumption may be inappropriate. An alternative assumption that is often made is that the free concentration in the liver can be estimated by dividing the total liver concentration by the liver:blood partition coefficient; that is, $C_{Lfree} = C_L/P_L$ [5]. This approximation is particularly useful for compounds whose metabolism is limited by hepatic blood flow at low concentrations. If the intent is to use *in vitro* estimates of the metabolic parameters (V_{max}, K_m, k_f) in the model, then the definition of the *in vivo* free concentration should be consistent with the conditions under which the *in vitro* estimates of intrinsic clearance were obtained. In principle, this could require adjusting for differences in binding between the *in vitro* medium and the tissue *in vivo*, although such adjustments are seldom performed in practice.

Metabolite Compartments In principle, the same considerations that drive decisions regarding the level of complexity of the PBPK model for the parent compound must also be applied for each of its metabolites, and their metabolites, and so on. As in the case of the parent compound, the first and most important consideration is the purpose of the model. If the concern is a direct parent compound effect and the compound is inactivated by metabolism, then there is no need for a description of metabolism beyond its role in the clearance of the parent compound. The model for methotrexate (Fig. 35.2) is an example of a parent compound model.

If one or more of the metabolites are considered to contribute to the efficacy or toxicity of a compound, it may also be necessary to provide a more complete description of the kinetics of the metabolites themselves. For example, in the case

of teratogenicity from all-trans retinoic acid, both the parent compound and several of its metabolites are considered to be toxicologically active; therefore, in developing the PBPK model for this compound it was necessary to include a fairly complete description of the metabolic pathways [19]. Fortunately, the metabolism of xenobiotic compounds often produces metabolites that are relatively water soluble, simplifying the description needed. In many cases, a classical one-compartment description may be adequate for describing the metabolite kinetics. In other cases, however, the description of the metabolite (or metabolites) may have to be as complex as that of the parent compound. If reactive intermediates produced during the metabolism of a compound are responsible for toxicity, a very simple description of the metabolic pathways might be adequate [43].

Target Tissues Typically, a PBPK model used in drug development applications will include compartments for any target tissues for the efficacy of the compound and could also include target tissues of toxicity if the model is to be used for assessing safety. The target tissue description may in some cases need to be fairly complicated, including such features as *in situ* metabolism, binding, and pharmacodynamic processes in order to provide a realistic measure of biologically effective tissue exposure.

A fundamental issue in determining the nature of the target tissue description required is the need to identify the active form of the compound. A compound may produce an effect directly, through its interaction with tissue constituents, or indirectly, through a metabolite. In the case of toxicity, it is often the metabolism of a compound that leads to undesired effects, either through the production of reactive metabolites during metabolism or due to the toxicity of a circulating metabolite.

The specific nature of the relationship between tissue exposure and response depends on the mechanism, or mode of action, involved. Rapidly reversible effects may result primarily from the current concentration of the compound in the tissue, while longer-term effects may depend on both the concentration and duration of the exposure. Although therapeutic effects are generally due to the administered compound, an active metabolite may extend efficacy or cause undesired side effects or toxicity. In general, the appropriate measure of tissue exposure for a toxic side effect of a compound may be different from the appropriate measure for its therapeutic effect. For example, the therapeutic effect of a drug may depend on the prolonged maintenance of a relatively low concentration sufficient to occupy a receptor in the target tissue, while its toxicity may result from transient, high rates of metabolism in the liver occurring shortly after dosing. In such a case, PBPK modeling of the concentration time course in the liver and target tissue for different dosing routes or regimens might help to maximize the therapeutic index for the compound. For a developmental toxicity, the concentration time course might also have to be convoluted with the window of susceptibility for a particular gestational event. The evaluation of the various modes of action for the beneficial and toxic effects of a compound is the most important step in a PK analysis and a principal determinant of the structure and level of detail that will be required in the PBPK model.

Uptake Routes Each of the relevant uptake routes for the compound must be described in the model. Often there are a number of possible ways to describe a

particular uptake process, ranging from simple to complex. As with all other aspects of model design, the competing goals of parsimony and realism must be balanced in the selection of the level of complexity to be used. The following examples are meant to provide an idea of the variety of model code that can be required to describe the various possible uptake processes.

Intravenous Administration (Bolus Dosing)

$$A_{B0} = Dose \cdot BW$$

where A_{B0} is the amount of compound in the blood at the time of dosing ($t = 0$), *Dose* is the administered dose (mg/kg), and *BW* is body weight (kg).

Intravenous Administration (Infusion) In the case where a steady-state approximation has been used to eliminate the blood compartment, we have

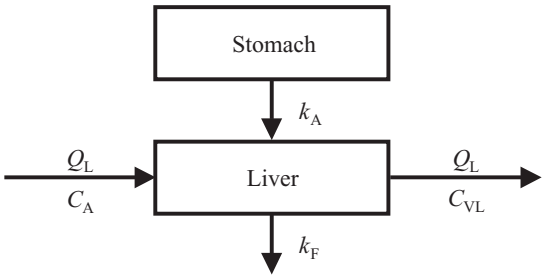
$$C_B = (Q_L \cdot C_{VL} + \cdots + Q_F \cdot C_{VF} + k_{IV})$$

where

$$k_{IV} = \begin{cases} Dose \cdot BW / t_{IV} & (t < t_{IV}) \\ 0 & (t > t_{IV}) \end{cases}$$

where t_{IV} is the duration of time over which the infusion takes place (h). In this case, the model code must be written with a "switch" to change the value of k_{IV} to zero at $t = t_{IV}$.

Oral Gavage For a compound that is completely absorbed in the stomach,



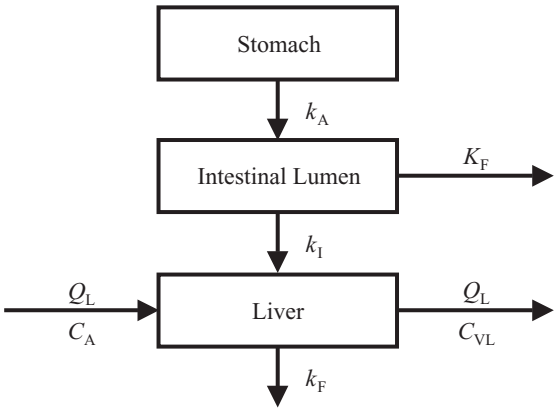
$$A_{ST0} = \text{Dose} \cdot \text{BW}$$

$$dA_{ST}/dt = -k_A \cdot A_{ST}$$

$$dA_L/dt = Q_L \cdot (C_A - C_L/P_L) - k_F \cdot C_L \cdot V_L/P_L + k_A \cdot A_{ST}$$

where A_{ST0} is the amount of compound in the stomach at the beginning of the simulation, A_{ST} is the amount of compound in the stomach at any given time, and k_A is a first-order rate constant (h^{-1}) describing uptake from the stomach.

For a compound that is incompletely absorbed,



$$A_{ST0} = Dose \cdot BW$$

$$dA_{ST}/dt = -k_S \cdot A_{ST}$$

$$dA_I/dt = k_S \cdot A_{st} - k_I \cdot A_I - K_F \cdot A_I/V_I$$

$$dA_L/dt = Q_L \cdot (C_A - C_{VL}) - k_F \cdot C_{Lfree} \cdot V_L + k_I \cdot A_I$$

where A_I is the amount of compound in the intestinal lumen (mg), k_I is the rate constant for intestinal absorption (h^{-1}), K_F is the fecal clearance (L/h), and V_I is the volume of the intestinal lumen (L).

The rate of fecal excretion of the compound is then

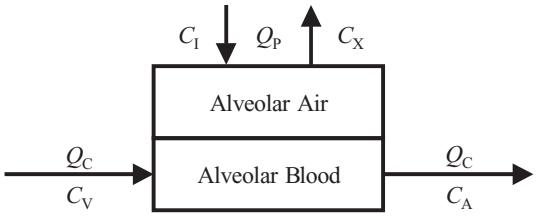
$$dA_F/dt = K_F \cdot A_I/V_I$$

The examples described above are highly simplified descriptions. For example, they describe uptake from the stomach or intestinal lumen directly to the liver, when in fact the uptake is into the tissues of the gastrointestinal (GI) tract with subsequent transport to the liver in the portal blood. While this simplification is adequate in some cases, a more accurate description may be necessary in others, such as when metabolism in the gut tissues is important or portal blood flow could limit uptake. The equations shown above also do not describe biliary excretion or other processes that might be important determinants of the intestinal concentration and fecal excretion of a compound over time. Again, these processes would need to be included in the full model description for compounds where these processes are important [19]. Note also that this simple formulation does not consider the plug flow of the intestinal contents and will not reproduce the delay that actually occurs in the appearance of a compound in the feces. Such a delay could be added using a delay function available in common simulation software, or multiple compartments could be used to simulate plug flow, as shown in the diagram of the methotrexate model (Fig. 35.2).

Although in some cases a simple, first-order model can adequately describe oral absorption, more physiologically representative approaches have been developed and shown to be useful for predicting the fraction absorbed, for example, a

compartmental approach such as the ACAT model [44] and a model describing the GI tract as a tube [45]. Simulation of oral absorption using physiologically based models represents another challenge because of the many processes involved such as the release, dissolution, degradation, metabolism, uptake, and absorption of a compound as it transits through the different segments of the digestive tract [46]. Oral absorption simulations require *in vitro* and *in silico* input data such as solubility, permeability, particle size, partition coefficient ($\log P$), ionization constant (pK_a), and dose [47, 48].

Inhalation For compounds that are volatile, it is necessary to describe the exchange of vapor between the lung air and blood in the alveolar region. This is true even if the compound is not administered by inhalation, because exhalation can be an important route of clearance for volatile compounds regardless of the dose route.



$$dA_{AB}/dt = Q_C \cdot (C_V - C_A) + Q_P \cdot (C_I - C_X)$$

where A_{AB} is the amount of compound in the alveolar blood (mg), C_V is the concentration of compound in the pooled venous blood (mg/L), C_A is the concentration of compound in the alveolar (arterial) blood (mg/L), Q_P is the alveolar (not total pulmonary) ventilation rate (L/h), C_I is the concentration of compound in the inhaled air (mg/L), and C_X is the concentration of compound in the alveolar air (mg/L). Assuming the alveolar blood is at steady state with respect to the other compartments,

$$dA_{AB}/dt = 0$$

Also, assuming lung equilibration (i.e., that the blood in the alveolar region has reached equilibrium with the alveolar air prior to exhalation),

$$C_X = C_A/P_B$$

where P_B is the blood : air partition coefficient.

Substituting into the equation for the alveolar blood and solving for C_A, we have

$$C_A = (Q_C \cdot C_V + Q_P \cdot C_I)/(Q_C + Q_P/P_B)$$

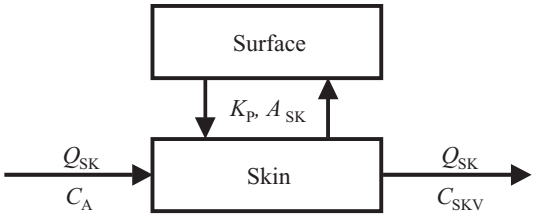
Note that the rate of elimination of the compound by exhalation is just $Q_P \cdot C_X$. The alveolar ventilation rate, Q_P, does not include the "deadspace" volume (the portion of the inhaled air that does not reach the alveolar region) and is therefore roughly 70% of the total respiratory rate. The concentration C_X represents the

"end-alveolar" air concentration; in order to estimate the average exhaled concentration (C_{EX}), the deadspace contribution must be included:

$$C_{EX} = 0.3C_I + 0.7C_X$$

PBPK models including more detailed physiological descriptions of inhalation exposures developed to understand toxicological effects of reactive vapors in the nasal cavity have been reviewed [49].

Dermal A simple model can be used to describe dermal absorption from a constant-concentration vehicle on the skin surface.



$$dA_{SK}/dt = K_P \cdot A_{SFC} \cdot (C_{SFC} - C_{SK}/P_{SKV})/1000 + Q_{SK} \cdot (C_A - C_{SK}/P_{SKB})$$

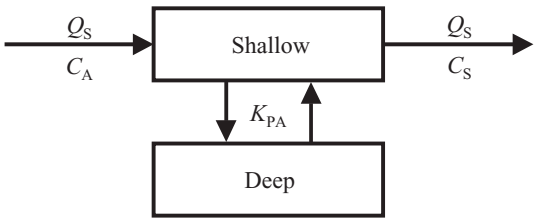
where A_{Sk} is the amount of compound in the skin (mg), K_P is the skin permeability coefficient (cm/h), A_{SFC} is the skin surface area (cm^2), C_{SFC} is the concentration of compound on the surface of the skin (mg/L), C_{SK} is the concentration of the compound in the skin (mg/L), P_{SK} is the skin : vehicle partition coefficient (i.e., the vehicle containing the compound on the surface of the skin), Q_{SK} is the blood flow to the skin region (L/h), C_A is the arterial concentration of the compound (mg/L), and P_{SKB} is the skin : blood partition coefficient.

Due to adding this compartment, the equation for the blood in the model must also be modified to add a term for the venous blood returning from the skin ($+Q_{SK} \cdot C_{SK}/P_{SKB}$), and the blood flow and volume parameters for the slowly perfused tissue compartment must be reduced by the amount of blood flow and volume for the skin. Approaches used to include the dermal exposure route in PBPK models have been reviewed [50]. Several reviews discuss the wide variety of available compartment models and provide guidance for choosing among them [51, 52].

Experimental Apparatus In some cases, in addition to compartments describing the animal–chemical system, it may also be necessary to include model compartments that describe the experimental apparatus in which measurements were obtained.

Distribution/Transport There are a number of issues associated with the description of the transport and distribution of the compound that must be considered in the process of model design. Discussions of the more common ones are included here.

Diffusion-Limited Transport Most of the PBPK models in the literature are flow-limited models; that is, they assume that the rate of tissue uptake of the compound is limited only by the flow of the compound to the tissue in the blood. While this assumption appears to be reasonable in general, for some compounds and tissues uptake may be diffusion limited. Examples of tissues for which diffusion-limited transport has often been described include the skin, placenta, brain, and fat. The model compartments described thus far have all assumed flow-limited transport. If there is evidence that the movement of a compound between the blood and a tissue is limited by diffusion, a two-compartment description of the tissue can be used with a "shallow" exchange compartment in communication with the blood and a diffusion-limited "deep" compartment that represents the actual tissue:



$$dA_S/dt = Q_S \cdot (C_A - C_S) - K_{PA} \cdot (C_S - C_D/P_D)$$
$$dA_D/dt = K_{PA} \cdot (C_S - C_D/P_D)$$

where A_S is the amount of compound in the shallow compartment (mg), Q_S is the blood flow to the shallow compartment (L/h), C_S is the concentration of compound in the shallow compartment (mg/L), K_{PA} is the permeability–area product for diffusion-limited transport (L/h), C_D is the concentration of compound in the deep compartment (mg/L), P_D is the tissue:blood partition coefficient, and A_D is the amount of compound in the deep compartment (mg).

Saturable Tissue Binding When there is evidence that saturable binding is an important determinant of the distribution of a compound into a tissue (such as evidence of dose-dependent tissue partitioning), a simple description of tissue binding can be added to the model. In this description, only free (unbound) compound is considered to be available for transport or clearance at any given moment in time. For example, in the case of saturable binding in the liver,

$$dA_L/dt = V_L\ dC_L/dt = Q_L \cdot (C_A - C_{Lfree}) - k_F \cdot C_{Lfree}$$

where A_L is the total (free plus bound) concentration of the compound in the liver (mg), C_{Lfree} is the concentration of free (unbound) compound in the liver (mg/L), and k_F is the rate constant for metabolism (h^{-1}).

The apparent complication in adding this equation to the model is that the change in the total amount of compound in the tissue (dA_L/dt) is needed for the mass balance, but the determinants of the kinetics are described in terms of the

free concentration in the tissue (C_{Lfree}). To solve for free in terms of total, we note that

$$C_L = C_{Lfree} + C_{Lbound}$$

where C_{Lbound} is the concentration of bound compound in the tissue (mg/L). We can describe the saturable binding with an equation similar to that for saturable metabolism:

$$C_{Lbound} = B_m \cdot C_{Lfree}/(K_d + C_{Lfree})$$

where B_m is the binding capacity (mg/L) and K_d is the binding affinity (mg/L). Substituting this equation into the previous one, we have

$$C_L = C_{Lfree} + B_m \cdot C_{Lfree}/(K_d + C_{Lfree})$$

Rewriting this equation to solve for the free concentration in terms of only the total concentration would result in a quadratic equation, the solution of which could be obtained with the quadratic formula. However, taking advantage of the iterative algorithm by which these PBPK models are exercised (as will be discussed later), it is not necessary to go to this effort. Instead, a much simpler implicit equation can be written for the free concentration (i.e., an equation in which the free concentration appears on both sides):

$$C_{Lfree} = C_L/(1 + B_m/(K_d + C_{Lfree}))$$

In an iterative algorithm, this equation can be solved at each time step using the previous value of C_{Lfree} to obtain the new value! A new value of C_L is then obtained from the mass balance equation for the liver using the new value of C_{Lfree}, and the process is repeated. An underlying assumption for this simple description of tissue binding is that the binding is rapidly reversible compared to the movement or clearance of free compound, such that equilibrium between free and bound chemical can be maintained.

In fact, at least two different computational approaches have been used to describe saturable binding in PBPK models. The concentration of free compound can either be estimated, as described above, from solving a conservation equation for total mass that apportions the total amount of compound between free and bound forms using the equilibrium dissociation constants, K_d, and binding maxima, B_m [53], or it can be estimated by explicitly including both "on" (association) and "off" (dissociation) rate constants, k_a and k_d [54]. In the latter case, the dissociation binding constant (with units of concentration) is the ratio of the two rate constants, k_d/k_a. The advantage of the rate constant approach is that it does not require the assumption that binding is fast compared to transport and clearance.

While these two computational approaches have usually been applied within tissues, they can also be readily applied to binding in blood if the concentrations and affinities of binding proteins are known. However, in most modeling of drugs, protein binding in blood is linear (not saturable at clinically relevant concentrations) and can be characterized by a single parameter, fraction unbound, rather

than estimates of concentrations of binding sites and their affinities for binding. Nevertheless, there are cases where protein binding is more appropriately described as a nonlinear process [55]. Alternative descriptions of blood binding will be discussed in more detail in the next section.

Binding in Blood Protein binding in blood can be a key determinant of drug disposition, affecting compound availability for interaction with therapeutic targets as well as for clearance. A high fraction bound in the blood also gives rise to concerns regarding potential drug–drug interactions that might displace bound drug and produce a transient increase in drug concentrations to potentially toxic levels. Methodologies to estimate drug binding and approaches for the quantitative description of this binding in PK models have been areas of intense interest over the past four to five decades. Consideration of blood binding faces two parallel challenges. First, when drugs are bound in capillary blood, what fraction should be regarded as available for transport into tissue? Second, how does the binding in blood influence blood:tissue partitioning? Historically, these questions have been addressed both in empirical descriptions and in PBPK models, and some care is required to reconcile the different approaches and arrive at a consistent quantitative treatment of blood binding and transport of compound throughout the body in both types of modeling approaches.

In the standard description of clearance of a compound from blood by tissue metabolism, binding in the blood is assumed to be linear and the fraction unbound, f_u, is simply multiplied by the intrinsic clearance, leading to a straightforward relationship:

$$CL = Q_T \cdot f_u \cdot CL_{int}/(Q_T + f_u \cdot CL_{int})$$

In this relationship, the maximal tissue clearance, even with a low fraction unbound, is total tissue blood flow. That is, all of the compound in the blood, whether bound or unbound, becomes available for clearance as long as the intrinsic clearance is sufficiently large. Note that in this description the fraction unbound is not a function of the clearance. In fact, the derivation of this equation rests on the assumption that dissociation of bound compound in the blood is fast compared to the rate of tissue clearance. If the uptake of a compound into the tissue is limited by the rate of dissociation of the compound from binding proteins in the blood, the simple formula above will overestimate its clearance.

In PBPK models, blood concentrations of bound and free compound can be described separately, as discussed in the previous section, and only free compound is generally considered to be available to participate in processes such as diffusion, metabolism, tissue reaction, and intercompartmental transfer. As in the case of tissue binding, the relationship of free to bound concentrations in the blood is generally calculated by knowledge of dissociation binding constants (K_d) and maximum concentrations of binding proteins (B_m), as describe previously. An example of this approach has been described in the case of a PBPK model for estradiol [55]. This approach differs from the simple clearance formula given above in that the fraction unbound can be a nonlinear function of the concentration of the compound in the blood. It shares, however, the assumption that the "on" and "off" rates for binding

are fast compared to rates of clearance. The alternative description of binding described in the previous section, which explicitly includes the binding rate constants, would be preferred in cases where this assumption may be violated.

Protein binding in blood is a critical component of drug action and drug efficacy. PK models need to carefully consider the manner in which binding can be introduced into the basic equations and track free concentrations at sites of action or at least within the plasma. Introduction of blood binding in PBPK models raises some conceptual challenges, especially in comparing conventional empirical approaches with PBPK approaches intended to track thermodynamically free concentrations throughout the body. Although simple descriptions are often adequate, careful consideration of the underlying kinetic processes and their relative rates for the compound and tissues of interest is required to assure that a particular modeling approach is appropriate [56].

Tissue:Blood Partitioning Regardless of the manner in which blood binding is implemented in PBPK models, another challenge arises in describing equilibration between blood and tissues. In general, both the blood and the tissues will contain free and bound forms of the compound. For equilibration, only the free compound in the plasma diffuses across the tissue capillary interface into the tissue, and at equilibrium between blood and tissue, the free concentration in the plasma and the tissue is expected to be equal (except in the case of active transport). However, the equilibrium relationship of the concentrations in tissues compared to the blood or plasma is typically described with empirical partition coefficients based on measurements of total concentrations of the compound. Differential binding in plasma and tissue will therefore influence apparent tissue partitioning.

The relationship between apparent tissue:blood partitioning and binding in blood versus tissue can be straightforwardly described, as long as no other factors affect distribution. Assuming that (1) there is no need to adjust for the effect of clearance, and (2) there is no evidence of active transport of the compound between blood and tissue, the free fraction in the tissue, f_{ut}, can then be estimated:

$$P_{tb} = P_{tp}/BPR = (f_{up}/f_{ut})/BPR$$

where P_{tb} is the tissue:blood partition coefficient, P_{tp} is the tissue:plasma partition coefficient, BPR is the blood to plasma ratio, f_{up} is the fraction unbound in the plasma, and f_{ut} is the fraction unbound in the tissue.
Then

$$f_{ut} = f_{up}/(P_{tb} \cdot BPR)$$

In fact, there are quite a number of different determinants of the apparent partitioning between blood and tissues:

- Partitioning due to lipophilicity
- Plasma binding
- Tissue binding

- Active transport
- Clearance processes
- Blood to plasma ratio (for converting tissue:plasma partitions to tissue:blood)

A measured or estimated partition coefficient may reflect any combination of these factors, and the modeler must be aware of this potential complexity in attempting to use a particular set of data on a compound. For example, if partition coefficients have been estimated from QSAR, they are likely to primarily reflect lipophilic partitioning and may need to be adjusted for differences in binding in plasma and tissues. Alternatively, the model can be designed to separately describe lipophilic partitioning, using the estimated partition coefficients, and binding, based on other data. *In vitro*-derived partition coefficients, on the other hand, may reflect both thermodynamic partitioning and binding, although disruption of the tissue architecture may alter the binding characteristics of the tissue. It is also necessary to ensure that no metabolic clearance of the compound occurs in either blood or tissue during the measurements. *In vivo*-derived partition coefficients may reflect lipophilicity, binding, and active transport, as well as the effect of any clearance processes [57]. Due to this complexity, it may in some cases be preferable to estimate model parameters for tissue partitioning by fitting the *in vivo* blood and tissue concentration data rather than trying to use it directly to calculate "partition coefficients" for the model.

Model Diagram As described in the previous sections, the process of developing a PBPK model begins by determining the essential structure of the model based on the information available on the compound's toxicity, mechanism of action, and PK properties. The results of this step can usually be summarized by an initial model diagram, such as those depicted in Fig. 35.2 and 35.3. In fact, in many cases a well-constructed model diagram, together with a table of the input parameter values and their definitions, is all that an accomplished modeler should need in order to create the mathematical equations defining a PBPK model. In general, there should be a one-to-one correspondence of the boxes in the diagram to the mass balance equations (or steady-state approximations) in the model. Similarly, the arrows in the diagram correspond to the transport or metabolism processes in the model. Each of the arrows connecting the boxes in the diagram should correspond to one of the terms in the mass balance equations for both of the compartments it connects, with the direction of the arrow pointing from the compartment in which the term is negative to the compartment in which it is positive. Arrows only connected to a single compartment, which represent uptake and excretion processes, are interpreted similarly.

The model diagram should be labeled with the names of the key variables associated with the compartment or process represented by each box and arrow. Interpretation of the model diagram is also aided by the definition of the model input parameters in the corresponding table. The definition and units of the parameters can indicate the nature of the process being modeled (e.g., diffusion-limited vs. flow-limited transport, binding vs. partitioning, saturable vs. first-order metabolism).

35.3 PBPK MODEL IMPLEMENTATION

The purpose of developing a PBPK model is to perform simulations and learn about the system (Fig. 35.1). But first, the model must be parameterized, coded using some type of software package, and tested to make sure it is working properly. Also, sensitivity analysis and other techniques must be used to understand the model and verify that key inputs are known with sufficient accuracy to result in reasonable simulation results.

35.3.1 Model Parameterization

Once the model structure has been determined, it still remains to identify the values of the input parameters in the model.

Physiological Parameters Estimates of the various physiological parameters needed in PBPK models are available from a number of sources in the literature, particularly for the human, monkey, dog, rat, and mouse [4, 26–30]. Estimates for the same parameter often vary widely, however, due both to experimental differences and to differences in the animals examined (age, strain, activity). Ventilation rates and blood flow rates are particularly sensitive to the level of activity [26, 28]. Data on some important tissues are relatively poor, particularly in the case of fat tissue. Table 35.2 shows typical values of a number of physiological parameters in several species.

Biochemical Parameters One large barrier to the application of PBPK models in preclinical drug development has been that tissue:plasma partition coefficients (P_{tp}) are too expensive to routinely measure. Partition coefficients can be determined by *in vivo* or *in vitro* measurements [31, 57, 58] or can be estimated from quantitative structure–activity relationship (QSAR) modeling. Perhaps the driving force behind the recent interest in PBPK modeling in the pharmaceutical industry was reported successes in developing methods for *a priori* predictions of P_{tp} values for volatile organic compounds based on their solubilities in the neutral lipid, phospholipid, and water fractions of tissues as estimated using a vegetable oil:water partition coefficient; the necessary tissue composition data has been tabulated for a variety of tissues [59–61]. This approach was eventually extended to using the mechanistic equations for predicting P_{tp} values for drugs [62]. Briefly, these mechanistic equations assume that the drug distributes homogeneously into the tissue and plasma by passive diffusion, where two processes are accounted for: (1) nonspecific binding to lipids estimated from drug lipophilicity data ($\log P$, $\log D$) and (2) specific reversible binding to common proteins present in plasma and tissue estimated from the fraction unbound in the plasma (f_{up}). These P_{tp} values can be used to estimate the volume of distribution [63]. Recent contributions have focused on improving methods for calculating P_{tp} values for moderate-to-strong bases by developing a method incorporating the electrostatic interactions with tissue acidic phospholipids [64] and for acids, very weak bases, neutrals, and zwitterions by incorporating the effect of drug ionization on distribution processes [65].

One of the greatest challenges is typically the characterization of metabolism, which can also make use of both *in vivo* and *in vitro* methods. For compounds

TABLE 35.2 Typical Physiological Parameters for PBPK Models

Species	Mouse	Rat	Monkey	Human
Ventilation				
Alveolar (L/h)[a]	29.0[b]	15.0[b]	15.0[b]	15.0[b]
Blood flows				
Total (L/h)[a]	16.5[c]	15.0[c]	15.0[c]	15.0[c]
Muscle (fraction)	0.18	0.18	0.18	0.18
Skin (fraction)	0.07	0.08	0.06	0.06
Fat (fraction)	0.03	0.06	0.05	0.05
Liver (arterial) (fraction)	0.035	0.03	0.065	0.07
Gut (portal) (fraction)	0.165	0.18	0.185	0.19
Other organs (fraction)	0.52	0.47	0.46	0.45
Tissue volumes				
Body weight (kg)	0.02	0.3	4.0	80.0
Body water (fraction)	0.65	0.65	0.65	0.65
Plasma (fraction)	0.04	0.04	0.04	0.04
RBCs (fraction)	0.03	0.03	0.03	0.03
Muscle (fraction)	0.34	0.36	0.48	0.33
Skin (fraction)	0.17	0.195	0.11	0.11
Fat (fraction)	0.10[d]	0.07[d]	0.05[d]	0.21
Liver (fraction)	0.046	0.037	0.027	0.023
Gut tissue (fraction)	0.031	0.033	0.045	0.045
Other organs (fraction)	0.049	0.031	0.039	0.039
Intestinal lumen (fraction)	0.054	0.058	0.053	0.053

[a]Scaled allometrically: $QC = QCC \cdot BW^{0.75}$.
[b]Varies significantly with activity level (range: 15.0–40.0).
[c]Varies with activity level (range: 15.0–20.0).
[d]Varies substantially (lower in young animals, higher in older animals).

cleared by hepatic metabolism, intrinsic clearance values determined *in vitro* with hepatocyte or microsomal substrate depletion or kinetic assays are typically used. Many researchers have described physiological methods for scaling hepatocyte and microsome data, including Zuegge et al. [66], Lavé et al. [67], Houston [68], Houston and Carlile [69], Obach [70], and Ito et al. [71]. Recently improved parameters for the physiological scaling of human hepatocyte and microsome data have been published [72].

Allometry The different types of physiological and biochemical parameters in a PBPK model are known to vary with body weight in different ways [24]. Typically, the parameterization of PBPK models is simplified by assuming standard allometric scaling [28], as shown in Table 35.3, where the scaling factors, b, can be used in the following equation:

$$Y = aX^b$$

where Y is the value of the parameter at a given body weight, X (kg), and a is the scaled parameter value for a 1 kg animal.

TABLE 35.3 Standard Allometric Scaling for Physiologically Based Pharmacokinetic Model Parameters

Parameter Type (units)	Scaling (power of body weight)
Volumes	1.0
Flows (volume per time)	0.75
Ventilation (volume per time)	0.75
Clearances (volume per time)	0.75
Metabolic capacities (mass per time)	0.75
Metabolic affinities (mass per volume)	0
Partition coefficients (unitless)	0
First-order rate constants (inverse time)	–0.25

While standard allometric scaling provides a useful starting point, or hypothesis, for cross-species scaling, it is not sufficiently accurate for some applications. In the case of the physiological parameters, the species-specific parameter values are generally available in the literature [4, 26–30] and can be used directly in place of the allometric estimates. For compound-specific parameters, *in vitro* data for metabolism, distribution, or absorption relevant to the species under consideration are used in most of the cases in preference to allometric estimates. However, allometric scaling might provide first parameter estimates when data is lacking.

Parameter Optimization In many cases, important parameter values needed for a PBPK model may not be available in the literature. In such cases it is necessary to measure them in new experiments, to estimate them by QSAR techniques, or to identify them by optimizing the fit of the model to an informative dataset. Even in the case where an initial estimate of a particular parameter value can be obtained from other sources, it may be desirable to refine the estimate by optimization. For example, given the difficulty of obtaining accurate estimates of the fat volume in rodents, a more reliable estimate may be obtained by examining the impact of fat volume on the kinetic behavior of a lipophilic compound. Of course, being able to uniquely identify a parameter from a kinetic dataset rests on two key assumptions: (1) that the kinetic behavior of the compound under the conditions in which the data was collected is sensitive to the parameter being estimated, and (2) that other parameters in the model, which could influence the observed kinetics, have been determined by other means and are held fixed during the estimation process. When it is necessary to estimate multiple parameters from *in vivo* PK data, using sensitivity analysis to verify that sufficient data are available and optimizing on individual parameters before performing a global optimization has been recommended [73].

The actual approach for conducting a parameter optimization can range from simple visual fitting, where the model is run with different values of the parameter until the best correspondence appears to be achieved, to use of a quantitative mathematical algorithm. The most common algorithm used in optimization is the least-squares fit. To perform a least-squares optimization, the model is run to obtain a set of predictions at each of the times a data point was collected. The square of the difference between the model prediction and data point at each time is calculated

and the results for all of the data points are summed. The parameter being estimated is then modified, and the sum of squares is recalculated. This process is repeated until the smallest possible sum of squares is obtained, representing the best possible fit of the model to the data.

In a variation on this approach, the square of the difference at each point is divided by the square of the prediction. This variation, known as relative least squares, is preferable in the case of data with an error structure that can be described by a constant coefficient of variation (i.e., a constant ratio of the standard deviation to the mean). The former method, known as absolute least squares, is preferable in the case of data with a constant variance. From a practical viewpoint, the absolute least-squares method tends to give greater weight to the data at higher concentrations and results in fits that look best when plotted on a linear scale, while the relative least-squares method gives greater weight to the data at lower concentrations and results in fits that look best when plotted on a logarithmic scale.

A generalization of this weighting concept is provided by the extended least-squares method. In the extended least-squares algorithm, the heteroscedasticity parameter can be varied from 0 (for absolute weighting) to 2 (for relative weighting) or can be estimated from the data. In general, setting the heteroscedasticity parameter from knowledge of the error structure of the data is preferable to estimating it from a dataset.

A common example of identifying PBPK model parameters by fitting kinetic data is the estimation of tissue partition coefficients from experiments in which the concentration of compound in the blood and tissues is reported at various time points. Using an optimization approach, the predictions of the model for the time course in the blood and tissues could be optimized with respect to the data by varying the model's partition coefficients. There is little difference in the strength of the justification for estimating the partition coefficients in this way as opposed to estimating them directly from the data (by dividing the tissue concentrations by the simultaneous blood concentration). In fact, the direct estimates would probably be used as initial estimates in the model when the optimization was started.

A major difficulty in performing parameter optimization results from correlations between the parameters. When it is necessary to estimate parameters that are highly correlated, it is best to generate a contour plot of the objective function (sum of squares) or confidence region over a reasonable range of values of the two parameters [74].

Mass Balance Requirements One of the most important mathematical considerations during model design is the maintenance of mass balance. Simply put, the model should neither create nor destroy mass. This seemingly obvious principle is often violated unintentionally during the process of model development and parameterization. A common violation of mass balance, which typically leads to catastrophic results, involves failure to exactly match the arterial and venous blood flows in the model. As described previously, the movement of compound in the blood (in units of mass per time) is described as the product of the concentration of compound in the blood (in units of mass per volume) times the flow rate of the blood (in units of volume per time). Therefore, to maintain mass balance, the sum of the blood flows leaving any particular tissue compartment must equal the sum of the blood flows entering the compartment. In particular, to maintain mass balance in the blood

compartment (regardless of whether it's actually a compartment or just a steady-state equation), the sum of the venous flows from the individual tissue compartments must equal the total arterial blood flow leaving the heart:

$$\sum Q_T = Q_C$$

Another obvious but occasionally overlooked aspect of maintaining mass balance during model development is that if a model is modified by splitting a tissue out of a lumped compartment, the blood flow to the separated tissue (and its volume) must be subtracted from that for the lumped compartment. Moreover, even though a model may initially be designed with parameters that meet the above requirements, mass balance may unintentionally be violated later if the parameters are altered during model execution. For example, if the parameter for the blood flow to one compartment is increased, the parameter for the overall blood flow must be increased accordingly or an equivalent reduction must be made in the parameter for the blood flow to another compartment. Particular care must be taken in this regard when the model is subjected to sensitivity or uncertainty analysis; inadvertent violation of mass balance during Monte Carlo sampling can lead to erroneous sensitivity results [39].

A similar mass balance requirement must be met for transport other than blood flow. For example, if the compound is cleared by biliary excretion, the elimination of compound from the liver in the bile must exactly match the appearance of compound in the gut lumen in the bile. Put mathematically, the same term for the transport must appear in the equations for the two compartments, but with opposite signs (positive vs. negative). For example, the following equation could be used to describe a liver compartment with first-order metabolism and biliary clearance:

$$dA_L/dt = Q_L \cdot (C_A - C_L/P_L) - k_F \cdot C_L \cdot V_L/P_L - K_B \cdot C_L$$

where K_B is the biliary clearance rate (L/h). The equation for the intestinal lumen would then need to include the term: $+K_B \cdot C_L$.

As a model grows in complexity, it becomes increasingly difficult to assure its mass balance by inspection. Therefore, it is a worthwhile practice to check for mass balance by including an equation in the model that adds up the total amount of compound in each of the model compartments, including metabolized and excreted compound, for comparison with the administered or inhaled dose.

35.3.2 Numerical Solution of Model Equations

The previous sections have focused on the process of designing the PBPK model structure needed for a particular application. At this point the model consists of a number of mathematical equations: differential equations describing the mass balance for each of the compartments and algebraic equations describing other relationships between model variables. The next step in model development is the coding of the mathematical form of the model into a form that can be executed on a computer. There are many options available for performing this process, ranging from programming languages such as Fortran, C, and MatLab to more sophisticated simulation software packages such as acslXtreme and Berkeley Madonna.

Mathematically, a PBPK model is represented by a system of simultaneous ordinary differential equations. Each of the differential equations describes the mass balance for one of the "state variables" (compartments) in the model. There may also be additional differential equations to calculate other necessary model outputs, such as the area under the concentration curve (AUC) in a particular compartment, which is simply the integral of the concentration over time. The resulting system of equations is referred to as simultaneous because the time courses of the compound in the various compartments are so interdependent that solving the equations for any one of the compartments requires information on the current status of all the other compartments; that is, the equations for all of the compartments must be solved at the same time. This kind of mathematical problem, in which a system is defined by the conditions at time zero together with differential equations describing how it evolves over time, is known as an *initial value problem*, and matrix decomposition methods can be used to obtain the simultaneous solution.

A number of numerical algorithms are available for solving such problems. They all have in common that they are stepwise approximations; that is, they begin with the conditions at time zero and use the differential equations to predict how the system will change over a small time step, resulting in an estimate of the conditions at a slightly later time, which serves as the starting point for the next time step. This iterative process is repeated as long as necessary to simulate the experimental scenario.

The more sophisticated methods, such as the Gear algorithm (named after the mathematician David Gear, who developed it), use a predictor–corrector approach, in which the corrector step essentially amounts to "predicting backwards" after each step forward, in order to check how closely the algorithm is able to reproduce the conditions at the previous time step. This allows the time step to be increased automatically when the algorithm is performing well, and to be shortened when it is having difficulty, such as when conditions are changing rapidly. However, due to the wide variation of the time constants (response times) for the various physiological compartments (e.g., fat vs. richly perfused), PBPK models often represent "stiff" systems. Stiff systems are characterized by state variables (compartments) with widely different time constants, which cause difficulty for predictor–corrector algorithms. The Gear algorithm was specifically designed to overcome this difficulty. It is therefore generally recommended that the Gear algorithm (or an alternative stiff system solver such as the Rosenbrock method) be used for executing PBPK models.

Regardless of the specific algorithm selected, the essential nature of the solution will be a stepwise approximation. However, all of the algorithms made available in computer software are convergent; that is, they can stay arbitrarily close to the true solution, given a small enough time step. On modern personal computers, even large PBPK models can be run to more than adequate accuracy in a reasonable timeframe.

35.3.3 Model Evaluation

This section discusses various issues associated with the evaluation of a PBPK model. Once an initial model has been developed, it must be evaluated on the basis

of its conformance with experimental data. In some cases, the model may be exercised to predict conditions under which experimental data should be collected in order to verify or improve model performance. Comparison of the resulting data with the model predictions may suggest that revision of the model will be required. Similarly, a PBPK model designed for one compound or application may be adapted to another compound or application, requiring modification of the model structure and parameters. It is imperative that revision or modification of a model is conducted with the same level of rigor applied during initial model development, and that structures are not added to the model with no other justification than that they improve the agreement of the model with a particular dataset.

In addition to comparing model predictions to experimental data, model evaluation includes assessing the biological plausibility of the model structures and input parameters, and the resulting confidence that can be placed in extrapolations performed by the model [75]. Both elements of testing the model—kinetic validation and mechanistic validation—are necessary to provide confidence in the model. Unfortunately, there is a temptation to accept kinetic validation alone, particularly when data for mechanistic validation are unavailable. It should be remembered, however, that the simple act of adding equations and parameters to a model will, in itself, increase the flexibility of the model to fit data. Therefore, every attempt should be made to obtain additional experimental data to provide support for the mechanistic hypothesis underlying the model structure.

Model Documentation In cases where a model previously developed by one investigator is being evaluated for use in a different application by another investigator, adequate model documentation is critical for evaluation of the model. The documentation for a PBPK model should include sufficient information about the model so that an experienced modeler could accurately reproduce its structure and parameterization. Usually the suitable documentation of a model will require a combination of one or more "box and arrow" model diagrams together with any equations that cannot be unequivocally derived from the diagrams. Model diagrams should clearly differentiate blood flow from other transport (e.g., biliary excretion) or metabolism, and arrows should be used where the direction of transport could be ambiguous. All tissue compartments, metabolism pathways, routes of exposure, and routes of elimination should be clearly and accurately presented. All equations should be dimensionally consistent and in standard mathematical notation. Generic equations (e.g., for tissue "*i*") can help to keep the description brief but complete. The values used for all model parameters should be provided, with units. If any of the listed parameter values are based on allometric scaling, a footnote should provide the body weight used to obtain the allometric constant as well as the power of body weight used in the scaling.

35.3.4 Model Validation

Internal validation consists of the evaluation of the mathematical correctness of the model [34]. It is best accomplished on the actual model code but, if necessary, can be performed on appropriate documentation of the model structure and parameters, as described earlier (assuming, of course, that the actual model code accurately reflects the model documentation). A more important issue regards the provision

of evidence for external validation (sometimes referred to as verification). The level of detail incorporated into a model is necessarily a compromise between biological accuracy and parsimony. The process of evaluating the sufficiency of the model for its intended purpose, termed *model verification*, requires a demonstration of the ability of the model to predict the behavior of experimental data different from that on which it was based.

Whereas a simulation is intended simply to reproduce the behavior of a system, a model is intended to confirm a hypothesis concerning the nature of the system. Therefore, model validation should demonstrate the ability of the model to predict the behavior of the system under conditions that test the principal aspects of the underlying hypothetical structure. While quantitative tests of goodness of fit may often be a useful aspect of the verification process, the more important consideration may be the ability of the model to provide an accurate prediction of the general behavior of the data in the intended application.

Where only some aspects of the model can be verified, it is particularly important to assess the uncertainty associated with the aspects that are untested. For example, a model of a compound and its metabolites that is intended for use in cross-species extrapolation to humans would preferably be verified using data in different species, including humans, for both the parent compound and the metabolites. If only parent compound data is available in the human, the correspondence of metabolite predictions with data in several animal species could be used as a surrogate, but this deficiency should be carefully considered when applying the model to predict human metabolism. One of the values of biologically based modeling is the identification of specific data that would improve the quantitative prediction of toxicity in humans from animal experiments.

In some cases it is necessary to use all of the available data to support model development and parameterization. Unfortunately, this type of modeling can easily become a form of self-fulfilling prophecy: models are logically strongest when they fail, but psychologically most appealing when they succeed [33]. Under these conditions, model verification can be particularly difficult, putting an additional burden on the investigators to substantiate the trustworthiness of the model for its intended purpose. Nevertheless, a combined model development and verification can often be successfully performed, particularly for models intended for interpolation, integration, and comparison of data rather than for true extrapolation.

Parameter Verification In addition to verifying the performance of the model against experimental data, the model should be evaluated in terms of the plausibility of its parameters. This is particularly important in the case of PBPK models, where the parameters generally possess biological significance and can therefore be evaluated for plausibility independent of the context of the model. The source of each model input parameter value should be identified, whether it was obtained from prior literature, determined directly by experiment, or estimated by fitting a model output to experimental data. Parameter estimates derived independently of tissue time course or dose–response data are preferred. To the extent feasible, the degree of uncertainty regarding the parameter values should also be evaluated. The empirically derived *Law of Reciprocal Certainty* states that the more important the model parameter, the less certain will be its value. In accordance with this principle, the

most difficult, and typically most important, parameter determination for PBPK models is the characterization of the metabolism parameters.

When parameter estimation has been performed by optimizing model output to experimental data, the investigator must assure that the parameter is adequately identifiable from the data [34]. Due to the confounding effects of model error, overparameterization, and parameter correlation, it is quite possible for an optimization algorithm to obtain a better fit to a particular dataset by modifying a parameter that in fact should not be identified on the basis of that dataset. Also, when an automatic optimization routine is employed, it should be restarted with a variety of initial parameter values to assure that the routine has not stopped at a local optimum. These precautions are particularly important when more than one parameter is being estimated simultaneously, since the parameters in biologically based models are often highly correlated, making independent estimation difficult. Estimates of parameter variance obtained from automatic optimization routines should be viewed as lower bound estimates of true parameter uncertainty since only a local, linearized variance is typically calculated. In characterizing parameter uncertainty, it is probably more instructive to determine what ranges of parameter values are clearly inconsistent with the data than to accept a local, linearized variance estimate provided by the optimization algorithm.

It is usually necessary for the investigator to repeatedly vary the model parameters manually to obtain a sense of their identifiability and correlation under various experimental conditions, although some simulation languages include routines for calculating parameter sensitivity and covariance or for plotting confidence region contours. Sensitivity analysis and Monte Carlo uncertainty analysis techniques can serve as useful methods to estimate the impact of input parameter uncertainty on the uncertainty of model outputs. However, care should be taken to avoid violation of mass balance when parameters are varied by sensitivity or Monte Carlo algorithms, particularly where blood flows are affected.

Sensitivity Analysis To the extent that a particular PBPK model correctly reflects the physiological and biochemical processes underlying the pharmacokinetics of a compound, exercising the model can provide a means for identifying the most important physiological and biochemical parameters determining the PK behavior of the compound under different conditions [39]. The technique for obtaining this information is known as *sensitivity analysis* and can be performed by two different methods. Analytical sensitivity coefficients are defined as the ratio of the change in a model output to the change in a model parameter that produced it. To obtain a sensitivity coefficient by this method, the model is run for the exposure scenario of interest using the preferred values of the input parameters, and the resulting output (e.g., brain concentration) is recorded. The model is then run again with the value of one of the input parameters varied slightly. Typically, a 1% change is appropriate. The ratio of the resulting incremental change in the output to the change in the input represents the sensitivity coefficient. It is usually more convenient to use log-normalized sensitivity coefficients, which represent the ratio of the fractional change in output to the fractional change in input. For example, if a 1% increase in an input parameter resulted in a 0.5% decrease in the output, the log-normalized sensitivity coefficient would be –0.5. Log-normalized sensitivity coefficients >1.0 in absolute value represent amplification of input error and would be a cause for concern. An

alternative approach is to conduct a Monte Carlo analysis, as described below, and then to perform a simple correlation analysis of the model outputs and input parameters. This type of approach is often referred to as *global sensitivity analysis* [76]. Both methods have specific advantages. The analytical sensitivity coefficient most accurately represents the functional relationship of the output to the specific input under the conditions being modeled. The advantage of the global sensitivity analysis is that it also reflects the impact of interactions between the parameters during the Monte Carlo analysis.

Uncertainty and Variability Analysis Evaluations of the uncertainty and/or the variability associated with the predictions of a PBPK model are often performed using the Monte Carlo simulation approach [77, 78]. In a Monte Carlo simulation, a probability distribution for each of the PBPK model parameters is randomly sampled, and the model is run using the chosen set of parameter values. This process is repeated a large number of times until the probability distribution for the desired model output has been created. Generally, 1000 iterations or more may be required to ensure the reproducibility of the mean and standard deviation of the output distributions as well as the 1st through 99th percentiles. To the extent that the input parameter distributions adequately characterize the uncertainty in the inputs, and assuming that the parameters are reasonably independent, the resulting output distribution will provide a useful estimate of the uncertainty associated with the model outputs. If simulations are performed so that the probability distribution for PBPK model parameters represents the variability expected in the human population, then the Monte Carlo analysis will result in the simulation of pharmacokinetics expected for a population.

In performing a Monte Carlo analysis, it is important to distinguish uncertainty from variability. As it relates to the impact of pharmacokinetics in risk assessment, uncertainty can be defined as the possible error in estimating the "true" value of a parameter for a representative ("average") person. Variability, on the other hand, should only be considered to represent true interindividual differences. Understood in these terms, uncertainty is a defect (lack of certainty), which can typically be reduced by experimentation, and variability is a fact of life, which must be considered regardless of the risk assessment methodology used. An elegant approach for separately documenting the impact of uncertainty and variability is "two-dimensional" Monte Carlo, in which distributions for both uncertainty and variability are developed and multiple Monte Carlo runs are used to convolute the two aspects of overall uncertainty. Unfortunately, in practice, it is often difficult to differentiate the contribution of variability and uncertainty to the observed variation in the reported measurements of a particular parameter.

Due to its physiological structure, many of the parameters in a PBPK model are interdependent. For example, the blood flows must add up to the total cardiac output and the tissue volumes (including those not included in the model) must add up to the body weight. Failure to account for the impact of Monte Carlo sampling on these mass balances can produce erroneous results. In addition, some physiological parameters are naturally correlated, such as cardiac output and respiratory ventilation rate, and these correlations should be taken into account during the Monte Carlo analysis.

Although sophisticated methods of uncertainty analysis can provide valuable information, very simple techniques can also be used as a way to effectively communicate uncertainty. By simply determining the minimum and maximum values of an uncertain but important model parameter, and performing a simulation for a range of values, the impact of that parameter on PK predictions can be illustrated. When predicting human pharmacokinetics based on preclinical data, there is always uncertainty. Quantifying key uncertainties and providing a range of possible outcomes that could all be reasonable based on the current knowledge of the PK properties of the compound will allow for more informed decision-making.

Collection of Critical Data As with model development, the best approach to model evaluation is within the context of the scientific method. The most effective way to evaluate a PBPK model is to exercise the model to generate a quantitative hypothesis; that is, to predict the behavior of the system of interest under conditions "outside the envelope" of the data used to develop the model (at shorter/longer durations, higher/lower concentrations, different routes, different species, etc.). In particular, if there is an element of the model that remains in question, the model can be exercised to determine the experimental design under which the specific model element can best be tested. For example, if there is uncertainty regarding whether uptake into a particular tissue is flow or diffusion limited, alternative forms of the model can be used to compare predicted tissue concentration time courses under each of the limiting assumptions under various experimental conditions. The experimental design and sampling time that maximize the difference between the predicted tissue concentrations under the two assumptions can then serve as the basis for the actual experimental data collection. Once the critical data has been collected, the same model can also be used to support a more quantitative experimental inference. In the case of the tissue uptake question just described, not only can the *a priori* model predictions be compared with the observed data to test the alternative hypotheses, but the model can also be used *a posteriori* to estimate the quantitative extent of any observed diffusion limitation (i.e., to estimate the relevant model parameter by fitting the data). If, on the other hand, the model is unable to reproduce the experimental data under either assumption, it may be necessary to reevaluate other aspects of the model structure. The key difference between research and analysis is the iterative nature of the former. It has wisely been said, "If we knew when we started what we had to do to finish, they'd call it search, not research."

35.4 GENERIC PBPK MODELS

Despite the clear value of compound-specific PBPK models developed by scientists with experience in kinetic modeling and designed to address kinetic issues specific to that compound, there is also a need for simpler modeling techniques that can readily be applied across diverse compounds by an inexperienced user. The past ten years have seen tremendous advances in the capabilities of generic PBPK models that can simulate pharmacokinetics for humans or preclinical species based on a combination of physicochemical properties and *in vitro* data. The generic PBPK

model has recently become an increasingly important tool in assessing DMPK properties in preclinical development. Recent work has demonstrated the value of applying generic PBPK models in early preclinical development [14, 21, 22, 79].

35.4.1 User-Friendly Software Packages Bringing PBPK Modeling to the Nonexpert

The possible benefits from having PBPK software packages available for scientists who are nonmodelers have been a topic of interest for many years. Such a tool would need to meet many criteria to be broadly useful. This tool would need to be user-friendly, fast, flexible, and requiring little mathematical expertise from the user. The import of data into the tool and the export of results from the tool would need to be fast and automatable. The required input would be clearly defined and difficult to enter incorrectly, making consistent use by scientists of varying backgrounds possible. The tool would ideally be applicable through all stages of preclinical through clinical development. The pharmaceutical industry now has many tools that meet some or all of these criteria. Tools using physiology-based whole body models for the simulation of the PK behavior including absorption, distribution, and elimination include GastroPlus™ (Simulations Plus Inc., www.simulations-plus.com), Simcyp (Simcyp, www.simcyp.com), PK-Sim® (Bayer Technology Services, www.pksim.com), MEDICI-PK (AT Computing in Technology GnbH, www.cit-wulkow.de), and Cloe PK® (Cyprotex, www.cyprotex.com).

35.4.2 Recent Advances in Generic PBPK Modeling Tools

GastroPlus, which is well known in the pharmaceutical industry for its capabilities in predicting oral absorption in preclinical species based on the ACAT model, has recently expanded to include the capability of PBPK modeling. In the most recent version, GastroPlus includes a physiological intestinal model for humans in fed and fasted states as well as models for the rat, dog, cynomolgus monkey, and mouse. Several additional modules are available for parameter optimization, for combining the absorption model with physiological and compartmental PK models, and for PD models. The software also includes clinical trial simulation capabilities and a powerful method of performing sensitivity analysis. Although currently only PBPK modules for the rat and human are available, users can create PBPK models for other species themselves by creating input files with appropriate physiological parameters. The performance of GastroPlus to predict absorption was evaluated by Parrott and Lavé [80]. In this study, GastroPlus was compared to iDEA™, another software to predict absorption that is no longer commercially available.

Another tool for predicting human pharmacokinetics, Simcyp (Simcyp Limited, Sheffield, UK), was previously known as a DDI clinical trial simulator but has expanded to include PBPK modeling capabilities. Simcyp utilizes fundamental scaling procedures described by Houston [68] for the prediction of *in vivo* hepatic clearance (CL_H) from *in vitro* metabolism data. These *in vitro* metabolism data can be obtained from individual cytochrome P450s (CYP) in human-expressed recombinant systems. These are used for predicting behavior not only in average individuals but also in whole populations or in special subpopulations. In order to predict

drug–drug interactions involving CYP, Simcyp utilizes the relationship between the inhibitor concentration at the active site *in vivo* and the inhibition constant (K_i) determined *in vitro*. Competitive inhibition, induction, and/or mechanism-based inactivation mechanisms can be investigated within this software, according to the principles described by Ito et al. [71] and Tucker et al. [81]. Simcyp not only predicts the mean value but also simulates the extremes in the population by applying a Monte Carlo approach. This software comes with a database of physiological properties for specific populations and of PK information for specific drugs on the market (e.g., the CYP3A4 substrate midazolam, the CYP3A4 inducer rifampicin, and the CYP3A4 inducer and inhibitor ritonavir).

Yet another tool, PK-Sim, developed as a user-friendly tool for PBPK modeling, has PBPK models in the mouse, rat, dog, monkey, and human. In the model, tissue concentrations depend on the blood flow rate to the tissue, the rate of permeation into the tissue, active transport processes into and out of the tissue, and the rate of metabolism within a tissue. Although this detailed description allows significant flexibility and complexity, the user-friendly interface also allows for simple simulations whereby the more complex features are not utilized. In PK-Sim, the GI tract is described as a single tube with physiologically relevant dimensions and spatially varying properties such as pH and surface area. The software has Monte Carlo capabilities, and simulations examining the impact of interindividual variability can be performed using the population PK module. Physiological parameters for people from 0 to 80 years old are provided, allowing simulations of pharmacokinetics in the young and the elderly. Also, the software has the capability of linking PK to PD behavior with a PK/PD module.

In a fresh approach to PBPK modeling, the new software MEDICI-PK was developed using a novel software concept aimed at providing increased flexibility while maintaining user-friendliness. Instead of adopting the traditional approach whereby user-friendliness is made possible by adopting a static model, in MEDICI-PK the system of differential equations is generated automatically when starting a simulation. This software allows for predictions of parent compound and multiple metabolites, and interactions (metabolic and otherwise) between compounds [82]. MEDICI-PK has PBPK modeling capabilities for multiple species (e.g., the human, mouse, and dog) that can be extended by the user, and also contains PD modeling capabilities.

Cloe-PK is a commercial tool aimed at prediction of human pharmacokinetics at the earliest stages of drug discovery [83]. The PBPK model includes 14 organs and tissues, clearance by metabolism and renal excretion, and diffusion-limited uptake in tissues. In each of the organ compartments, the capillary, intracellular, and extracellular spaces are explicitly included. Using *in vitro* and *in silico* data as input, this software can predict human IV and oral *AUC* from clinical trial data within 2-fold and 3.75-fold, respectively (www.cyprotex.com/products/pk_howwell.htm). Studies on the accuracy of the model for predicting PK behavior in the rat and human have been published [21, 22] and illustrate the utility of this software for predicting pharmacokinetics and ranking compounds based on minimal data and *in silico* parameters.

These software packages are exceptionally useful tools, and we expect them to be increasingly used in the pharmaceutical industry. However, their implementation may require a modeling and simulation expert to determine appropriate

applications and methods of use and to perform validation exercises to convince the scientists involved with the preclinical development of drugs that the packages do indeed work. Additionally, in-house PBPK expertise and models will still be necessary because these standard tools do not allow the flexibility to simulate every situation that will arise. For example, currently some generic PBPK tools do not yet have the capability to simulate exposures to a parent compound and a metabolite, which could be of interest for simulating the pharmacokinetics of prodrugs or investigating possible PK interactions between the parent and metabolite. Also, generic PBPK software packages have sophisticated capabilities that may require an expert modeler to determine appropriate ways to use (and not misuse) the features (e.g., GastroPlus has the capability of simulating enterohepatic cycling, and PK-Sim can incorporate saturable and nonsaturable metabolism in multiple tissue compartments). In addition, the availability of such tools simplifies the technical use of PBPK models; however, a good understanding of the models and underlying equations is still mandatory in order to guarantee good interpretation of output.

35.5 INTEGRATING PRECLINICAL DATA USING THE PBPK MODEL

Here, we provide examples of how PBPK modeling is a valuable tool in several stages of drug development. During the lead identification (LI) and lead optimization (LO) stages, limited data is available. During the clinical candidate selection, more data is available. Finally, a rich dataset is available prior to entry into humans. The availability of data and issues that arise at each stage dictate the utility of PBPK modeling.

35.5.1 Preclinical Data Useful for PBPK Modeling

Much of the data typically generated in the preclinical development process used to characterize key aspects of ADME can be used in PBPK model development (Table 35.1). The first information generated includes *in silico* parameters (e.g., polar surface area, pK_a, and log P values are calculated). Metabolic stability studies (e.g., in microsomes or hepatocytes) are often considered critical to determine if hepatic metabolism is a major route of elimination and if first-pass metabolism might result in unacceptably low bioavailability [84, 85]. Screens for permeability and solubility are often implemented early in the process. Plasma protein binding might be measured to determine if a compound will have a sufficient free concentration for therapeutic efficacy [86]. The blood-to-plasma ratio, BPR, might be measured to provide a rational basis for the appropriate biological fluid for assay (e.g., blood or plasma) and to aid in interpreting PK data [42]. Also, screens specific to a disease area might be implemented. For example, a P-glycoprotein (P-gp) screen might be used to determine if a compound will be able to penetrate the central nervous system.

Single-dose pharmacokinetic (SDPK) studies in a rodent species might be performed to determine if a compound has drug-like PK properties and adequate bioavailability. Later studies might include SDPK studies in a nonrodent species. Hepatocyte or microsomal clearance data can be scaled to estimate the *in vivo* metabolic clearance in preclinical species and humans [70, 87]. The scaled clearance

in preclinical species can be compared to clearance in SDPK studies to determine if hepatic metabolism is a major route of elimination in preclinical species. If the clearance seen in SDPK studies is higher than the clearance scaled from hepatocyte or microsome data, urine and/or bile might be collected in SDPK studies to provide additional information on mechanisms of clearance.

These studies provide pharmaceutical scientists with qualitative information on the potential human PK behavior of a compound. Using PBPK modeling, the results of the various preclinical assays can be integrated to provide a quantitative prediction of human pharmacokinetics [88]. During preclinical development, DMPK data are constantly being generated. Therefore, the human PK projection will change as more information becomes available. A PBPK model can act as a repository of current information and is easily updated when new PK or PD data becomes available. An important feature of PBPK models is that they can be used to determine the key data that should be generated.

35.5.2 Lead Identification and Optimization Stages

Drug discovery is increasingly "data rich" with high throughput chemistry generating numerous compounds that are rapidly screened for pharmacological and PK properties. Determination of *in vivo* pharmacokinetics is considerably more costly and slower than *in vitro* screening, and so there is interest in optimizing resources by using simulation to prioritize compounds. Physiologically based pharmacokinetics can be used at this stage to prioritize compounds prior to *in vivo* experimentation—getting an estimate of the expected PK profile of new drug candidates in humans and providing some mechanistic understanding of the compound's properties and of the relevance of the assays used in the screening strategy.

Because of the mechanistic basis of PBPK models, when they do not adequately describe animal PK data, this means that a biological phenomenon affecting pharmacokinetics has not been included in the model and is not represented by the assays used to screen the compounds. Therefore, if a PK issue for a promising compound becomes apparent, PBPK modeling allows you to determine which mechanisms are consistent with the observed data. This information can be used to guide further experimentation to arrive more rapidly at the desired information. Understanding pharmacokinetics in preclinical species using PBPK modeling can also provide a scientific basis for determining which preclinical species are most relevant to humans, thereby improving the scientific rationale of the selected screening strategy.

The emerging technology of generic PBPK modeling has been shown in recent studies to have potential as a valuable tool for assessing the pharmacokinetics of compounds in the early stages of drug development. For example, recent papers reported studies on applying generic PBPK modeling to predict rat pharmacokinetics [21] and human pharmacokinetics [22] following IV administration of test compound. These studies were conducted to evaluate the commercial PBPK modeling package Cloe PK [83]. The PBPK model included 14 organs and tissues, clearance by metabolism and renal excretion, and diffusion-limited uptake in tissues. For these rat and human models, model input included molecular weight, octanol/water partitioning, octanol/water distribution coefficient at a pH of 7.4, hepatic intrinsic metabolic clearance, and the unbound fraction in plasma. Model development involved

the use of a training dataset consisting of 82 compounds for the rat model and 69 compounds for the human model. After the models were developed, they were tested using data from test datasets consisting of 134 compounds in the rat and 18 compounds in the human. Using this approach to rank compounds and select the 25% most likely to have the best exposure (i.e., AUC) resulted in 61% of the best compounds being selected, which is a 2.4-fold improvement over random selection [21]. Brightman et al. [22] concluded that "the generic PBPK model is potentially a powerful and cost-effective tool for predicting the mammalian pharmacokinetics of a wide range of organic compounds, from readily available *in vitro* inputs only."

In a similar study, Parrott et al. [79] studied applying generic PBPK modeling to predict rat pharmacokinetics following IV or PO administration of test compound. This rat PBPK model included 11 tissue compartments and clearance by metabolism in the liver; uptake in tissues was assumed to be perfusion limited. GastroPlus was used to simulate oral absorption. For this model, the necessary input included structure-based predictions of lipophilicity, ionization, and protein binding, intrinsic clearance based on rat hepatocyte data, experimentally measured aqueous solubility, and artificial membrane permeability. To improve the prediction of AUC following oral administration of compounds, particularly for compounds with $\log P > 4$, it was necessary to use solubility in simulated intestinal fluid since aqueous solubility apparently underestimates *in vivo* solubility for highly lipophilic compounds. Parrott et al. [79] noted that "overall, this evaluation shows that generic simulation may be applicable for typical drug-like compounds to predict differences in PK parameters of more than twofold based upon minimal measured input data." The authors recommend that, for applying the method for new series of compounds outside the range of the training dataset, the model be verified for several compounds before it is generally applied.

35.5.3 Clinical Candidate Selection

PBPK modeling has a great potential to assist clinical candidate selection where numerous factors must be considered and data related to the pharmacokinetics and pharmacodynamics of a compound needs to be combined and compared in a rational way. This potential was illustrated by Parrott et al. [14], who demonstrated the use of PBPK modeling to select the best compound from among five candidates for the clinical lead. The preclinical data for the five candidates was integrated and the efficacious human doses and associated internal exposures were estimated. For this calculation, the PBPK models were linked to an E_{max} PD model so that the dose resulting in a 90% effect could be identified. This example showed that the PBPK approach facilitates a sound decision on the selection of the optimal molecule to be progressed by integrating the available information and focusing the attention onto the expected properties in human. Importantly, the method can include estimates of variability and uncertainty in the predictions to verify that decisions are based on significant differences between the compounds.

35.5.4 Supporting Entry into Humans

After a clinical candidate has been selected, the first-in-human (FIH) dose must be selected. There are many ways of selecting the FIH dose. For example, in therapeutic

areas other than oncology, FIH dose estimates can be determined by multiplying the no-observed-adverse-effect-level (NOAEL) from preclinical toxicology studies by a safety factor, by using human data for a similar compound when they are available, or by using a PK model based on preclinical data to determine the dose that will result in a systemic exposure identified as therapeutic based on preclinical pharmacology data [89]. When this last approach is adopted, it is often referred to as performing a human PK extrapolation.

The first step of the human PK extrapolation is to identify the internal measure of exposure (e.g., the C_{min}, C_{max}, or AUC) believed to be efficacious in humans based on pharmacology data. Next, a human PK model for IV exposures is developed based on all preclinical data. This PK model can be developed in many ways, including PBPK modeling [13]. The oral exposure route is added to the human IV PK model. Again, there are many ways to model oral absorption, for example, by using an empirical first-order oral absorption rate constant or using the physiological ACAT model. Finally, once the model is developed, the dose that will result in the therapeutic exposure is determined. The estimated efficacious dose and other information (e.g., the C_{min}, C_{max}, AUC(0–24 h), CL, V_{ss}, $t_{1/2}$) are reported. PK projections can be based on a single or repeated (e.g., steady-state) exposure. At this stage it is important to understand the uncertainty of the FIH dose estimate.

Uncertainty can be illustrated by presenting a range of results (e.g., dose, AUC) from different models, or a range of results for different values of a key parameter that is not known with great certainty. If uncertainty is too great, additional experiments can be designed to aid in narrowing the possible values of key parameters. If uncertainty is extensive and cannot be reduced with additional experimentation, it is perhaps better to simply state that uncertainty is too great to predict human pharmacokinetics than to report a human PK projection that is not likely to be correct. PBPK modeling can be used as a tool to understand the quantitative impact of uncertainty from key knowledge gaps and also helps to minimize uncertainty due to species differences in PK properties.

In its best form, the human PK extrapolation is an integration of all preclinical data (e.g., *in vivo* data for the rodent and nonrodent, and *in vitro* data in the corresponding preclinical species as well as human) to provide a scientifically defensible estimate (extrapolation) of the likely pharmacokinetics of a compound in humans. Luttringer et al. [90] recently examined the ability of PBPK modeling to predict human pharmacokinetics based on preclinical species, using epiroprim as a test compound due to significant species differences in its PK properties. By incorporating information on species differences in PK properties from *in vitro* studies (e.g., in protein binding, the blood-to-plasma ratio, and intrinsic clearance in hepatocytes), PBPK modeling was able to reduce the uncertainty inherent in interspecies extrapolation and to provide a better prediction of human pharmacokinetics than allometric scaling or by direct scaling of hepatocyte data.

Recently, Jones et al. [13] reported similar results in a comparison between empirical and physiologically based approaches for the human PK extrapolation. Human pharmacokinetics of 19 compounds that had entered into humans was predicted using Dedrick plot analysis and PBPK modeling. A strategy for predicting human pharmacokinetics by focusing on methods for understanding the effects of absorption, distribution, and elimination from a physiological perspective was

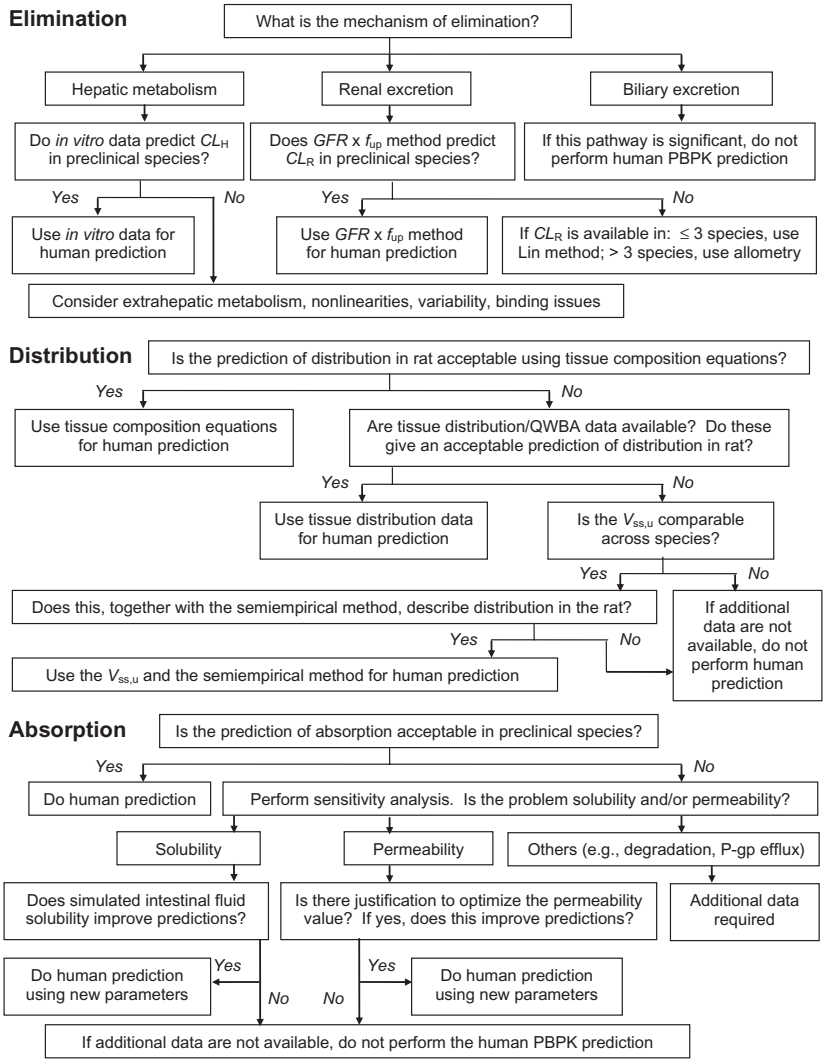


FIGURE 35.4 A strategy for applying PBPK modeling to predict human pharmacokinetics prior to FIH. CL_H, hepatic clearance; CL_R, renal clearance; f_{up}, unbound fraction in plasma; *GFR*, glomerular filtration rate; QWBA, quantitative whole-body autoradiography; $V_{ss,u}$, steady-state volume of distribution of unbound drug. (Adapted from Ref. 13.)

developed (Fig. 35.4). The ability of PBPK modeling to predict pharmacokinetics in preclinical species was tested, and the human pharmacokinetics was only predicted if the model could predict pharmacokinetics in preclinical species. Based on this criterion, for 70% of the 19 compounds included in the study, a human PK prediction could be made. Jones et al. [13] noted: "The prediction accuracy for these compounds in terms of the percentage of compounds with an average-fold error of <2-fold was 83%, 50%, 75%, 67%, 92% and 100% for apparent oral clearance (CL/F), apparent volume of distribution during terminal phase after oral administration

(V-z/F), terminal elimination half-life (t1/2), peak plasma concentration (C-max), area under the plasma concentration-time curve (AUC) and time to reach C-max (t(max)), respectively." Simulated plasma concentrations and PK parameters were compared with human data so that the accuracy of the prediction methods could be assessed. The human PK data were more accurately predicted by the PBPK modeling approach than by the empirical approach. Using the strategy proposed by Jones et al. [13], the model development guides the strategy for gathering the data necessary for a complete understanding of likely human PK behavior.

Poor predictions with PBPK models are often a result of incomplete knowledge resulting in processes not correctly incorporated into the model (e.g., for biliary clearance and enterohepatic recirculation there are limited options for quantitatively predicting the effects on human pharmacokinetics). For such situations, an alternative method of performing the human PK extrapolation (e.g., allometric scaling) might seem attractive. However, allometric scaling is based on the assumption that clearance is proportional to $BW^{0.75}$ and that steady-state volume of distribution is proportional to BW^{1} due to physiological properties (i.e., the same physiological properties that are incorporated in PBPK models). If PBPK modeling does not appear to be a good method for a compound, there is no reason to believe that allometric scaling or other empirical methods will work either. Additionally, developing methods for including increasingly complex PK mechanisms (e.g., first-pass metabolism and transporters in the gut, EH cycling, biliary excretion, and multiple pathways of elimination) is an active area of research, and methods for predicting human pharmacokinetics even with PK complications will soon be possible.

35.6 EXAMPLES OF THE USE OF PBPK MODELING IN DRUG DEVELOPMENT

In this section, two examples are provided of successful PBPK models for drugs that have been developed in the past: methotrexate (a cancer therapeutic) and all-*trans*-retinoic acid (a cancer therapeutic and skin treatment). Two areas in which PBPK modeling will become increasingly important in the future are then discussed: evaluation of PK variability and modeling of pharmacodynamics.

35.6.1 Methotrexate

The PBPK model for methotrexate (MTX) provides an excellent example of the iterative nature of the process of developing a PBPK model for a drug. The stated rationale for the approach used was "basing the model, as much as possible, on established, independently verifiable, physiological concepts" [5]. For the initial model development [91], a single IV dose of 3 mg/kg, which falls in the range of clinical treatment levels, was evaluated in CDF-1 male mice. Key observations regarding the behavior of the kinetic data included an unusually large initial drop in the plasma MTX concentration, indicating rapid uptake, tissue localization, and excretion (MTX is not metabolized extensively in mice). A subsequent asymptotic leveling of the concentration curves for all tissues was taken as evidence for zero-order uptake of MTX from the gut. A rapid early increase in the concentration of

MTX in the small intestine, with a peak gut lumen:plasma concentration ratio of about 100, demonstrated the importance of enterohepatic recycling.

Based on these observations, an initial MTX model was developed that included five compartments: plasma, muscle, liver, kidneys, and GI tract tissue/lumen [91]. The authors also derived reduced model structures with three compartments (plasma/body, liver, gut lumen) or two compartments (plasma/body plus gut lumen) to expedite solution of the associated system of equations. Flow-limited transport was assumed in all versions of the model, except as described below. The model incorporated a time-delay term to account for bile transport and holding time. Biliary clearance rates were estimated by bile duct cannulation experiments. To account for GI travel time and fecal excretion delays, time-delay functions were also applied in the gut lumen. Renal clearance was determined by comparison of the integrated plasma concentration data with cumulative urinary excretion data. Plasma protein binding was estimated at 25%. Comparison of experimental data and model predictions showed good agreement in general, although the model overpredicted gut lumen concentrations for times less than 60 minutes, probably due to the simple time-delay description of biliary transport.

In order to refine their initial model, Bischoff et al. [5] studied a variety of dose levels of MTX in several species, including humans. The additional data reproduced the initial data's features of (1) a rapid drop in MTX plasma concentrations and a corresponding increase in gut lumen concentrations, indicating the importance of tissue uptake and biliary secretion; (2) a peak gut lumen:plasma ratio of approximately 100; and (3) linear binding of MTX in tissues as plasma concentrations increased above 0.1 μg/mL, indicating nonlinear binding at low concentrations. The authors speculated that this phenomenon was probably due to strong binding to dihydrofolate reductase.

A revised PBPK model (Fig. 35.2) was developed to describe the more extensive data. Renal clearance of MTX was determined by comparing the time integral of plasma concentration with cumulative urine formation after intraperitoneal (IP) or IV administration. Tissue:plasma equilibrium ratios were derived from constant infusion experiments and/or the portion of the IV pulse injection curve after initial redistribution. Constant tissue:plasma equilibrium ratios at high concentrations indicated linear binding, while at lower concentrations, equilibrium ratios were represented by the sum of linear nonspecific binding and strong binding (presumed to be associated with dihydrofolate reductase).

An important feature of the revised model was its use of multicompartment submodels for biliary secretion and GI transport (Fig. 35.2). The original model used a mathematical time-delay (step function) to simulate bile formation and secretion from the liver. The abrupt introduction of bile into the GI tract lumen at the delay time caused the model to overshoot the data in this time period. In the revised model, biliary secretion was represented by a three-compartment submodel in which a series of discrete compartments was able to produce a smoother "S-shaped" bile concentration efflux curve.

MTX transit through the GI tract was modeled using an approach similar to that used for biliary secretion. Due to the tubular flow nature of the gut lumen, an assumption of uniform mixing would not predict the correct time course for concentrations appearing in the feces. Therefore, the GI tract was divided into four distinct regions with the feces exiting from the last compartment. An assumption of

zero-order absorption from the GI tract that was adequate for the single-dose level described in the initial modeling was not adequate for the wider range of dose levels investigated in the follow-up study. The revised model therefore provided for both saturable and nonsaturable GI tract absorption. In the absence of detailed data indicating otherwise, absorption characteristics were assumed to be the same for all regions, but specific location-dependent absorption characteristics could be included using this approach.

Comparison of model predictions and experimental data demonstrated that a single model structure was able to describe MTX distribution and excretion reasonably well for the mouse, rat, dog, and human, using species-specific parameters. The greatest uncertainty in the model was in the kinetics describing intestinal absorption. The authors concluded that GI tract absorption was not readily saturable, and both saturable and nonsaturable absorption should be included in the model. Based on the observed kinetic behavior at very low doses, the authors concluded that strong, saturable nonlinear binding occurred in the liver and kidney, probably related to binding with dihydrofolate reductase.

35.6.2 All-*trans*-Retinoic Acid

A PBPK model for all-*trans*-retinoic acid (ATRA; tretinoin) was developed in order to provide a coherent description of the absorption, distribution, metabolism, and excretion of the compound and its metabolites across species and routes of administration [19]. The goal of developing such a model was to provide a more biologically relevent dose measure than administered dose for assessing the human teratogenic risk from ATRA.

The PBPK model developed for ATRA provided a full physiological description for ATRA, with compartments for plasma, liver, gut, intestinal lumen, fat, skin, richly perfused tissues, slowly perfused tissues, placenta, and embryo (Fig. 35.3). Both oxidation (to the 4-oxo derivative) and glucuronidation of ATRA were described with saturable kinetics. Conversion to the 13-*cis* isomer (13-*cis*-RA; isotretinoin) and the subsequent metabolism of that compound were also included (not shown). Simpler compartmental descriptions were used for the metabolites, since there was no evidence that they preferentially partitioned into any of the body tissues. A third metabolic pathway, side chain oxidation producing CO_2, was also included. Oral uptake was described by zero-order stomach emptying and first-order uptake from the intestinal lumen. Dermal uptake was described by a two-compartment model, with compartments representing the stratum corneum and viable epidermis. Distribution was assumed to be flow limited except for dermal uptake and transplacental transfer, which were assumed to be diffusion limited. Excretions into urine and feces were modeled as first-order processes, with all chemicals being excreted in the feces and only glucuronides being excreted in the urine. Enterohepatic recirculation of ATRA and its metabolites was also described.

The physiological parameters for adult animals were obtained from Brown et al. [30]. Gestational parameters were based on previous modeling of rats [92, 93]. Partition coefficients were based on distribution studies with mice [94] and with a human placenta [95]. The ATRA volume of distribution calculated using these partitions, 1.1 L/kg, agrees with measured values. Biliary excretion was adjusted on the basis of data from rats with exteriorized bile ducts [96, 97]. The metabolic

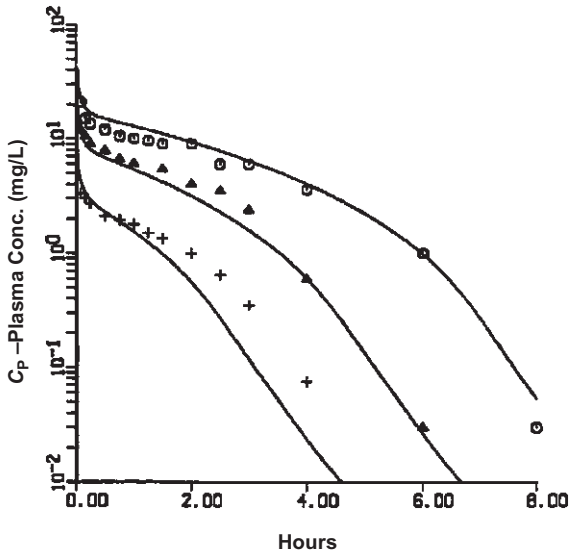


FIGURE 35.5 Simulation of plasma concentration of all-*trans*-retinoic acid in the plasma of nonhuman primates following intravenous (IV) dosing at 5, 2.5, and 1 mg/kg.

parameters were adjusted using data for IV administration of ATRA in rats [97] and monkeys [98], as well as from metabolite measurements [96, 99]. A key difference in the metabolism of ATRA across species is the predominance of the oxidative pathway in the rodent [96, 97], in contrast with the predominance of the glucuronide pathway in the primate [99].

The PBPK model for IV dosing of ATRA in the monkey (Fig. 35.5) was scaled allometrically to predict the kinetics for oral dosing of human leukemia patients with 1.1 mg/kg ATRA [100]. The only parameters adjusted in this extrapolation were those describing the rate of oral uptake. All other parameters were calculated from those for the monkey. The resulting model provided an excellent description of the kinetics for humans with oral dosing (Fig. 35.6). It was also able to reproduce the observed kinetics for total radioactivity following topical administration of ATRA (Fig. 35.7). In contrast to the kinetic data, which could only provide an estimate of total exposure to ATRA plus its metabolites, the PBPK model was able to provide separate estimates of internal exposure to ATRA and its active and inactive metabolites. An important result of the modeling was to demonstrate that the low dose rate associated with dermal exposure results in high efficiency clearance of ATRA to its inactive glucuronide metabolites, as opposed to oral dosing, where the higher dose rate leads to a greater proportion of active oxidative metabolites.

The model was used to simulate oral clinical dosing with ATRA, as well as minimal teratogenic doses of ATRA in the primate and rodent. Based on literature data on the teratogenic potential of the various chemical species, the most appropriate dose surrogate could be either C_{max} or AUC for the total concentration of active retinoids (ATRA + 4-oxo-ATRA + 13-*cis*-RA + 4-oxo-13-*cis*-RA). The glucuronides are not included in this dose measure since they do not cross the placenta. On

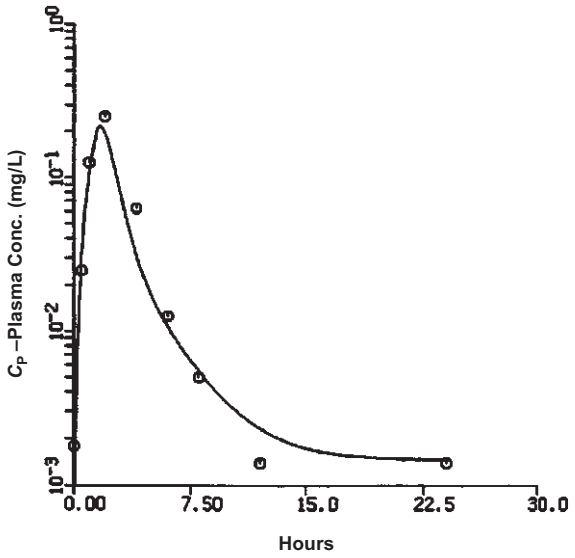


FIGURE 35.6 Simulation of all-*trans*-retinoic acid concentration in plasma of human subject receiving an oral dose of 1.1 mg/kg.

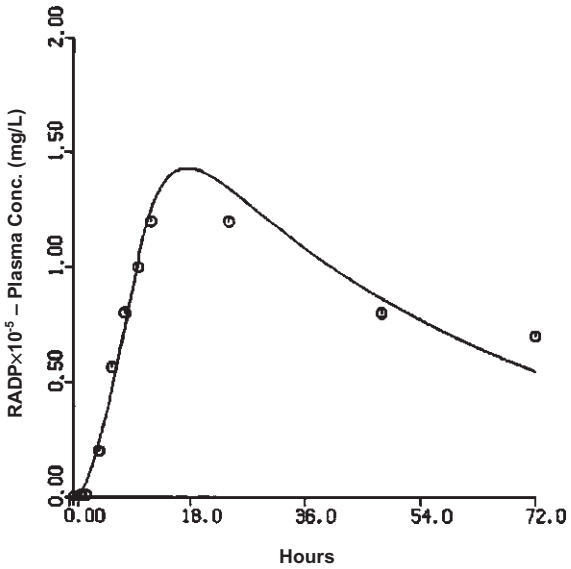


FIGURE 35.7 Simulation of total radiation in plasma following topical treatment of human subject with 50 micrograms of all-*trans*-retinoic acid.

the other hand, based on activity at retinoic acid receptors it could be argued that the most appropriate dose surrogate could be the peak concentration or area under the curve for ATRA alone. In either case, maternal plasma levels were used as a surrogate for fetal levels, based on evidence from animal studies that concentrations achieved in maternal and fetal plasma are similar. The calculated

TABLE 35.4 Comparison of Dose Surrogates for Retinoic Acid Teratogenicity

			All-*trans*-Retinoic Acid		Total Active Retinoids		Total Retinoids
	Route	Dose (mg/kg)	C_{max} (ng/mL)	AUC (ng·h/mL)	C_{max} (ng/mL)	AUC (ng·h/mL)	C_{max} (ng·eq/mL)
Minimal teratogenic doses (all-*trans*-RA)							
Mouse	Oral	4.0	1,048	1,852	2,681	12,658	3,107
Rat	Oral	2.5	943	2,029	1,918	13,554	2,051
Monkey	Oral	5.0	1,830	3,714	2,294	5,962	4,983
Clinical doses (human)							
ATRA	Oral	1.1	218	695	264	1,088	1,237
13-*Cis*	Oral	1.1	654[a]	3,154[a]	1,033	7,103	1,148

[a]Reflects concentration of 13-*cis*-RA rather than all-*trans*-RA.

dose surrogates, as well as the estimated peak plasma level for total retinoids (which includes the glucuronides), for several species are shown in Table 35.4.

One test of a useful dose surrogate is that similar values should be calculated at similar effect levels across species. For a minimal teratogenic effect, all of the dose surrogates in Table 35.4 (including administered dose) are within a factor of 2–3 across species. The most consistent dose surrogate is the C_{max} for total active retinoids, which is essentially constant across species. Based on this dose measure, the internal exposure of patients receiving oral ATRA treatment for cancer is below the threshold for teratogenic effects by about a factor of 7–10. However, this comparison assumes that the maternal plasma concentration profile is representative of fetal exposure. If one takes into consideration the longer period of organogenesis in the human (around 35 days) as compared to the rodent (around 10 days) and assumes, as a worst case, fetal exposure at the maximum maternal concentration throughout the entire period, the margin of safety could be as low as 2–3. It is of interest that the kinetics of 13-*cis*-RA in the human are considerably different from those of ATRA. 13-*cis*-RA has a much longer half-life than ATRA in the human and oxidation, rather than glucuronidation, is the dominant form of metabolism. The calculated plasma concentrations and AUC values for total active retinoids following oral treatment with 13-*cis*-RA are in the same range as those causing teratogenic effects in animals. This result is consistent with the observation of teratogenic effects associated with the human use of 13-*cis*-RA (isotretinoin, Table 35.4). This PBPK model was used by the FDA in its evaluation of the safety of a topical skin treatment containing ATRA.

35.6.3 Future Directions

Interindividual Variability Because of the heterogeneity of the human population, it is generally expected that there will be a broad range of responses to the biological effects of drugs. This heterogeneity is produced by interindividual variations in physiology, biochemistry, and molecular biology, reflecting both genetic and environmental factors, and results in differences among individuals in the biologically effective tissue dose associated with a given administered dose

(pharmacokinetics) as well as in the response to a given tissue dose (pharmacodynamics). Often it is possible to distinguish specific classes of individuals, such as infants or the elderly, who appear to be more susceptible to a specific effect. PBPK modeling provides the capability to quantitatively describe the potential impact of PK factors on the variability of individual response. Because the parameters in a PBPK model have a direct biological correspondence, they provide a useful framework for determining the impact of observed variations in physiological and biochemical factors on the population variability in dosimetry.

For example, PBPK models can be used to determine the impact of differences in key metabolism enzymes, whether due to multiple genotypic expression, such as polymorphisms, or just due to normal variation in enzyme activities within the general population. Other potential modulators of sensitivity that can be addressed quantitatively with a PBPK model include physical condition, level of activity, disease states, age, hormonal status, and interactions with other chemicals and drugs. In each case, the PBPK model provides a quantitative structure for determining the effect of these various factors on the relationship between the administered dose and the internal (biologically effective) target tissue exposure. When coupled with Monte Carlo analysis, the PBPK model provides a method to assess the quantitative impact of these sources of variability on individual response (as opposed to average population response) by comparing model predicted internal doses over the distribution of individual parameter values.

It is useful to consider the total variability among humans in terms of three contributing sources: (1) the variation across a population of "normal" individuals at the same age (e.g., young adults); (2) the variation across the population resulting from their different ages (e.g., infants or the elderly); and (3) the variation resulting from the existence of subpopulations that differ in some way from the "normal" population (e.g., due to genetic polymorphisms). A fourth source of variability, health status, should also be considered. To the extent that the variation in physiological and biochemical parameters across these population dimensions can be elucidated, PBPK models can be used together with Monte Carlo methods to integrate their effects on the *in vivo* kinetics of a compound and predict the resulting impact on the distribution of responses (as represented by target tissue doses) across the population.

There has sometimes been a tendency in drug development to use information on the variability of a specific parameter, such as the *in vitro* activity of a particular enzyme, as the basis for expectations regarding the variability in dosimetry for *in vivo* exposures. However, whether or not the variation in a particular physiological or biochemical parameter will have a significant impact on *in vivo* dosimetry is a complex function of interacting factors. In particular, the structures of physiological and biochemical systems frequently involve parallel processes (e.g., blood flows, metabolic pathways, excretion processes), leading to compensation for the variation in a single factor. Moreover, physiological constraints may limit the *in vivo* impact of variability observed *in vitro*. For instance, high affinity intrinsic clearance can result in essentially complete metabolism of all the compound reaching the liver in the blood; under these conditions, variability in amount metabolized *in vivo* would be more a function of variability in liver blood flow than variability in metabolism *in vitro*. Thus, it is often true that the whole (the *in vivo* variability in dosimetry) is less than the sum of its parts (the variability in each of the PK factors).

The overall PK variability across a population is a function of many compound-specific, genetic, and physiological factors. Due to the complex interactions among these factors, speculation regarding the extent of population variability on the basis of the observed variation in a single factor can be highly misleading. Analysis using PBPK modeling and Monte Carlo techniques provides a more reliable approach for estimating population PK variability. PBPK modeling can also be useful in a more qualitative sense, to determine whether there is reason for concern regarding a particular age-group that might be more sensitive due to PK differences. Similar analyses can be performed to determine whether exposure during special life stages, such as gestation or lactation, represents a significant concern.

Modeling of Pharmacodynamics The growing popularity of the PBPK modeling approach represents a movement from simpler kinetic models toward more biologically realistic descriptions of the determinants that regulate disposition of drugs in the body. To a large extent, the application of these PBPK models to study the time courses of compounds in the body is simply an integrated systems approach to understanding the biological processes that regulate the delivery of drugs to target sites. Many PBPK models integrate information across multiple levels of organization, especially when describing interactions of compounds with molecular targets, such as reversible binding of ligands to specific receptors, as in the case of methotrexate binding to dihydrofolate reductase [5, 101]. In such cases, the PBPK models integrate molecular, cellular, organ level, and organism-level processes to account for the time courses of compounds, metabolites, and bound complexes within organs and tissues in the body. The system under scrutiny in PBPK models is more the integrated physiological system, appropriate enough for a discipline defined as physiologically based modeling.

The main goal of PBPK models is quite simple—to predict the target tissue dose of compounds and their metabolites at target tissues and, in some cases, to describe interactions in target tissues. PBPK models once developed are extensible. They can be used to extrapolate to various other conditions because of their biological fidelity. While the goal in applying these models is to predict dosimetry, it is important to remember that the overall goal of using PBPK modeling in efficacy and safety assessment with drugs is broader than simply estimating tissue dose, regardless of the level of detail provided in the interactions of compounds with tissue constituents. The goal in the larger context is to understand the relationship between dose delivered to target tissues and the biological sequelae of the exposure of target tissues to compounds. The specific steps that lead from these dose metrics to tissue, organ, and organism-level responses have usually been considered part of the pharmacodynamic (PD) process. In general, PD models used in drug evaluation have been more empirical, utilizing simple effect compartments correlated with blood or tissue concentrations of active compound. Another inexorable development will be expansion of the systems approaches into the PBPD arena. This latter area will represent a systems biology approach for describing perturbations of biological systems by compounds and the exposure/dose conditions under which these perturbations become sufficiently large to pose significant health risks or sufficiently large to achieve specific therapeutic outcomes.

The systems biology approach (Fig. 35.8) focuses on normal biological function and the perturbations associated with exposure to compounds. Perturbations of

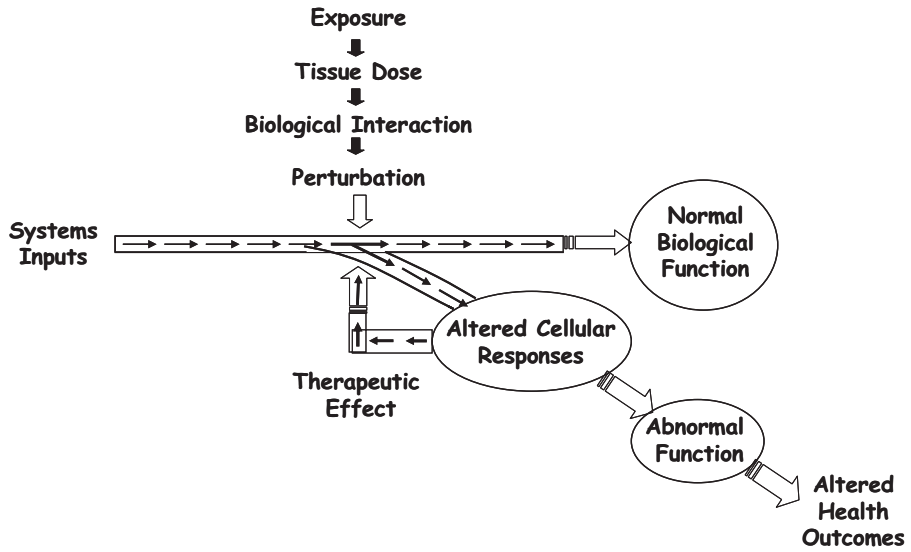


FIGURE 35.8 Diagram of the approach for understanding the pharmacological and toxicological effects of compounds in terms of their interaction with the biological system. The horizontal axis represents the biological component of the interaction, and the vertical axis represents the chemical component. Drugs can both restore altered biological function (efficacy) and produce altered function (toxicity).

biological processes by compounds lead to either adverse responses (toxicity) or restoration of normal function to a compromised tissue (efficacy). The effects of compounds, whether for good or ill, can best be described by PBPK approaches linked through PBPD models of responses of cellular signaling networks. Toxicity and efficacy are then defined by an intersection of compound action with the biological system. Toxicology and pharmacology are disciplines at the interface of chemistry/pharmacokinetics (primarily embedded in the vertical component) and biology/pharmacodynamics (primarily captured by the horizontal chain). Clearly, the main differences in the next generation of systems approaches in PK and PD modeling will be the increasingly detailed descriptions of biology afforded by new technologies and the expansion of modeling tools available for describing the effects of compounds on biological signaling processes.

35.7 CONCLUSIONS AND FUTURE PERSPECTIVES

It is ironic that PBPK modeling of drugs now appears to lag behind modeling of environmental contaminants [102], since the concept of PBPK modeling was first described in the context of drug disposition, in the seminal work of Teorell [1, 2]. In the pharmaceutical industry, noncompartmental "model-free" PK analyses are the standard practice, despite the fact that these methods are useful only for summarizing the characteristics of a dataset (e.g., volume of distribution, mean retention time, terminal half-life) and do not provide the advantages inherent in PBPK modeling

(hypothesis testing, prediction, etc.). Their principal advantages are that they are rapid and inexpensive to perform.

However, in recent years there has been increasing pressure on the pharmaceutical industry to accelerate the drug development process, and PBPK modeling has repeatedly been identified as one of the technologies that could prove useful to this end [12, 102–104]. Because the collection of ADME data on a drug is a required element of drug development, much of the data necessary for developing a PBPK model is often available. The PBPK model offers the opportunity to make better use of these data, by serving as a structured repository for quantitative information on the compound, a conceptual framework for hypothesis testing, and a quantitative platform for prediction.

The rapid development of computational chemistry [105], genomics [106], and high throughput screening [107] has brought increasing attention to the discovery phase of drug development, including growing interest in "discovery toxicology" [108]. PBPK modeling can play a complementary role to two other technologies that are finding increasing use in drug discovery: QSAR analysis and genomics. QSAR can be used to estimate compound-specific parameters for the PBPK model, while genomic data can provide mode of action insights that drive model structure decisions. In this scenario, the PBPK model provides a quantitative biological framework for integrating the physicochemical characteristics of the drug candidate, together with *in vitro* data on its ADME and toxicity, within the constraints of the fundamental physiological and biochemical processes governing compound behavior *in vivo*. This approach is particularly effective when used consistently during drug development, because the information gained from modeling of previous candidate compounds can greatly facilitate model development for new compounds with similar structures or properties.

As the drug development process proceeds, the model can be iteratively informed and refined on the basis of the data being collected, and in turn the model can serve as a platform for *in silico* hypothesis testing and experimental design. As the model becomes more robust, it can also be employed for extrapolation (e.g., selection of first human dose) and for simulation (e.g., Monte Carlo analysis for design of clinical trials). The physiological structure of the PBPK model makes it a perfect platform for conducting evaluations of alternative dosing methods and regimens, and for investigating the impact of genetic-, age-, and disease-related differences in physiology and metabolism on drug kinetics. Of particular importance, by using a PBPK model the pharmacodynamic effects of a drug can be investigated more directly, relating the effects to the concentration in the tissue (e.g., the brain) where the compound interacts with the biological system, rather than attempting to elucidate a potentially indirect relationship with a concentration in the central (e.g., plasma) compartment. By obtaining quantitative information on the dose–responses for both the efficacy and toxicity of the compound, the PBPK model can be exercised to evaluate the potential to increase the efficacy/toxicity ratio of the drug through manipulation of dose rate and dose route using novel drug delivery systems. These and other attributes of PBPK models for organizing and interpreting diverse datasets, with the specific goals of understanding efficacy and toxicity, are reviving interest in applying these tools in drug development and evaluation [109–113]. The availability of increasingly sophisticated tools that can make predictions even with

early preclinical data will encourage increasing application of PBPK modeling in preclinical development.

ACKNOWLEDGMENTS

The authors thank Dr. Carl Brown, Dr. Werner Rubas, and Dr. Phil Worboys for reviewing the manuscript for this chapter and providing valuable discussion and insight.

REFERENCES

1. Teorell T. Kinetics of distribution of substances administered to the body. I. The extravascular mode of administration. *Arch Int Pharmacodyn* 1937;57:205–225.
2. Teorell T. Kinetics of distribution of substances administered to the body. I. The intravascular mode of administration. *Arch Int Pharmacodyn* 1937;57:226–240.
3. Andersen ME. Saturable metabolism and its relation to toxicity. *Crit Rev Toxicol* 1981;9:105–150.
4. Bischoff KB, Brown RG. Drug distribution in mammals. *Chem Eng Prog Symp Ser* 1966;62(66):33–45.
5. Bischoff KB, Dedrick RL, Zaharko DS, Longstreth JA. Methotrexate pharmacokinetics. *J Pharm Sci* 1971;60:1128–1133.
6. Collins JM, Dedrick RL, Flessner MF, Guarino AM. Concentration dependent disappearance of fluorouracil from peritoneal fluid in the rat: experimental observations and distributed modeling. *J Pharm Sci* 1982;71:735–738.
7. Farris FF, Dedrick RL, King FG. Cisplatin pharmacokinetics: applications of a physiological model. *Toxicol Lett* 1988;43:117–137.
8. Andersen ME, Yang RSH, Clewell HJ, Reddy MB. Introduction: a historical perspective of the development and application of PBPK models. In Reddy MB, Yang RSH, Clewell HJ III, Andersen ME, Eds. *Physiologically Based Pharmacokinetic Modeling: Science and Applications*. Hoboken, NJ: John Wiley & Sons; 2005, pp 1–18.
9. McMullin TS. Drugs. In Reddy MB, Yang RSH, Clewell HJ III, Andersen ME, Eds. *Physiologically Based Pharmacokinetic Modeling: Science and Applications*. Hoboken, NJ: John Wiley & Sons; 2005, pp 273–296.
10. Pott O'Brien W. Antineoplastic agents. In Reddy MB, Yates RSH, Clewell HJ III, Andersen ME, Eds. *Physiologically Based Pharmacokinetic Modeling: Science and Applications*. Hoboken, NJ: John Wiley & Sons; 2005, pp 297–317.
11. Lupfert C, Reichel A. Development and application of physiologically based pharmacokinetic-modeling tools to support drug discovery. *Chem Biodiversity* 2005;2:1462–1486.
12. Nestorov I. Whole body pharmacokinetic models. *Clin Pharmacokinet* 2003;42:883–908.
13. Jones HM, Parrott N, Jorga K, Lave T. A novel strategy for physiologically based predictions of human pharmacokinetics. *Clin Pharmacokinet* 2006;45:511–542.
14. Parrott N, Jones H, Paquereau N, Lavé T. Application of full physiological models for pharmaceutical drug candidate selection and extrapolation of pharmacokinetics to man. *Basic Clin Pharmacol Toxicol* 2005;96:193–199.

15. Baxter LT, Zhu H, Mackensen DG, Jain RK. Physiologically-based pharmacokinetic model for specific and nonspecific monoclonal-antibodies and fragments in normal-tissues and human tumor xenografts in nude-mice. *Cancer Res* 1994;54:1517–1528.
16. Baxter LT, Zhu H, Mackensen DG, Butler WF, Jain RK. Biodistribution of monoclonal-antibodies—scale-up from mouse to human using a physiologically-based pharmacokinetic model. *Cancer Res* 1995;55:4611–4622.
17. Aarons L. Editors' view. Physiologically based pharmacokinetic modeling: a sound mechanistic basis is needed. *Br J Clin Pharm* 2005;60(6):581–583.
18. Dedrick RL, Bischoff KB. Species similarities in pharmacokinetics. *Fed Proc* 1980; 39:54–59.
19. Clewell HJ, Andersen ME, Wills RJ, Latriano L. A physiologically based pharmacokinetic model for retinoic acid and its metabolites. *J Am Acad Dermatol* 1997;36: S77–S85.
20. Reddy MB, Yang RSH, Clewell HJ III, Andersen ME, Eds. *Physiologically Based Pharmacokinetic Modeling: Science and Applications*. Hoboken, NJ: John Wiley & Sons; 2005.
21. Brightman FA, Leahy DE, Searle GE, Thomas S. Application of a generic physiologically based pharmacokinetic model to the estimation of xenobiotic levels in rat plasma. *Drug Metab Dispos* 2006;34:84–93.
22. Brightman FA, Leahy DE, Searle GE, Thomas S. Application of a generic physiologically based pharmacokinetic model to the estimation of xenobiotic levels in human plasma. *Drug Metab Dispos* 2006;34:94–101.
23. Malaty LI, Kuper JJ. Drug interactions of HIV. Protease inhibitors. *Drug Safety* 1999;20:147–169.
24. Adolph EF. Quantitative relations in the physiological constitutions of mammals. *Science* 1949;109:579–585.
25. Dedrick RL. Animal scale-up. *J Pharmacokinet Biopharm* 1973;1:435–461.
26. Astrand P, Rodahl K. *Textbook of Work Physiology*. New York: McGraw-Hill; 1970, pp 157–160, 206–211.
27. International Commission on Radiological Protection (ICRP). Report of the Task Group on Reference Man. ICRP Publication 23; 1975, pp 228–237, 280–285, 325–327.
28. Environmental Protection Agency (EPA). Reference physiological parameters in pharmacokinetic modeling. EPA/600/6–88/004. Washington, DC: Office of Health and Environmental Assessment; 1988.
29. Davies B, Morris T. Physiological parameters in laboratory animals and humans. *Pharm Res* 1993;10:1093–1095.
30. Brown RP, Delp MD, Lindstedt SL, Rhomberg LR, Beliles RP. Physiological parameter values for physiologically based pharmacokinetic models. *Toxicol Indust Health* 1997;13(4):407–484.
31. Jepson GW, Hoover DK, Black RK, McCafferty JD, Mahle DA, Gearhart JM. A partition coefficient determination method for nonvolatile chemicals in biological tissues. *Fundam Appl Toxicol* 1994;22:519–524.
32. Clewell HJ. Coupling of computer modeling with *in vitro* methodologies to reduce animal usage in toxicity testing. *Toxicol Lett* 1993;68:101–117.
33. Yates FE. Good manners in good modeling: mathematical models and computer simulations of physiological systems. *Am J Physiol* 1978;234:R159–R160.
34. Carson ER, Cobelli C, Finkelstein L. *The Mathematical Modeling of Metabolic and Endocrine Systems. Model Formulation, Identification, and Validation*. Hoboken, NJ: John Wiley & Sons; 1983, pp 23–45, 113–127, 217–231.

35. Rescigno A, Beck JS. Perspectives in pharmacokinetics. The use and abuse of models. *J Pharmacokinet Biopharm* 1987;15(3):327–344.

36. Himmelstein KJ, Lutz RJ. A review of the application of physiologically based pharmacokinetic modeling. *J Pharmacokinet Biopharm* 1979;7:127–145.

37. Gerlowski LE, Jain RK. Physiologically based pharmacokinetic modeling: principles and applications. *J Pharm Sci* 1983;72:1103–1126.

38. Nestorov IA, Aarons LJ, Arundel PA, Rowland M. Lumping of whole-body physiologically based pharmacokinetic models. *J Pharmacokinet Biopharm* 1998;26(1):21–46.

39. Clewell HJ, Lee T, Carpenter RL. Sensitivity of physiologically based pharmacokinetic models to variation in model parameters: methylene chloride. *Risk Anal* 1994;14: 521–531.

40. Campain J. Metals and inorganic compounds. In Reddy MB, Yang RSH, Clewell HJ III, Andersen ME, Eds. *Physiologically Based Pharmacokinetic Modeling: Science and Applications*. Hoboken, NJ: John Wiley & Sons; 2005, pp 239–270.

41. Lin JH. Applications and limitations of interspecies scaling and *in vitro* extrapolation in pharmacokinetics. *Drug Metab Dispos* 1998;26:1202–1212.

42. Hinderling PH. Red blood cells: a neglected compartment in pharmacokinetics and pharmacodynamics. *Pharmacol Rev* 1997;49:279–295.

43. Andersen ME, Clewell HJ, Gargas ML, Smith FA, Reitz RH. Physiologically-based pharmacokinetics and the risk assessment for methylene chloride. *Toxicol Appl Pharmacol* 1987;87:185–205.

44. Agoram B, Woltosz WS, Bolger MB. Predicting the impact of physiological and biochemical processes on oral drug bioavailability. *Adv Drug Deliv Rev* 2001;50(Suppl 1): S41–S67.

45. Willmann S, Schmitt W, Keldenich J, Dressman JB. A physiologic model for simulating gastrointestinal flow and drug absorption in rats. *Pharm Res* 2003;20:1766–1771.

46. Semino G, Lilly P, Andersen ME. A pharmacokinetic model describing pulsatile uptake of orally-administered carbon tetrachloride. *Toxicology* 1997;117(1):25–33.

47. Chaturvedi PR, Decker CJ, Odinecs A. Prediction of pharmacokinetic properties using experimental approaches during early drug discovery. *Curr Opin Chem Biol* 2001;5(4): 452–463.

48. Cai H, Stoner C, Reddy A, Freiwald S, Smith D, Winters R, Stankovic C, Surendran N. Evaluation of an integrated *in vitro–in silico* PBPK (physiologically based pharmacokinetic) model to provide estimates of human bioavailability. *Int J Pharm* 2006;308(1–2): 133–139.

49. Dennison JE, Andersen ME. Reactive vapors in the nasal cavity. In Reddy MB, Yang RSH, Clewell HJ III, Andersen ME, Eds. *Physiologically Based Pharmacokinetic Modeling: Science and Applications*. Hoboken, NJ: John Wiley & Sons; 2005, pp 375–387.

50. Reddy MB. PBPK modeling approaches for special applications: dermal exposure models. In Reddy MB, Yang RSH, Clewell HJ III, Andersen ME, Eds. *Physiologically Based Pharmacokinetic Modeling: Science and Applications*. Hoboken, NJ: John Wiley & Sons; 2005, pp 375–387.

51. McCarley KD, Bunge AL. Pharmacokinetic models of dermal absorption. *J Pharm Sci* 2001;90(11):1699–1719.

52. Roberts MS, Anissimov YG, Gonsalvez RA. Mathematical models in percutaneous absorption (Reprinted from *Percutaneous Adsorption* 1999;3–55). *J Toxicol-Cutaneous Ocular Toxicol* 2001;20:221–270.

53. Andersen ME, Mills JJ, Gargas ML, Kedderis L, Birnbaum LS, Neubert D, Greenlee WF. Modeling receptor-mediated processes with dioxin: implications for pharmacokinetics and risk assessment. *Risk Anal* 1993;13(1):25–36.
54. Kohn MC, Lucier GW, Clark GC, Sewall C, Tritscher AM, Portier CJ. A mechanistic model of effects of dioxin on gene expression in the rat liver. *Toxicol Appl Pharmacol* 1993;120(1):138–154.
55. Plowchalk DR, Teeguarden J. Development of a physiologically based pharmacokinetic model for estradiol in rats and humans: a biologically motivated quantitative framework for evaluating responses to estradiol and other endocrine-active compounds. *Toxicol Sci* 2002;69(1):60–78.
56. Mendel CM. The free hormone hypothesis: distinction from the free hormone transport hypothesis. *J Androl* 1992;13(2):107–116.
57. Lam G, Chen M, Chiou WL. Determination of tissue to blood partition coefficients in physiologically-based pharmacokinetic studies. *J Pharm Sci* 1982;71(4):454–456.
58. Lin JH, Sugiyama Y, Awazu S, Hanano M. *In vitro* and *in vivo* evaluation of the tissue-to-blood partition coefficients for physiological pharmacokinetic models. *J Pharmacokinet Biopharm* 1982;10(6):637–647.
59. Pelekis M, Poulin P, Krishnan K. An approach for incorporating tissue composition data into physiologically based pharmacokinetic models. *Toxicol Ind Health* 1995;11: 511–522.
60. Poulin P, Krishnan K. A biologically-based algorithm for predicting human tissue—blood partition coefficients of organic chemicals. *Hum Exp Toxicol* 1995;14:273–280.
61. Poulin P, Krishnan K. An algorithm for predicting tissue:blood partition coefficients of organic chemicals from *n*-octanol:water partition coefficient data. *J Toxicol Environ Health* 1995;46:117–129.
62. Poulin P, Theil FP. *A priori* prediction of tissue:plasma partition coefficients of drugs to facilitate the use of physiologically-based pharmacokinetic models in drug discovery. *J Pharm Sci* 2000;89:16–35.
63. Poulin P, Theil F. Prediction of pharmacokinetics prior to *in vivo* studies. 1. Mechanism-based prediction of volume of distribution. *J Pharm Sci* 2002;91:129–156.
64. Rodgers T, Leahy D, Rowland M. Physiologically based pharmacokinetic modeling 1: Predicting the tissue distribution of moderate-to-strong bases. *J Pharm Sci* 2005;94: 1259–1276.
65. Rodgers T, Rowland M. Physiologically based pharmacokinetic modelling 2: Predicting the tissue distribution of acids, very weak bases, neutrals and zwitterions. *J Pharm Sci* 2006;95:1238–1257.
66. Zuegge J, Schneider G, Coassolo P, Lavé T. Prediction of hepatic metabolic clearance—comparison and assessment of prediction models. *Clin Pharmacokinet* 2001;40:553–563.
67. Lavé T, Coassolo P, Reigner B. Prediction of hepatic metabolic clearance based on interspecies allometric scaling techniques and *in vitro in vivo* correlations. *Clin Pharmacokinet* 1999;36:211–231.
68. Houston JB. Relevance of *in-vitro* kinetic-parameters to *in-vivo* metabolism of xenobiotics. *Toxicol In Vitro* 1994;8:507–512.
69. Houston JB, Carlile DJ. Prediction of hepatic clearance from microsomes, hepatocytes, and liver slices. *Drug Metab Rev* 1997;29:891–922.
70. Obach RS. Prediction of human clearance of twenty-nine drugs from hepatic microsomal intrinsic clearance data: an examination of *in vitro* half-life approach and nonspecific binding to microsomes. *Drug Metab Dispos* 1999;27:1350–1359.

71. Ito K, Iwatsubo T, Kanamitsu S, Nakajima Y, Sugiyama Y. Quantitative prediction of *in vivo* drug clearance and drug interactions from *in vitro* data on metabolism, together with binding and transport. *Annu Rev Pharmacol Toxicol* 1998;38:461–499.
72. Barter ZE, Bayliss MK, Beaune PH, Boobis AR, Carlile DJ, Edwards RJ, Houston JB, Lake BG, Lipscomb JC, Pelkonen OR, Tucker GT, Rostami-Hodjegan A. Scaling factors for the extrapolation of *in vivo* metabolic drug clearance from *in vitro* data: reaching a consensus on values of human microsomal protein and hepatocellularity per gram of liver. *Curr Drug Metab* 2007;8:33–45.
73. Reddy MB, Andersen ME, Morrow PE, Dobrev ID, Varaprath S, Plotzke KP, Utell MJ. Physiological modeling of inhalation kinetics of octamethylcyclotetrasiloxane in humans during rest and exercise. *Toxicol Sci* 2003;72:3–18.
74. Blau GE, Neely WB. Dealing with uncertainty in pharmacokinetic models using SIMUSOLV. In *Drinking Water and Health*, Vol. 8. Washington, DC: National Research Council; 1987, pp 185–207.
75. Cobelli C, Carson ER, Finkelstein L, Leaning MS. Validation of simple and complex models in physiology and medicine. *Am J Physiol* 1984;246:R259–R266.
76. Gueorguieva I, Nestorov IA, Rowland M. Reducing whole body physiologically based pharmacokinetic models using global sensitivity analysis: diazepam case study. *J Pharmacokinet Pharmacodyn* 2006;33(1):1–27.
77. Clewell HJ. The use of physiologically based pharmacokinetic modeling in risk assessment: a case study with methylene chloride. In Olin S, Farland W, Park C, Rhomberg R, Scheuplein L, Starr T, Wilson J, Eds. *Low-Dose Extrapolation of Cancer Risks: Issues and Perspectives*. Washington, DC: ILSI Press; 1995.
78. Clewell HJ, Andersen ME. Use of physiologically-based pharmacokinetic modeling to investigate individual versus population risk. *Toxicology* 1996;111:315–329.
79. Parrott N, Paquereau N, Coassolo P, Lavé T. An evaluation of the utility of physiologically based models of pharmacokinetics in early drug discovery. *J Pharm Sci* 2005;94: 2327–2343.
80. Parrott N, Lavé T. Prediction of intestinal absorption: comparative assessment of GASTROPLUS (TM) and IDEA (TM). *Eur J Pharm Sci* 2002;17:51–61.
81. Tucker GT, Houston JB, Huang SM. Optimizing drug development: strategies to assess drug metabolism/transporter interaction potential—toward a consensus. *Pharm Res* 2001;18:1071–1080.
82. Telgmann R, von Kleist M, Huisinga W. Software supported modelling in pharmacokinetics. *CompLife* 2006;216–225.
83. Leahy DE. Integrating *in vitro* ADMET data through generic physiologically based pharmacokinetic models. *Expert Opin Drug Metab Toxicol* 2006;2:619–628.
84. Lavé T, Dupin S, Schmitt C, Valles B, Ubeaud G, Chou RC, Jaeck D, Coassolo P. The use of human hepatocytes to select compounds based on their expected hepatic extraction ratios in humans. *Pharm Res* 1997;14:152–155.
85. Thompson TN. Early ADME in support of drug discovery: the role of metabolic stability studies. *Curr Drug Metab* 2000;1:215–241.
86. Poggesi I. Predicting human pharmacokinetics from preclinical data. *Curr Opin Drug Discov Dev* 2004;7:100–111.
87. Riley RJ, McGinnity DF, Austin RP. A unified model for predicting human hepatic, metabolic clearance from *in vitro* intrinsic clearance data in hepatocytes and microsomes. *Drug Metab Dispos* 2005;33:1304–1311.
88. Poulin P, Theil FP. Prediction of pharmacokinetics prior to *in vivo* studies. II. Generic physiologically based pharmacokinetic models of drug disposition. *J Pharm Sci* 2002;91:1358–1370.

89. Reigner BG, Blesch KS. Estimating the starting dose for entry into humans: principles and practice. *Eur J Clin Pharmacol* 2002;57:835–845.
90. Luttringer O, Theil F-P, Poulin P, Schmitt-Hoffmann AH, Guentert TW, Lavé T. Physiologically based pharmacokinetic (PBPK) modeling of disposition of epiroprim in humans. *J Pharm Sci* 2003;92:1990–2007.
91. Bischoff KB, Dedrick RL, Zaharko DS. Preliminary model for methotrexate pharmacokinetics. *J Pharm Sci* 1970;59:149–154.
92. Fisher JW, Whittaker TA, Taylor DH, Clewell H III, Andersen ME. Physiologically based pharmacokinetic modeling of the pregnant rat: a multiroute exposure model for trichloroethylene and its metabolite, trichloroacetic acid. *Toxicol Appl Pharmacol* 1989;99: 395–414.
93. O'Flaherty EJ, Scott W, Schreiner C, Beliles RP. A physiologically based kinetic model of rat and mouse gestation: disposition of a weak acid. *Toxicol Appl Pharmacol* 1992;112:245–256.
94. Kalin JR, Starling ME, Hill DL. Disposition of all-*trans*-retinoic acid in mice following oral doses. *Drug Metab Dispos* 1981;9:196–201.
95. Asai M, Faber W, Neth L, di Sant'Agnese PA, Nakanishi M, Miller RK. Human placental transport and metabolism of all-*trans*-retinoic acid *in vitro*. *Placenta* 1991;12: 367–368.
96. Zile MH, Inhorn RC, DeLuca HF. Metabolites of all-*trans*-retinoic acid in bile: identification of all-*trans*- and 13-*cis*-retinoyl glucuronides. *J Biol Chem* 1982;257:3537–3543.
97. Swanson BN, Frolik CA, Zaharevitz DW, Roller PP, Sporn MB. Dose-dependent kinetics of all-*trans*-retinoic acid in rats. Plasma levels and excretion into bile, urine, and faeces. *Biochem Pharmacol* 1981;30:107–113.
98. Adamson PC, Balis FM, Smith MA, Murphy RF, Godwin KA, Poplack DG. Dose-dependent pharmacokinetics of all-*trans*-retinoic acid. *JNCI* 1992;84:1332–1335.
99. Kraft JC, Slikker W Jr, Bailey JR, Roberts LG, Fischer B, Wittfoht W, Nau H. Plasma pharmacokinetic and metabolism of 13-*cis*- and all-*trans*-retinoic acid in the cynomolgus monkey and the identification of 13-*cis*- and all-*trans*-retinoyl–glucuronides. *Drug Metab Dispos* 1991;19:317–324.
100. Muindi JRF, Frankel SR, Huselton C, DeGrazia F, Garland WA, Young CW, Warrell RP Jr. Clinical pharmacology of oral all-*trans* retinoic acid in patients with acute promyelocytic leukemia. *Cancer Res* 1992;52:2138–2142.
101. Dedrick RL. Pharmacokinetic and pharmacodynamic considerations for chronic hemodialysis. *Kidney Int* 1975;7(Suppl 2):S7–S15.
102. Rowland M, Balant L, Peck C. Physiologically based pharmacokinetics in drug development and regulatory science: a workshop report (Georgetown University, Washington, DC, 29–30, May 2002). *AAPS PharmSci* 2004;6(1):E6.
103. Peck CC, Barr WH, Benet LZ, Collins J, Desjardins RE, Furst DE, et al. Opportunities for integration of pharmacokinetics, pharmacodynamics, and toxicokinetics in rational drug development. *J Pharm Sci* 1992;81(6):605–610.
104. Charnick SB, Kawai R, Nedelman JR, Lemaire M, Niederberger W, Sato H. Perspectives in pharmacokinetics. Physiologically based pharmacokinetic modeling as a tool for drug development. *J Pharmacokinet Biopharm* 1995;23:217–229.
105. Jorgensen WL. The many roles of computation in drug discovery. *Science* 2004;303(5665): 1813–1818.
106. Ricke DO, Wang S, Cai R, Cohen D. Genomic approaches to drug discovery. *Curr Opin Chem Biol* 2006;10(4):303–308.

107. Lahoz A, Gombau L, Donato MT, Castell JV, Gomez-Lechon MJ. *In vitro* ADME medium/high-throughput screening in drug preclinical development. *Mini Rev Med Chem* 2006;6(9):1053–1062.

108. van de Waterbeemd H, Gifford E. ADMET *in silico* modelling: towards prediction paradise? *Nat Rev Drug Discov* 2003;2(3):192–204.

109. Blesch KS, Gieschke R, Tsukamoto Y, Reigner BG, Burger HU, Steimer JL. Clinical pharmacokinetic/pharmacodynamic and physiologically based pharmacokinetic modeling in new drug development: the capecitabine experience. *Invest New Drugs* 2003; 21(2):195–223.

110. Lin JH, Lu AYH. Role of pharmacokinetics and metabolism in drug discovery and development. *Pharmacol Rev* 1997;49:403–449.

111. Lin J, Sahakian DC, de Morais SMF, Xu JJ, Polzer RJ, Winter SM. The role of absorption, distribution, metabolism, excretion and toxicity in drug discovery. *Curr Top Med Chem* 2003;3:1125–1154.

112. Poulin P, Schoenlein K, Theil FP. Prediction of adipose tissue:plasma partition coefficients for structurally unrelated drugs. *J Pharm Sci* 2001;90:436–447.

113. Theil FP, Guentert TW, Haddad S, Poulin P. Utility of physiologically based pharmacokinetic models to drug development and rational drug discovery candidate selection. *Toxicol Lett* 2003;138:29–49.

36

MATHEMATICAL MODELING AS A NEW APPROACH FOR IMPROVING THE EFFICACY/TOXICITY PROFILE OF DRUGS: THE THROMBOCYTOPENIA CASE STUDY

ZVIA AGUR,[1,2] MORAN ELISHMERENI,[1] YURI KOGAN,[1] YURI KHEIFETZ,[1] IRIT ZIV,[2] MEIR SHOHAM,[2] AND VLADIMIR VAINSTEIN[1,2]

[1]*Institute for Medical Biomathematics (IMBM), Bene-Ataroth, Israel*
[2]*Optimata Ltd., Ramat-Gan, Israel*

Contents

36.1 Introduction
- 36.1.1 Biomathematics and Its Use for Rationalizing Drug Treatment Strategies: A Short History
- 36.1.2 Aims of This Chapter

36.2 Thrombopoiesis
- 36.2.1 Biology
- 36.2.2 Mathematical Modeling

36.3 Thrombocytopenia
- 36.3.1 Pathophysiology
- 36.3.2 Current Therapy
- 36.3.3 Novel Cytokine Therapy

Preclinical Development Handbook: ADME and Biopharmaceutical Properties, edited by Shayne Cox Gad
Copyright © 2008 John Wiley & Sons, Inc.

36.4 Modeling Drug Effects on Thrombopoiesis
36.4.1 Toxicity Modeling: Interleukin-11 (IL-11)
36.4.2 Efficacy Modeling: Thrombopoietin (TPO)
36.4.3 Modeling Combination Therapy: Chemotherapy and TPO Support
36.5 Using the Validated Model for Predicting Improved Drug Efficacy/Toxicity Profile
36.5.1 Model Validation by Retrospective Human Study Results: IL-11 and TPO
36.5.2 Model Validation in Prospective Animal Trials: TPO Applied to the Virtual Mouse and Virtual Monkey
36.5.3 Predicting the Optimal TPO Efficacy/Toxicity Ratio in Monkeys
36.6 Using the Thrombopoiesis Model for Predicting an Unknown Animal Toxicity Mechanism
36.7 Transition to Phase I
36.8 Conclusion
References

36.1 INTRODUCTION

Despite recent innovations, many life-threatening diseases still lack effective treatments. In March 2004, the U.S. Food and Drug Administration (FDA) agency issued a major report that identifies both the problems and the potential solutions for bringing more breakthroughs in medical science to patients, as quickly and efficiently as possible. The report looks at the development processes for drugs, biologics, and medical devices and calls for a joint effort of industry, academic researchers, product developers, patient groups, and the FDA to identify key problems and to develop solutions: "A new product development toolkit—containing powerful new scientific and technical methods such as computer-based predictive models . . . is urgently needed to improve predictability and efficiency along the critical path from laboratory concept to commercial product" [1]. The role of the present chapter is to demonstrate how the science of biomathematics can be harnessed for improving the solution of safety issues in the critical path of drug development, in general, and in the transition from the preclinical phases to Phase I, in particular.

36.1.1 Biomathematics and Its Use for Rationalizing Drug Treatment Strategies: A Short History

A new synthesis of ecology and "hard" biology, called biomathematics, emerged in the second half of the 20th century in the scientific community. Its role was to rationalize complex biological processes. Thus, in contrast to experimental biologists, who work at the microscopic cellular level and develop analytical tools that are analogous to the still camera in photography, biomathematicians develop formulae, which effectively animate these shots, allowing us to understand the dynamics of the complex process we are investigating. Biomathematics has enabled the development of a range of new theories dealing with significant problems of disease progression and control, hitherto beyond the reach of "snapshot", experimental biology.

But in spite of these efforts, until recently the biomedical research community was unanimous in viewing biological systems as too complex to enable accurate retrieval by mathematical models. This declarable mistrust in the power of biomathematics left the biomedical sciences lagging behind other sciences, as an immature sequel of experimental observations. In recent years, the somewhat disillusioned postgenomic era has rediscovered biological complexity, renaming it "system biology." It seems that, finally, biomathematicians are becoming legitimate and almost beloved children of the scientific community.

In the 1980s, notions from population dynamics have been used by Agur and colleagues to develop relatively simple formulae describing the growth patterns of interwoven populations of healthy and cancerous cells, formulae that have resulted in new drug regimens where the toxicity of chemotherapy has been significantly reduced [2, 3, 63]. The power of mathematics here was to prove the universality of the theoretical results and therefore to justify and encourage collaboration with cancer research experimentalists. The latter not only verified the theory in the laboratory, but also pinpointed the feasibility and strength of the theory-to-lab arrow [4, 5].

In the above mentioned mathematical models, populations are subjected to a loss process due to randomly occurring environmental disturbances, which are effective only during a portion of the life cycle. The models are studied over a large range of time scales of the environmental change and for different degrees of variance in the system parameters. Analysis shows that the expected survival time of the population has a strong nonmonotonic dependence on the relation between the duration of the disturbance-resistant life stages and the periodicity of the environmental disturbance. This effect, termed *resonance phenomenon*, was found at integer and fractional multiple of this relation. Interestingly, persistence in all harshly varying environments is shown to depend on the degree of resonance in the environmental and population processes [2, 6–8, 64].

The universality of the resonance phenomenon, and its implication that the frequency of environmental disturbances determines population growth, seemed to offer attractive possibilities for the control of cancer. Thus, Agur and colleagues have shown, both theoretically and experimentally, how the resonance phenomenon could be employed for choosing cytotoxic drug regimens that allow discrimination between different target cell populations. More specifically, it was asserted that one could determine the period of drug pulses, so as to maximize the elimination of malignant cells and, at the same time, to minimize the destruction of drug-susceptible host cells.

In the first stage, it was necessary to investigate the generality of the resonance phenomenon for the dynamics of different host cell populations. To allow analytical tractability, and hence parameter-independent conclusions, deliberately crude mathematical models of the cancer patient were constructed, making simplified assumptions that both tumor and target host tissues are cells that vary only in cell-cycle parameters. The spatial arrangement of these cells was hence ignored. The interest was focused on comparing the overall behavior of the tumor to that of the host target tissues under different chemotherapy regimens of cell-cycle phase-specific drugs, and on finding regimens that are selective to cancer cells. The conviction was that only a simplified model can clarify the underlying properties of the biomedical scenario. Model analysis showed that the resonance phenomenon is valid when

considering drug-induced myelotoxicity and tumor progression. Specifically, the mathematical analysis suggested that the efficacy/toxicity ratio of cell-cycle phase-specific drugs would be maximized at an integer or fractional multiple of the mean cycle time of the host target populations (this being denoted the *Z-method*). This applies either when mean cancer cell-cycle parameters differ from those of the target host cell population, or when those are similar but the variation in the distribution of their cell cycle is larger [3, 9, 10].

It seemed mandatory, already at this level of qualitative understanding of the system, to carefully examine the plausibility of applying the Z-method to cancer and host cells. To this end, a series of laboratory experiments was launched, first examining the effect of drug-pulsing rhythm on cell proliferation, *in vitro*, and then checking how varying the pulsing rhythm of different drugs will affect disease progression on the level of the whole organism.

Applying an antimetabolite chemotherapeutic drug, cytarabine (ara-C), to lymphoma cells *in vitro*, it was experimentally shown that when total drug dose and total treatment duration were kept constant, drug schedules exerting significantly higher cell growth were those possessing periodicity that was an integer multiple of the average population cell-cycle time, as evaluated by rates of DNA synthesis. In equivalent *in vivo* experiments, mice were treated by short ara-C pulses, having different distributions of the interdosing intervals, including stochastically determined periodicity. Toxicity was evaluated by spleen weight, differential peripheral blood measurements, kinetic measurements of bone marrow cell proliferation (with bromodeoxiuridine labeling and flow cytometry analysis), and by overall animal survival. Results of these trials proved the superiority of the Z-method in controlling cell proliferation. In particular, it was shown that when the interdosing interval is an exact multiple of the intermitotic time of bone marrow stem and progenitor cells, cell-cycle kinetics are less affected, myelotoxicity is minimal, and survival time of tumor-bearing mice is maximal [3–5, 11].

The above experiments demonstrate that regimens employing a drug period, which coincides with the inherent periodicity of bone marrow cells, protect the bone marrow rather well, leading to increased life expectancy of cancer-bearing mice. In contrast, other regimens, notably those employing intervals that are randomly distributed around the same mean periodicity, are extremely toxic. In general, this work is a proof of the concept that by using a rational drug scheduling, based on the Z-method, it is feasible to control drug toxicity exerted on the bone marrow of cancer-bearing mice, while at the same time delaying their tumor progression. This conclusion has been further supported under more realistic and complex tumor growth models [12, 13] and under physiologically based mathematical models of human hematopoiesis [14].

The above described mathematical models added important new insights on drug treatment strategies, by considering fundamental effects on cellular dynamics. Yet, to enable mathematical tractability, drug-related characteristics were treated very simplistically. For this reason, only qualitative conclusions can be drawn from these model analyses. Now that the proof of concept has been provided, the models are becoming increasingly instrumental in planning concrete treatment strategies. To this end, modeling of the underlying pathological and physiological processes in a patient is wedded with the detailed relevant pharmacokinetics (PK) and pharmacodynamics (PD) [15, 65]. By uniting in one framework the pharmacological properties of the drug with the dynamic properties of the cells in the target tissues, one

obtains an improved understanding of how the timing of drug administration—the interdosing interval, drug fractionation, and other aspects of treatment scheduling—may affect the patient. Biomathematics has the power of integrating the vast biomedical and pharmaceutical knowledge into a concise formal language, which enables intensive calculations of the outcomes of complex processes. These calculations, being by far more comprehensive and accurate than any human intuition can be, justify their use for rational treatment design at any stage of the critical path, especially when partial preclinical results collected in several species are to be used for predicting the human response.

36.1.2 Aims of This Chapter

In this chapter, we discuss the application of mathematical modeling tools to elucidate the hematological disorder thrombocytopenia in different animal species, and to accurately describe the efficacy and safety of the thrombocytopenia-alleviating drugs, thrombopoietin and interleukin-11. Model validation in mice, monkeys, and humans, by the use of diverse experimental information, is discussed, as well as the use of animal models for predicting human safety and for improving patient treatment.

36.2 THROMBOPOIESIS

Any mathematical model describing a biological process is based on a verbal model of the process, that is, on an algorithm concisely describing its essential physiological "flow." We devote this section to a brief presentation of the verbal model of thrombopoiesis, and to the subsequent description of a mathematical model, constituting the essence of platelet development.

36.2.1 Biology

Platelets are components of the hematopoietic system, being the nucleus-lacking derivatives of megakaryocytes (MKs). Platelets function primarily in processes of thrombus formation and vascular repair, but also have roles in natural immunity and metastatic tumor biology. Platelet counts in healthy humans average 150–400 billion cells per liter of blood, a homeostasis that is crucial to maintain. Low counts may lead to severe hemorrhage, renal failure, and other disorders, while high counts indicate poor prognosis with respect to cardiovascular diseases and malignancies. Thrombopoiesis, the formation of blood platelets, has been studied for the last century, although critical advances in our understanding of the unique processes that accompany it are only of the last decade. We refer the reader to Fig. 36.1 for an illustration of the process and to the literature for a more elaborate description [16–19].

Normal platelet formation begins with bone marrow progenitors of the lineage, which descend from hematopoietic stem cells and proliferate in response to certain growth factors. The next stages in the sequence involve the immature forms of MKs (promegakaryoblasts and megakaryoblasts), which then develop into larger, mature MKs. As the cells mature into MKs, they gradually lose their ability to divide but

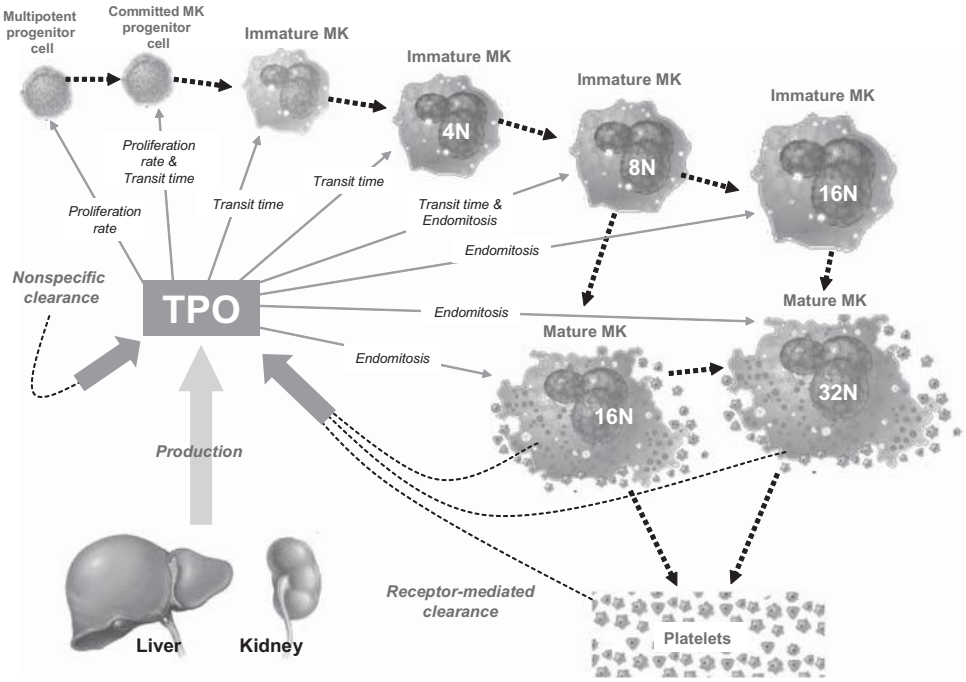


FIGURE 36.1 The process of thrombopoiesis. Uncommited progenitors in the bone marrow (hematopoietic stem cells) proliferate and develop into commited progenitors of the megakaryocyte (MK) lineage, which further develop into immature forms of MKs (promegakaryoblasts and megakaryoblasts). These then develop into larger, mature MKs. Maturation of cells is coupled with loss of the mitotic ability, but endomitosis and polyploidity are maintained until the early stages of MK fragmentation and systemic distribution of platelets. Thrombopoietin (TPO), derived from the liver and kidney constitutively, is a primary mediator of the platelet formation process and is sequestered by platelets and MKs, as well as nonspecifically.

maintain the function of DNA synthesis, thereby undergoing endomitosis and attaining a polyploid state. Finally, MK fragmentation occurs, resulting in release of platelets, first to bone marrow sinusoids and then to the systemic circulation. Radiolabeling studies indicate that the amount of platelets normally consumed by hemostasis is very small and constant. The highly regulated process of platelet consumption is induced by their adhesion to von Willebrand factor (vWF) and extracellular matrix components of damaged blood vessel wall underlying the endothelium. Following platelet adhesion, a clot is formed and the vessel wall is recovered. With a life span of approximately 10 days, unconsumed platelets that senesce are removed by macrophages of the reticuloendothelial system, mostly in the spleen.

Thrombopoietin (TPO), a glycoprotein produced by the liver and kidney constitutively and by the bone marrow upon demand, is characterized as the primary regulator of platelet formation. Although the focus was set on TPO in the late 1960s, it was successfully cloned only in 1992. TPO acts in all stages of thrombopoiesis, its receptors being expressed on each cell type in the lineage. Interestingly, systemic and bone marrow levels of TPO are inversely correlated to platelet numbers: due

to high affinity platelet-bearing TPO receptors, increased amounts of platelets result in high internalization of TPO, forming successful autoregulation of the thrombopoiesis. Slightly less significant cytokines, namely, the interleukins 3, 6, 11, and stem cell factor (SCF), stromal cell-derived factor 1 (SDF-1), and granulocyte macrophage colony-stimulating factor (GM-CSF), were also identified as modulators in normal platelet formation, each acting in different developmental phases, and some acting in synergy with others. Studies indicate that surrounding tissue, comprised of fibroblasts, endothelial cells, and macrophages, is also capable of augmenting thrombopoiesis, although these environmental factors are not thought to be critical since platelets are easily produced also *in vitro*.

The manipulation of molecular and genetic techniques in the last two decades has greatly boosted the understanding of biological pathways and mechanisms involved in platelet formation. Nonetheless, at the current stage, the regulation of thrombopoiesis, the central molecular components taking part in it, and their significance for therapeutic intervention in platelet-associated illnesses are yet to be clarified.

36.2.2 Mathematical Modeling

Although the intricacies of thrombopoiesis are far from being fully elucidated, current knowledge enabled the verbalization and subsequently the mathematical formalization of a basic thrombopoiesis-describing model. Schematized in Fig. 36.2, and elaborated elsewhere, the model divides the entire thrombopoietic lineage into 17 compartments. Every compartment, except for the first, is represented by time-dependent age distribution, where the number of cells is given as a function of discrete age (time spent in the compartment) and time. The number of cells in the first compartment is a function of time only. There are six groups of compartments in the model, in accordance with the above-mentioned structure of the thrombopoietic lineage. The subdivision of the six groups is as follows: (1) one compartment of lineage-uncommitted progenitors (UCP), (2) one compartment of lineage-committed progenitors (CP), (3) six compartments of endomitotic progenitors (EP), (4) four compartments of developing progenitors (DP), (5) four compartments of MKs, and (6) one compartment of blood-circulating platelets.

The first compartment, UCP, refers to all bone marrow hematopoietic progenitor cells that can differentiate into more than one line (e.g., pluripotent stem cells, CFU-GEMM). We assume one homogeneous UCP population, as its division into various subpopulations is not feasible, since kinetic data regarding the various subpopulations of the UCP compartment (i.e., rates of proliferation, maturation, and self-renewal) is rather scarce. In our model, cells of this compartment proliferate at a certain rate (α_{UCP}) and differentiate into MKs or other precursors. Based on previous studies showing that the probabilities of stem cell differentiation into any given hematopoietic lineage are constant, it was assumed that a fixed proportion of mature uncommitted progenitor cells flows into the thrombopoietic lineage (φ_{UCP}). Apoptotic cell death may have a significant effect on cell numbers in the proliferating compartments. Thus, we included its effect together with the effect of cell proliferation in the total amplification of cell number in a specific compartment. Since no information is currently available concerning apoptosis in the nonproliferating MK compartments, this issue was disregarded in these compartments.

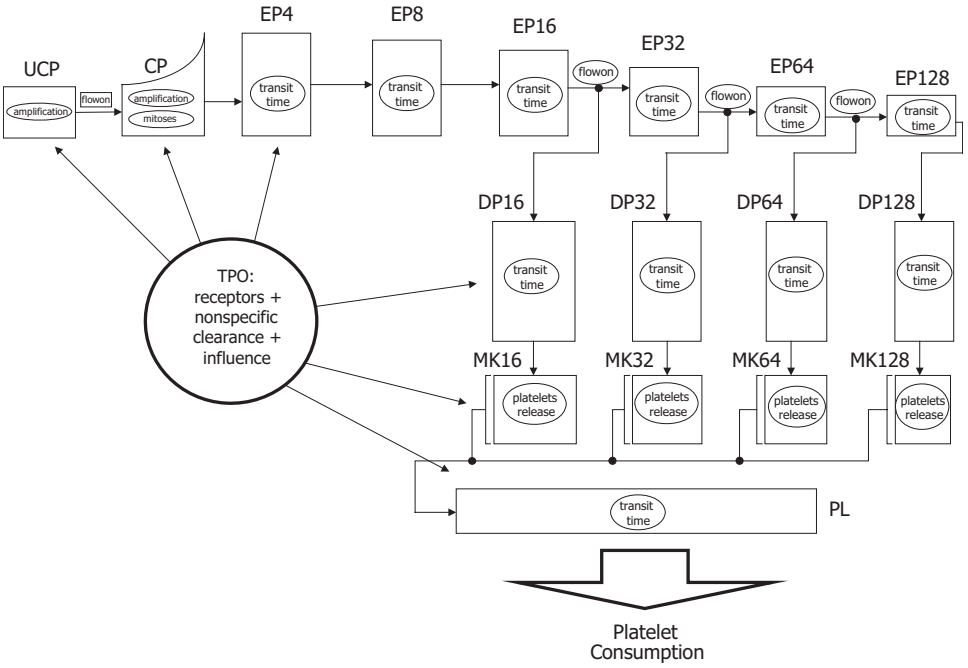


FIGURE 36.2 A scheme of the thrombopoiesis mathematical model. The model consists of 17 compartments, which can be grouped into six clusters: (1) one compartment of lineage-uncommitted stem cell progenitors (UCP), (2) one compartment of lineage-committed progenitors (CP), (3) six compartments of endomitotic progenitors (EP) of ploidies 4N, 8N, 16N, 32N, 64N, and 128N, (4) four compartments of developing progenitors (DP) of ploidies 16N, 32N, 64N, and 128N, (5) four compartments of megakaryocytes (MKs) of ploidies 16N, 32N, 64N, and 128N, and (6) one compartment of individual, blood-circulating platelets. Relevant key parameters included in the kinetic calculations of the different compartments are amplification rate, flow-on fraction (flowon), transit time, and rate of platelet release. The arrows indicate the direction of intercompartmental cell flow.

The CP compartment stands for an age distribution of progenitor cells already committed to the thrombopoietic lineage, but still capable of proliferation. The compartment is characterized by a transit time (τ_{CP}) and a number of mitoses (N_m). The latter represents the average number of possible cell divisions at that stage. This number may be noninteger, considering that certain cells can be quiescent and undergo fewer mitoses than others. Cells leaving CP enter the first of the six EP compartments, which comprises cells that have lost proliferation ability and yet are not sufficiently mature to release platelets. Thus, this subgroup of compartments, namely, EP4, EP8, EP16, EP32, EP64, and EP128, are formed according to the biologically known sequence of cells of the MK lineage bearing ploidy of 4N, 8N, 16N, 32N, 64N, and 128N, respectively. These endomitotic precursors cannot divide but continue endomitosis. The cells that enter the EP4 compartment are of ploidy 2N, at the exit they have ploidy 4N, and so on for subsequent EP compartments. It is assumed that MKs can release platelets only after reaching the 16N-ploidy phase. Hence, to arrive at platelet production in our model, the EP16 compartment must

be entered. After cells spend their designated transit time (τ_{EP}) in an EP compartment, they can move to the next EP compartment. Fractions of cells that continue endomitosis after moving through EP16, EP32, or EP64 are designated φ_{EP16}, φ_{EP32}, and φ_{EP64}, respectively, where in normal conditions $\varphi_{EP64} = 0$.

Alternatively, cells at the EP16, EP32, or EP64 stage may stop the endomitotic process by entering the relevant DP compartment, which is represented by four subgroups of cells. DP cells of 16N, 32N, 64N, and 128N ploidy increase their cytoplasmic contents prior to platelet production. Cells that have stopped endomitosis after exiting EP16 compartment enter into DP16; cells that have stopped endomitosis after exiting EP32 compartment enter into DP32, and so forth. After spending a certain amount of time (τ_{DP}) in the DP compartment, cells pass to the corresponding MK compartment. The four subcompartments of this stage signify cells capable of releasing platelets. MK16 compartment receives cells exiting from DP16, MK32 receives cell exiting from DP32, and so on. As in previous compartments, here too the cells are distributed over age (time spent in the compartment), yet there is no predefined transit time. Instead, the new cells entering MK are assumed to have some initial releasing capacity, indicating the number of potential platelets, or total platelets volume, to be released until the cell is exhausted. This capacity is assumed to be larger for cells of larger ploidy. Cells release platelets continuously, and their releasing capacity is consumed until it drops to zero, thereupon disappearing from the compartment.

The last compartment, PL, represents platelet counts distributed by age (time spent in blood after the release). Distribution of mean platelet volume (MPV) is also computed in order to allow calculations of platelet degradation. The platelets are readily consumed by the body in an age-independent manner, and in terms of volume (platelet number multiplied by MPV). There is also a maximal life span for old platelets, so that all nonconsumed platelets disappear upon reaching a maximal age (denoted by τ_{PL}). New platelets appear at every time step, as released by MK cells. This release is also described in terms of volume, and at every time step the amount and MPV are evaluated for the new platelets, taking into account the relative contributions of MK cells of different ploidies.

The formal description of the cellular compartments is supplemented by the model for the endogenous TPO, which regulates the dynamics of the process. A one-compartment PK model for TPO, with a constant production and a linear nonspecific clearance, is applied. In addition, there is an alternative, specific clearance of TPO, achieved through the consumption by the cells (receptor binding and internalization). To include this in the model, distributions of receptors per cell in all the line-committed compartments (CP and the groups that follow) are incorporated. Formulae are constructed for receptor numbers distributed over cell age. Receptors, constantly produced by the cells, excluding platelets that have no nucleus, bind free TPO and are internalized. To reflect the nonspecific clearance of TPO, Michaelis–Menten behavior is assumed for TPO-receptor kinetics.

The major stabilizing feedback in the model is exerted via the effects of TPO on the cells throughout the lineage. Kinetic parameters of the model's compartments are functions of TPO concentrations. In the UCP compartment, the amplification rate is an increasing function of the TPO concentration. Similarly, the number of mitoses in the CP compartment is an increasing function of TPO. In contrast, the transit times in CP, EP, and DP, and the EP flow-on (fraction of cells that continue

endomitosis) are decreasing functions of the TPO concentration. Finally, the MPV of released platelets (and consequenty the loss of cell volume) is an increasing function of the TPO concentration in the MK compartments. For all the dependencies listed above, sigmoid functions with saturation for large values of TPO concentration are used. In addition to this feedback, a TPO-independent feedback on cell proliferation in the model, or a "crowding effect," is included as well. The amplification rate in UCP and the number of mitoses in CP are decreasing functions of cell numbers in these compartments, respectively. This represents internal regulation of cell proliferation in these stages. Such functions are also assumed to have a sigmoid form.

The model is mathematically formalized according to the above description, using discrete difference equations. The variables of the model (e.g., cell numbers) are represented as functions of discrete time points, with a certain step Δt. The set of the model equations describes the recursive calculation of the system state for the current time point, using the state of the system at previous time points. For the specific clearance model, steady-state approximations are used, as these processes are on a much faster time scale than all the rest of the model. The model is simulated using a C++ code, and its parameters are estimated either directly from experimental measurements or by fitting the model to the published experimental data. The validation of the model is further described in Section 36.5.

36.3 THROMBOCYTOPENIA

Setting the essential rules for depicting thrombopoiesis, as explained in Section 36.2, it is possible to evaluate not only the homeostatic behavior of the system but also its irregularities. Diversion from normal steady-state thrombopoiesis can arise from various reasons and can have several physiological consequences. In this section, we discuss some of the main mechanisms leading to low platelet count, termed thrombocytopenia (TP). Both current and future therapeutic avenues will be illustrated.

36.3.1 Pathophysiology

The concise summary of TP pathophysiology, presented in this section, is based on extensive reviews of this pathology in the current hematology literature [16, 20, 21]. The clinical significance of TP, characterized by a blood platelet count of less than 150,000 cells per microliter, stems from the major role of platelets in the process of normal hemostasis. Low platelet counts lead to diminished ability of hemostasis and, consequently, increased bleeding propensity. Yet there are important exceptions to this rule. First, clinically significant bleeding occurs regularly only when the amount of platelets decreases below 10,000–20,000/μL. Second, exact clinical manifestation of this disorder depends on the underlying pathophysiological mechanisms. While TP induced by low platelet production leads to increased risk of bleeding, TP caused by excessive platelet consumption may result in an elevated risk of thromboembolism.

TP can be caused by one or more of the following mechanisms (elaborated in the following section): (1) decreased platelet production, (2) increased sequestration of platelets, or (3) their accelerated destruction. TP induced by the first mechanism,

impaired production of platelets, accompanies a variety of bone marrow pathologies. Congenital hereditary decreased production TP, one of these cases, is very rare. It can be caused by malfunctioning TPO receptor signaling (e.g., amegakaryocytic TP) or by impaired MK fragmentation into mature platelets. The more common syndrome is acquired decreased production TP. This form of TP can be a result of pathological bone marrow infiltration in hematopoietic malignancies (leukemias and lymphomas) or in massive metastases of extramedullary solid tumors. Alternatively, this could occur in myelodysplastic syndromes and vitamin B_{12} deficiency, when intrinsic maturation defects arise in the early hematopoietic progenitors, with involvement of 1–3 hematopoietic lines. Extrinsic inhibitors of hematopoietic progenitor proliferation, such as (1) cytotoxic drugs (anticancer chemotherapy), (2) circulating autoantibodies to MKs (immune thrombocytopenic purpura, systemic lupus erythematosus, etc.), (3) proinflammatory cytokines (sepsis), or (4) various viral infections (EBV, CMV, HIV, etc.), can induce this TP form as well.

Increased sequestration TP, the second mechanism, is a common finding in splenomegaly of any cause. A frequent consequence of splenic enlargement is increased pressure in the portal vein, which causes draining of blood from the spleen into the liver. This syndrome, referred to as portal hypertension, is present in a variety of chronic liver diseases and in cases of portal vein thrombosis due to hypercoagulation states. In portal hypertension, increased sequestration is often the only cause of TP. Other diseases with splenomegaly generally produce TP of a combined etiology. For example, splenomegaly is associated with conditions of leukemia and lymphoma, in which bone marrow infiltration results in decreased platelet production. Similar combinations of TP mechanisms appear in several infectious disorders (e.g., brucellosis and visceral leishmaniasis) and inflammatory diseases (e.g., Felty's syndrome and systemic juvenile rheumatoid arthritis).

Pathologically accelerated platelet destruction (the third mechanism of TP) can be induced by either increased consumption or physical factors. Physical platelet destruction occurs upon increased blood shear stress near valvular and intravascular prosthetic devices. There are varying disorders of increased platelet consumption by pathological uncontrolled coagulation. Thrombotic thrombocytopenic purpura (TTP) and hemolytic uremic syndrome (HUS) are associated with thrombosis, rather than bleeding, despite low platelet count. Recent progress in TTP research reveals that the underlying pathology involves decreased or absent function of a protease known as a disintegrin and metalloproteinase with a thrombospondin type 1 motif, member 13 (ADAMTS13), responsible for specific cleavage of vWF. As a consequence, large multimers of vWF are formed, and they initiate bouts of platelet adhesion and activation. Conversely, pathogenesis of HUS is incompletely understood. Since this disorder appears typically after certain bacterial infection, it is assumed that cross-reactive antibodies are responsible for platelet activation in this syndrome. Disseminated intravascular coagulation (DIC), distinct from the latter two disorders by its simultaneous induction of both thrombosis and bleeding, is a common feature of several severe illnesses including overwhelming sepsis, poisoning due to snake bites, amniotic fluid embolism, and fat embolism. The pathogenesis of DIC includes uncontrolled activation of intravascular coagulation pathways, leading to increased platelet consumption.

Accelerated destruction TP can also be attributed to immunological disorders. The most recognized disorder of this type is immune (idiopathic) thrombocytopenic

purpura (ITP). The underlying pathology consists of formation of autoantibodies against specific platelet surface antigens. Platelets covered with autoantibodies are effectively and prematurely destroyed by the phagocytes of the reticuloendothelial system. In the minority of cases, presence of autoantibodies to MKs is also suspected, which results in TP of mixed etiology—both decreased production and accelerated destruction. Other diseases with autoimmune platelet destruction include systemic lupus erythematosus and antiphospholipid antibody syndrome. Drug-induced immune TP was observed upon the use of many exogenous factors, including heparin, gold, antibiotics, and anti-inflammatory drugs. In these cases, antibodies are formed against the complex of a drug with platelet surface antigens. In heparin-induced TP, thrombotic complications are common (similar to those in TTP), since antibodies lead to excessive platelet activation in addition to increased clearance.

To examine the risk of TP in new drugs, or in yet to be tried drug regimens, the PK and PD of the drug should be simulated superimposed on a mathematical model of the underlying TP mechanism. However, how to determine the specific TP mechanism in each particular case is a very challenging task. While certain clues can be received from the patient's medical history, physical examination, and peripheral blood smear, bone marrow biopsy is frequently required in order to evaluate the number of MKs. Low numbers are indicative of decreased production, while increased numbers are associated with accelerated destruction. Some cases remain undefined, even after thorough laboratory investigation and manipulation of extensive tools. The type of TP guides further clinical workup for specific underlying pathology as well as possible treatment options.

36.3.2 Current Therapy

In light of the different mechanisms for TP, treatment is diverse and highly dependent on the underlying cause. Generally, we can divide current therapy into treatments directed against pathophysiological mechanisms, and symptomatic treatment of TP-induced bleeding/thrombosis. In the majority of the cases, platelet counts do not drop below 10,000–20,000 per microliter of blood, so that serious bleeding complications do not develop. Treatment of the underlying causes includes withdrawal of the offending stimulus (e.g., discontinuation of an immunogenic drug), removal of vWF complexes by plasma exchange in TTP, replacement of mechanical prosthesis by a biological one, and specific treatment of malignancies and infections.

It is imperative to identify accelerated platelet destruction by the reticuloendothelial system, for which splenectomy and/or administration of intravenous immunoglobulins (IVIGs) is indicated in refractory cases. Splenectomies lead to decreased autoantibody production and remove a large fraction of phagocytes responsible for platelet destruction. IVIGs, on the other hand, saturate antibody-binding receptors on the phagocytes and suppress their interaction with antibody-covered platelets and MKs. Therefore, theoretically, IVIGs should be more effective in cases of MK-specific antibodies. This hypothesis, however, has not been examined clinically, due to technical difficulties in identifying antibody specificity in particular patients. Importantly, neither a splenectomy nor IVIG therapy is effective in cases of direct complement-mediated antibody toxicity to platelets and MKs.

Symptomatic treatment of TP-associated bleeding disorders consists mainly of transfusion of donor platelets. Platelet transfusions are commonly used, with approximately 9 million units yearly applied in the United States alone. Although repeated platelet transfusions may aid in preventing bleeding, they can transmit both viral and bacterial infections and can cause alloimmunization, which requires HLA-matched donors. Health care costs and inconvenience to patients also pose a concern. Furthermore, this treatment must be repeated on a regular and frequent basis, due to the short half-life of donor platelets (3–4 days), and since the underlying causes of TP are left untreated. Platelet transfusions are of especially low efficacy in immunologically mediated TP that involve an even shorter platelet half-life.

36.3.3 Novel Cytokine Therapy

Over the past fifteen years, attempts to find new therapies to replace platelet transfusions in the treatment of thrombocytopenic disorders have naturally been focused on the growth factors involved in normal thrombopoiesis (see Section 36.2). Interleukin-11 (IL-11), discovered in 1990 to be a thrombopoietic growth factor secreted from bone marrow stromal cells, was the first candidate for this purpose. The genetically engineered form of this protein, recombinant human IL-11 (rhIL-11), was evaluated for treatment in patients with nonmyeloid malignancies that suffered from chemotherapy-induced thrombocytopenia and did, in fact, produce a dose-dependent increase in platelets. RhIL-11, approved in 1997 for prevention of severe drug-induced thrombocytopenia, is currently the only cytokine licensed in the United States for this purpose. However, with its only modest thrombopoietic activity and its use often associated with intolerable side effects, IL-11 has not satisfied the demands for an efficacious thrombopoietic agent to be applied in the clinical setting [22–24].

In light of the central role of TPO in the proliferation and survival of MKs and increased platelet production, its potential to replace standard platelet transfusion therapy and improve platelet harvesting efficacy in donors seems even greater than that of IL-11 [22, 25]. Recombinant human TPO (rhTPO) has been examined for exogenous application in patients with primary thrombocytopenic disorders, as well as for treatment of chemotherapeutically induced myelosuppression in cancer patients. However, Phase I studies with rhTPO in healthy individuals remain disappointing. In a trial that was aimed at improving platelet yields in donors, some of them developed immune-mediated TP due to appearance of autoantibodies to native TPO. Evaluation of rhTPO therapy has also encountered difficulties due to delayed peak platelet response and neutralizing antibodies formed against the pegylated molecule. It is believed that most complications are caused by significant antigenic differences between the native and recombinant TPO proteins. As a result, this molecule currently remains in its developmental stage and is not yet approved. Small TPO analogues and synthetic TPO-derived agents are currently being developed to bypass immunogenicity-related problems [26–34].

Mathematical modeling of thrombopoiesis (as described in Section 36.2) and drug-induced TP (as will be shown in Section 36.6) can aid in disentangling disease dynamics and in deciphering pathophysiological mechanisms underlying the disease. In particular, mathematical models of TPO-affected thrombopoiesis and of IL-11-induced side effects enable one to propose improved treatment schedules for both

drugs, obtaining maximum efficacy and substantially improved safety (see Sections 36.4 and 36.5). In turn, preclinical validation of these improved regimens can give new hope for clinical application of these cytokines in their multiple arenas.

36.4 MODELING DRUG EFFECTS ON THROMBOPOIESIS

Innovative cytokine-based therapeutics of IL-11 and TPO (see Section 36.3) developed for application in thrombopoiesis-related syndromes and for efficiently harvesting donor platelets have been extensively studied in the last decade or so. Yet, even today, toxicity-related limitations of each of these molecules prevent their clinical applicability. The following section is dedicated to mathematical models focusing on both beneficial and detrimental consequences of these therapeutic avenues, and on the manner by which such models may be used to suggest improved treatment strategies.

36.4.1 Toxicity Modeling: Interleukin-11 (IL-11)

Although IL-11 has been approved for treating drug-induced TP for almost a decade, its induction of intolerable toxic effects has impeded its therapeutic use. The cytokine has been shown to elicit a wide range of side effects, mainly associated with blood volume expansion (BVE). These include complications of various grades of edema, anemia, pleural effusion, and cardiac arrhythmia [23].

An initial and generalized perspective on this issue required a mathematical model of IL-11-induced BVE. However, the definitive mechanism underlying IL-11-mediated water accumulation is yet to be discovered, and the incomplete data [23, 35] restrict the possibility to produce a concrete and reliable model for this problem. Instead, a novel biomathematical approach was developed so that not one but several mathematical models, each representing an alternative mechanism for BVE following IL-11 therapy, were devised and evaluated [36]. The underlying assumption here was that by concurrently simulating multiple models, which formally describe alternative mechanisms, but all producing the same fluid-retentive behavior, it is possible to faithfully depict this effect despite the obscurity of the actual mechanism and related data. Accordingly, convergence of all models to yield unified BVE dynamics was the characteristic by which their success and predictive ability was measured. Furthermore, since the range of different models that capture the behavior of stable biological systems (e.g., body water homeostasis) is assumed to be relatively narrow, the chances of arriving at a reliable model was considered even greater in the drug-afflicted BVE setting [36].

Three closely related biologically based models were constructed using ordinary differential equations (ODEs) and standard Michaelis–Menten kinetics. The models incorporated basic water regulation properties (blood volume, pressure, and vascular compartments) and endocrinal feedback effects (compartments for BVE-upregulating and BVE-downregulating hormones), together with the IL-11-induced perturbation of the system. Notably, a short-term neuronal influence or long-term permanent structural changes were not considered, restricting the modeling to the therapeutic time scale. The variation between the different models was expressed in (1) the component directly affected by IL-11, being either blood volume or blood

vessels, and (2) the components affected by the endocrinal hormones, being both vessels and volume (full effect) or only volume (partial effect). Thus, model 1 assumes IL-11-induced vessel enlargement and full endocrinal feedback; model 2 assumes IL-11-induced volume expansion and full endocrinal function; and model 3 assumes IL-11-induced volume expansion and partial endocrinal function. The models were identical in all other assumptions.

Dynamics of subcutaneously administered IL-11 were represented by a one-compartment PK model, with first-order absorption from the external tissue. IL-11 concentrations in the tissue (I_T) and plasma (I_P) are given by

$$\dot{I}_T = -c_1 I_T \tag{36.1}$$

and

$$\dot{I}_P = f c_1 I_T - c_2 I_P \tag{36.2}$$

where I_T ($t = 0$) is the administered IL-11 concentration and I_P ($t = 0$) = 0. The coefficient c_1 denotes the rate of drug transport from the primary tissue to the plasma, c_2 is the drug clearance rate, and the fraction of transferred drug, an indicator of bioavailability, is f.

Blood pressure was described by considering its classical correlation to heart rate, stroke volume, and systemic vascular resistance. As heart rate variability was disregarded in experiments, and an inverse relationship between vascular resistance and vascular capacity was assumed, blood pressure was described to be a function of blood volume and the vascular capacity (expressed in terms of vessel surface):

$$P(t) = \left(\frac{V(t)}{S(t)^{3/2}} \right)^{n_0} \tag{36.3}$$

The function $P(t)$ is blood pressure at time t, $S(t)$ denotes overall vessel surface at time t, $V(t)$ is blood volume at time t, and n_0 is a parameter. Steady-state values of pressure and overall vessel surface and volume were given by P_{st}, S_{st}, and V_{st}, respectively.

Dynamics of the BVE-upregulating hormones (H_U) and the BVE-downregulating hormones (H_D) were subjected to blood pressure variations and were therefore given by

$$\dot{H}_U = \alpha_1 g(P_{st} - P(t)) - d_1 H_U(t) \tag{36.4}$$

and

$$\dot{H}_D = \alpha_2 g(P(t) - P_{st}) - d_2 H_D(t) \tag{36.5}$$

respectively. The description is general and does not refer to hormonal concentrations per se, but rather to effects associated with endocrinal deviations. In Eqs. 36.4 and 36.5, formation rates (α_1, α_2) and degradation rates (d_1, d_2) of the endocrinal

effects were taken as constants, and blood pressure deviations from steady state allowed formation of each factor using the function

$$g(x)=\begin{cases}x & \text{if} \quad x>0\\ 0 & \text{if} \quad x\le 0\end{cases} \tag{36.6}$$

The vascular structure was described in two-dimensional units, for example, by relating to the average surface of the inner endothelium layer of blood vessels. IL-11-induced vessel surface enlargement (in model 1) and H_U-induced vasoconstriction or H_D-induced vasodilation (in models 1 and 2) were described by biologically compatible nonlinear functions. As described earlier, model 3 does not enable vascular resizing in response to IL-11 or hormones. All three models, however, incorporate simple intrinsic feedback effects to vessel steady state in blood vessel dynamics. Thus, the equations for models 1, 2, and 3 are given by Eqs. 36.7, 36.8, and 36.9, respectively:

$$\dot{S}=\frac{\beta_0(I_P(t))^{r_0}}{k_0+(I_P(t))^{r_0}}-\frac{\beta_1(H_U(t))^{r_1}}{k_1+(H_U(t))^{r_1}}+\frac{\beta_2(H_D(t))^{r_2}}{k_2+(H_U(t))^{r_2}}+\beta_3(S_{st}-S(t)) \tag{36.7}$$

$$\dot{S}=-\frac{\beta_1(H_U(t))^{r_1}}{k_1+(H_U(t))^{r_1}}+\frac{\beta_2(H_D(t))^{r_2}}{k_2+(H_U(t))^{r_2}}+\beta_3(S_{st}-S(t)) \tag{36.8}$$

and

$$\dot{S}=\beta_3(S_{st}-S(t)) \tag{36.9}$$

Vascular modification rates in response to IL-11, H_U, and H_D are denoted as β_0, β_1 and β_2, respectively, and β_3 is the coefficient of direct vessel surface regulation. Parameters k_0, k_1, k_2 and r_0, r_1, r_2 are positive.

Volume dynamics were initially characterized by water absorption–excretion differences. Absorption rates were assumed not to deviate from steady-state values, whereas excretion rates were taken as susceptible to (1) systemic blood pressure deviations, known to specifically act on renal water excretion, and (2) the IL-11-induced effects. The function of blood volume was therefore described by the difference between absorption rates, which were constant (A_{st}), and excretion rates, which were set as the pressure-related difference between normal steady-state excretion (E_{st}) and the excretion in the IL-11 scenario (E_{drug}):

$$\dot{V}=A_{st}-\left(\frac{P(t)}{P_{st}}\right)^{n_1}(E_{st}-E_{drug}(t)) \tag{36.10}$$

The power coefficient n_1 sets the strength of the dependence of the volume changes on the pressure variation. Assuming equal steady-state absorption and excretion rates ($A_{st}=E_{st}$) under normal conditions, Eq. 36.10 turns into

$$\dot{V}=E_{st}\left(1-\left(\frac{P(t)}{P_{st}}\right)^{n_1}\right)+\left(\frac{P(t)}{P_{st}}\right)^{n_1}(E_{drug}(t)) \tag{36.11}$$

Excretion of volume in the therapeutic scenario (i.e., the term E_{drug}) was assumed to be affected by the hormones in all three models. As described above, in models 2 and 3 it was additionally assumed that the drug directly influences volume excretion. Both of these effects (IL-11 and hormone mediated) were assumed to be nonlinear and were introduced into the volume dynamics given in Eq. 36.11. For model 1, this gave

$$\dot{V} = E_{\text{st}}\left(1-\left(\frac{P(t)}{P_{\text{st}}}\right)^{n_1}\right)+\left(\frac{P(t)}{P_{\text{st}}}\right)^{n_1}\left(\frac{\gamma_1(H_{\text{U}}(t))^{q_1}}{m_1+(H_{\text{U}}(t))^{q_1}}-\frac{\gamma_2(H_{\text{D}}(t))^{q_2}}{m_2+(H_{\text{D}}(t))^{q_2}}\right) \tag{36.12}$$

while for models 2 and 3, this gave

$$\dot{V} = E_{\text{st}}\left(1-\left(\frac{P(t)}{P_{\text{st}}}\right)^{n_1}\right)+\left(\frac{P(t)}{P_{\text{st}}}\right)^{n_1}\left(\frac{\gamma_0(I_{\text{P}}(t))^{q_0}}{m_0+(I_{\text{P}}(t))^{q_0}}+\frac{\gamma_1(H_{\text{U}}(t))^{q_1}}{m_1+(H_{\text{U}}(t))^{q_1}}-\frac{\gamma_2(H_{\text{D}}(t))^{q_2}}{m_2+(H_{\text{D}}(t))^{q_2}}\right) \tag{36.13}$$

The IL-11-, H_{U}-, and H_{D}-afflicted rates of water excretion are denoted γ_0, γ_1, and γ_2, respectively. Parameters m_0, m_1, m_2, and q_0, q_1, q_2 are positive constants.

Subsequent calibration of the models was accomplished by obtaining and utilizing data from a human study of IL-11 safety, and their predictive ability was evaluated under different regimens of IL-11 therapy. These stages of the work are further described in Section 36.5.

36.4.2 Efficacy Modeling: Thrombopoietin (TPO)

As illustrated in Section 36.3, platelet deficiencies hamper the development of improved therapeutic regimens for hematology and oncology patients, as well as in their clinical management [22, 27]. The possible use of TPO to abrogate these disorders has also been debated (Section 36.3). The PK of rhTPO therapy was mathematically modeled in terms of ODEs and solved numerically using the Euler method. This extension was simulated in conjunction with the thrombopoiesis model described in Section 36.2 (see also Refs. 37 and 38). The independent PK model for rhTPO was similar in its structure to that of endogenous TPO, although the kinetic parameters were assumed to be different. The reason for this lies in the fact that exogenously administered synthetic molecules have been shown to differ from the endogenous analogues in a number of characteristics [32]. The model extension also assumes competitive binding of TPO and rhTPO to cell receptors. When describing the PD of the drug, its effects were considered similar to those of the endogenous protein, the latter already existing in the model. Parameter calibration of the model, as well as its retrospective and prospective validation in different species, is detailed in Section 36.5.

36.4.3 Modeling Combination Therapy: Chemotherapy and TPO Support

The consideration of TPO as a potential candidate for alleviating chemotherapy-induced TP in patients with malignant disorders (see Section 36.3) introduces the

issue of combination therapy. The addition of TPO to a cytotoxic-drug-affected scenario, allowing restoration of the damaged thrombopoietic system, can be described via minor manipulation of the basic mathematical model. To do this, one should take into account the effect of chemotherapeutic drugs on the thrombopoietic lineage. Chemotherapy nonspecifically damages all dividing cells, particularly progenitor cells of the thrombopoietic lineage. These targets are represented by the UCP and CP compartments of the TPO model (Section 36.2). Accordingly, the model assumes that the cytotoxic drug eliminates dividing cells in a concentration-dependent manner and, possibly (depending on the drug), in a cell-cycle phase-specific manner. The model incorporates the PK of the drug, to obtain the time course of drug concentrations in blood and bone marrow. Subsequently, a PD model for this drug is applied: the apoptosis probability of a dividing cell is calculated as a function of its position in the cycle and of the current drug concentration.

After constructing such a model and validating it, drug developers and treating physicians can explore the unlimited space of possible conjugate treatments, in which the side effects of chemotherapy are suppressed by use of exogenous TPO. The model allows examining different treatment regimens, predicting their possible outcomes, and selecting the best possible treatment strategies, while avoiding adverse effects, such as those observed in clinical trials of TPO. This identification of improved treatment strategies can be done for the general population, as well as on a patient-specific basis, the latter requiring the specific model parameters of the treated patient, which can be evaluated using the individual platelet profiles post drug intervention.

36.5 USING THE VALIDATED MODEL FOR PREDICTING IMPROVED DRUG EFFICACY/TOXICITY PROFILE

As explained in Section 36.3, clinical evaluation of IL-11 and TPO was obstructed due to safety problems. It was therefore imperative to investigate the mathematical models of TPO-mediated thrombopoiesis and IL-11-induced fluid retention (Sections 36.2 and 36.4), in order to suggest how to overcome the limitations involved in the development of these drugs. We show in this section how species-specific model parameters can be evaluated and the means by which retrospective and prospective validation of the mathematical models is achieved. Thereafter we discuss model use for predicting improved chemotherapy and supportive administration regimens.

36.5.1 Model Validation by Retrospective Human Study Results: IL-11 and TPO

Since modeling IL-11-mediated BVE has employed the specially developed multiple modeling approach (see Section 36.4), the previously depicted diverse models are considered validated and of predictive capability only upon their arrival at unified volume dynamics. The study therefore consisted of two essential steps: experimentally based calibration and parallel assessment of model simulation-derived BVE behavior. These procedures are described next [36].

In the first stage, model parameters were successfully calibrated to retrospectively retrieve clinically evaluated blood volume measurements following daily IL-11 administration of 25 μg/kg doses to healthy volunteers for a week [35]. The data

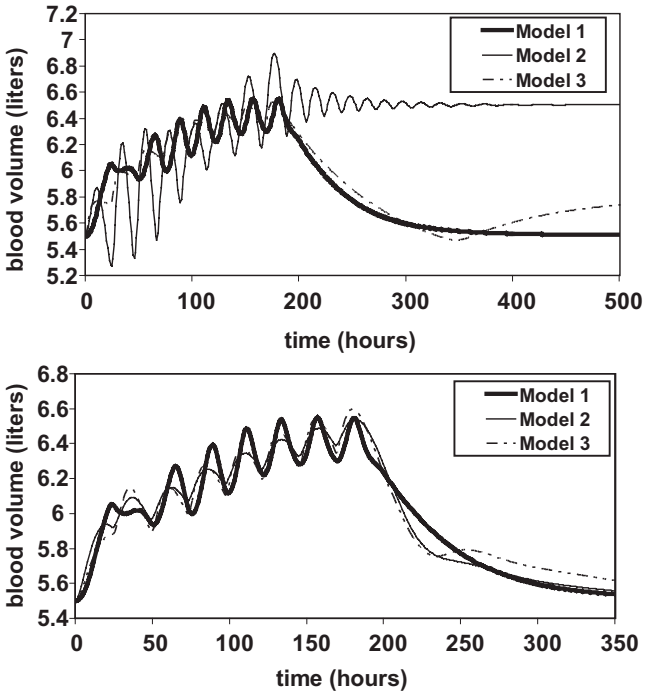


FIGURE 36.3 Comparison of alternative mathematical models for BVE dynamics following calibration by results of a clinical IL-11 study. Blood volume (liters) measured during one week of IL-11 therapy (7 daily doses of 25 μg/kg) was taken from a previous study in healthy humans. Three models, calibrated with data from either the therapeutic days (upper panel) or both the therapeutic and post-therapeutic windows (lower panel), were simulated under the described experimental treatment schedule. (Data adapted from Ref. 36.)

that served for approximation were collected during the first week, that is, within the therapeutic time frame. However, subsequent simulations of the models under the same regimen failed to generate unified behavior of BVE dynamics (Fig. 36.3, upper panel). In contrast, when simulations were preceded by calibration of the models using data from stages both within therapy (the first week) and up to one month following treatment termination, the output dynamics were highly similar between the models (Fig. 36.3, lower panel). In fact, the observed high correlation between the numbers of experimental points used for model calibration, and the models' increased similarity (data not shown), strengthened the possibility that by using more data points, model similarity and thus reliability and clinical predictability can be improved.

In the second stage of the work, the predictability of the models was evaluated in a wider therapeutic spectrum. The models were simulated under IL-11 treatment strategies of various durations, various interdosing intervals, and various dose intensities, where model-derived dynamics were again compared to assess the model robustness in portraying BVE dynamics. Highest values of similarity between models, as shown by the difference index, were observed when the average IL-11 dose per day of the tested treatment was close to that of the experimental treatment

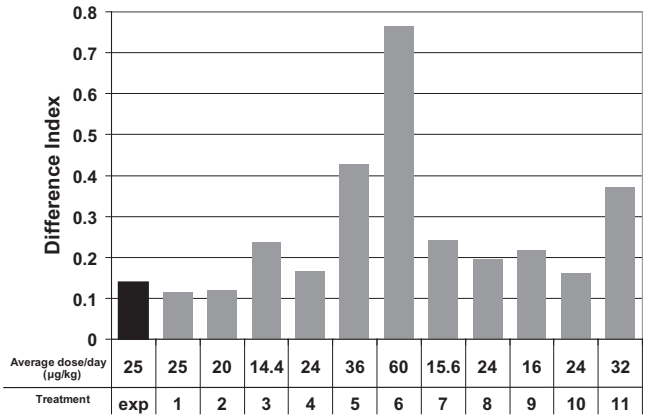


FIGURE 36.4 Model-derived BVE dynamics in therapeutic regimens that are close to experimental schedules in average dose per day values. Model simulations under the experimental schedule (treatment exp) and other regimens of various durations, doses, and interdosing intervals (treatments 1–11), following calibration with clinical measurements, are compared using the difference index. (Data adapted from Ref. 36.)

of daily 25 μg/kg doses (see Fig. 36.4 as an example). This suggests that in this example of an obscure toxicity mechanism, one can trust the model-derived BVE predictions for various IL-11 treatments, provided their average daily dose of IL-11 is in proximity to that used in the original clinical experiment.

The mathematical method applied in the case of IL-11 shows that given preliminary experimental data from various stages of therapy, beginning at phases within the therapeutic window and ending at the recuperated steady state, the different models reliably predict dynamics of water retention within a certain span of IL-11-administration strategies. Considering the recommended IL-11 levels (10–100 μg/kg/day), and the above model-derived conclusions, clinical studies evaluating BVE within concentrations of 10, 20, 30, . . . μg/kg/day are required to form a complete predictability frame of BVE within all relevant treatment scenarios. This would then allow appraisal of the clinical applicability of each of these IL-11 therapy schedules, as well as others.

As in the above-presented process of IL-11 model evaluation, clinical information was used for the TPO case. A thrombopoiesis computational model was designed on the basis of the mathematical description of TPO-induced thrombopoiesis (elaborated in Sections 36.2 and 36.4), to enable simulation and evaluation of *in vivo* platelet formation and to suggest therapeutic TPO regimens of improved efficacy and reduced immunogenicity [38]. The computer model was adjusted and validated for murine, simian, and human cases, as will be elaborated later.

Currently, human validation of the thrombopoiesis computer model is possible only in retrospective, as the drug has not yet undergone the appropriate regulatory procedures enabling human administration. To retrospectively validate the model, it was calibrated using a set of biologically realistic parameter values, so that homeostatic behavior (i.e., a normative count of 320,000 platelets/μL blood) was retrieved in untreated conditions. Next, simulation of the computerized model under

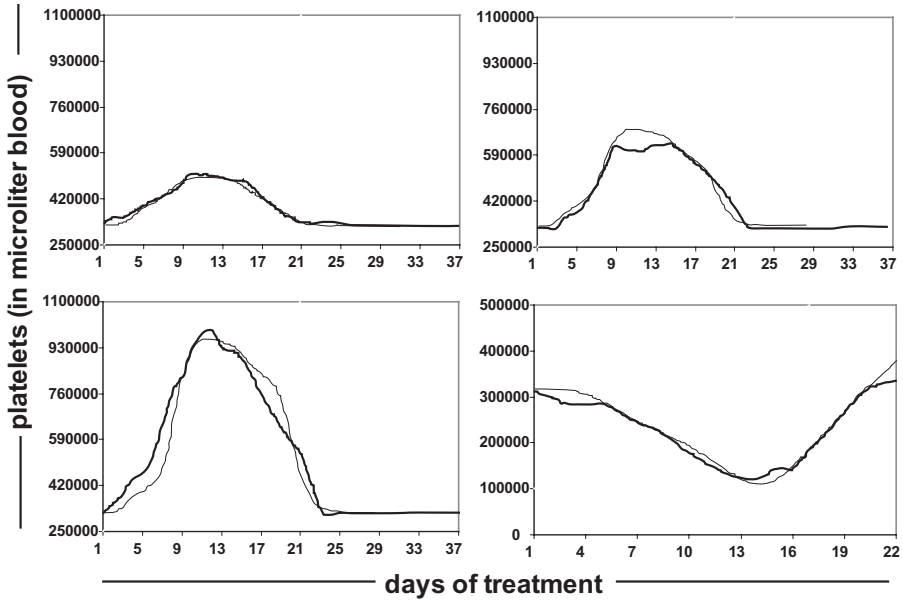


FIGURE 36.5 Model predictions of platelet profiles in patients treated by TPO and chemotherapy compared to clinical results. Average platelet counts in human patients are plotted, following a single IV bolus rhTPO administration of 0.3 μg/kg (upper left panel), 1.2 μg/kg (upper right panel), or 2.4 μg/kg (lower left panel), or an IV infusion of doxorubicin for 3 days, the total dose being 90 mg/m^2 (lower right panel). Simulation-generated curves are shown by thick lines; clinical results are shown by thin lines.

recombinant human TPO (rhTPO) administration was carried out. Data from a clinical trial [39], which included PK information (i.e., rhTPO concentration in blood) and accurate platelet counts in response to different TPO dosages, served the calibration process: three patients were assigned to a single IV bolus administration of each of the four dosages 0.3, 0.6, 1.2, or 2.4 μg/kg. The three platelet count curves for each dosage were averaged and a single parameter set, which enabled the model to accurately retrieve platelet dynamics observed under the various treatment regimens, as shown in Fig. 36.5, was identified. This parameter set was determined as the representative for the "average patient."

While TPO therapies pose many questions, such as its effects on elevated platelet counts in clonal thrombocytosis, the opposite problem, namely, that of reduced platelet counts, introduces equally significant challenges. Since TP is a common dose-limiting side effect of cancer chemotherapeutics, as discussed in Sections 36.3 and 36.4, accurate predictions of the chemotherapeutically reduced platelet dynamics are of importance when planning treatments. To allow predicting the effect of cytotoxics on thrombopoiesis in individual patients, the average "Virtual Patient" was tested for its ability to retrieve the outcomes of a standard chemotherapeutic treatment by doxorubicin. The model was successfully calibrated in reference to clinical published experimental data [40], as shown by Figure 36.5 (lower right panel) and improved TPO regimens were suggested. Prospective validation of the generality and clinical predictability of the model is warranted. A different

biomathematical approach, elaborated in Section 36.7, uses data from human and animal cell cultures and from preclinical studies that are available in the pharmaceutical industry, in order to develop therapeutic strategies with minimal suppression of thrombopoiesis.

In conclusion, the thrombopoiesis computer model was successfully calibrated to accurately retrieve relevant clinical information reflecting TPO therapy, as well as chemotherapy, but it is yet to undergo prospective human validation. Importantly, the models described here for different thrombopoietic growth factors are each targeted toward opposing aspects of therapy: while the IL-11 mathematical model attempts to define the toxicity associated with drug-induced alleviation of TP, the computerized TPO model is aimed at accurately predicting the direct beneficial results of such therapy on platelet restoration.

36.5.2 Model Validation in Prospective Animal Trials: TPO Applied to the Virtual Mouse and Virtual Monkey

To use the model predictions for clinical decision making, one must still substantiate the superiority of the model-suggested improved TPO regimens. This task must be carried out in animals first, not only due to safety issues, but also because typically in such cases, the agent in question is not yet approved for the treatment of patients. Once a proof of concept in animals is provided for its power to suggest improved regimens, the model can become instrumental during the clinical phases of drug development, for avoiding excessive and unnecessary toxicity and for reducing the number of patients in Phase I of the clinical development. These steps are expected to pave the road for routine clinical use of the computer-based prediction tool.

The underlying assumption in this work was that improved TPO schedules are those employing the smallest drug doses required to achieve the desired efficacy. This assumption is based on a biomathematical study that examined the effect of dose intensities on drug immunogenicity. Results of this work suggest that for a given immunoreactive system, there exists a critical drug dose for which the relevant immunogenic threshold is expected to be exceeded, thus affecting patient health [41].

To validate the model's predictions in preclinical experiments with BALB/c mice and rhesus monkeys, the thrombopoiesis model was calibrated to reflect murine or simian thrombopoiesis. This was achieved by using literature-derived data. The species-adapted models, Virtual Mouse and Virtual Monkey, were subsequently used to adjust the improved TPO treatment to the species in question and test this treatment in animal experiments. This work is described in Ref. 38.

Parameter calibration of the thrombopoiesis computer model was performed for fine-tuning the model to accurately describe thrombopoiesis in each species. This work involved definition of a biologically realistic range of values for each parameter in murine thrombopoiesis [28, 42–47] and simian thrombopoiesis [22, 48–54], which were then entered as the initial parameter values, subsequently to be fine-tuned according to the specific tested population. Ability of the model to retrieve platelet profiles in each animal group was then tested.

Next, the prediction accuracy of the thrombopoiesis computer model was validated in mice. Specifically, by simulating the model it was predicted that platelet counts, similar to those achieved with the accepted TPO administration schedule, can also be generated under different schedules of appreciably reduced TPO doses (Fig. 36.6, upper panel). Hence, two different administration regimens were

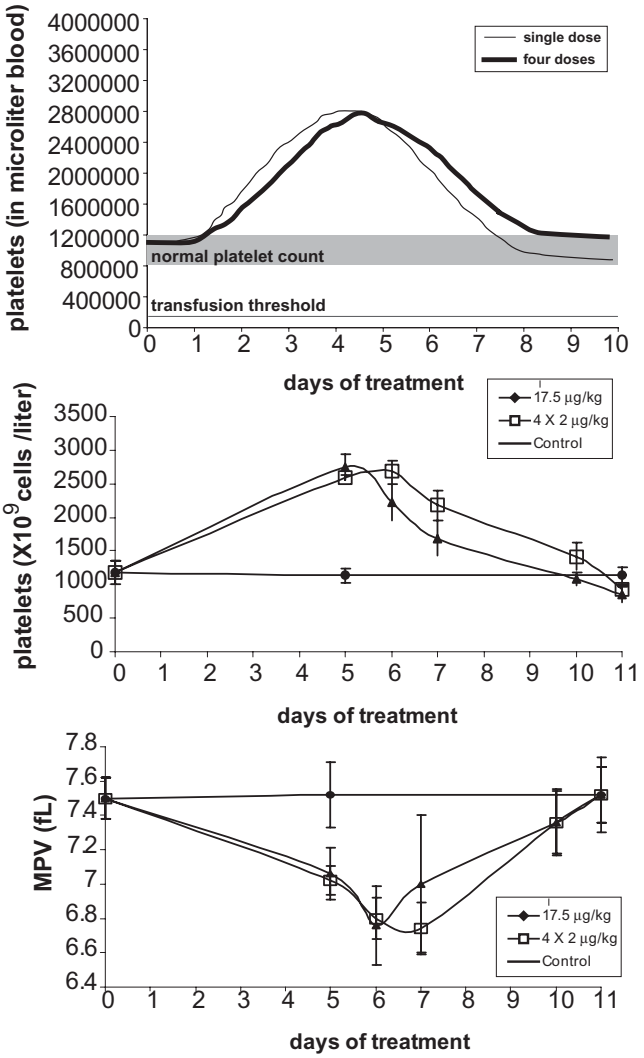


FIGURE 36.6 Model predictions of platelet profiles in mice treated by TPO as compared to experimental results. (Upper panel) The thrombopoiesis model-generated predictions indicating similar efficacy in platelet formation between a "conventional" single-dose TPO treatment of 17.5 µg/kg, and a model-suggested reduced TPO treatment of four daily doses of 2 µg/kg each, comprising only 10–45% of the standard regimen. Experimental results of platelet formation (middle panel) and MPV measurements (lower panel) following conventional rmTPO therapy (black diamonds) and the alternative therapy (white squares) in mice, according to the above schedules, validate the model predictions. Treatments are initiated at day 0. Average ± SD of five mice are shown, per each entry. (Data adapted from Refs. 37 and 38.)

experimentally applied to mice clustered in two experimental arms, and their subsequent responses were compared. Mice of the first arm (A) received a standard regimen consisting of a single injection of 17.5 μg/kg recombinant murine TPO (rmTPO), which was well below the reported saturating level [42]. The second arm (B) tested the model-generated proposition that the same platelet yields can be obtained in mice receiving a total dose of 8 μg/kg rmTPO, divided over four equal daily injections, whereas the null hypothesis here was that a significantly smaller total dose of rmTPO would be less efficient in elevating the platelet counts.

The results of the experiments, presented in Fig. 36.6 (middle panel), clearly show that the platelet profile of arm A (a regimen of one 17.5 μg/kg rmTPO injection) is similar to the profile of arm B (applying a regimen of four daily 2 μg/kg rmTPO doses). The differences are statistically insignificant, as evaluated by the Student's t-test. The average profiles of both arm A and B peaked at fairly the same time (day 5 vs. day 6, respectively) and at similar mean platelet counts of $2741 \pm 193 \times 10^9$/L and $2685 \pm 164 \times 10^9$/L, respectively. The latter schedule resulted in a slightly extended thrombocytosis. MPV, known to decrease in platelet production induced by low dose TPO in mice [55], was compared between arm A and arm B as well (Fig. 36.6, lower panel). Results show that the familiar phenomenon of MPV reduction also occurred similarly in both groups. Once again, arm A had preceded arm B in reaching its nadir by about 24 hours (6.76 fL on day 6, vs. 6.74 fL on day 7, respectively). Specific adverse effects were not observed following either treatment.

In order to evaluate in rhesus monkeys the efficacy of the treatment regimen, already validated in mice, we first checked the ability of the simian thrombopoiesis model to predict individual monkey responses to different TPO treatments. Next, the simian response to the model-suggested schedule was simulated and the resulting predictions were compared with the platelet counts that were experimentally obtained under the model-suggested schedule.

To this end, model parameters were first evaluated to fit the empirical platelet profile of a single rhesus monkey. The quantitatively adequate simulations of thrombopoiesis response to treatment were apparent from their resemblance to the empirical results (Fig. 36.7). This calibrated model was further validated in several other monkeys, each receiving a different drug schedule (see schedule in Fig. 36.8, top panel).

Results in Fig. 36.9 demonstrate that the model predictions run remarkably close to the empirical data points. Note that as the platelet counts were monitored in these monkeys only once weekly, a mismatch is introduced into the comparison between the empirical results and the daily predicted counts. Thus, there is no reason to assume that the peaks in the predicted responses on days that were not tested empirically did not actually take place.

36.5.3 Predicting the Optimal TPO Efficacy/Toxicity Ratio in Monkeys

Once verified, the Virtual Rhesus model was simulated for identifying an improved TPO administration regimen. The model-based regimen was then evaluated for verifying its improved efficacy and safety profile. This was done in two monkeys (see Fig. 36.8, bottom panel). The resulting elevation in platelet counts peaked at 1700–

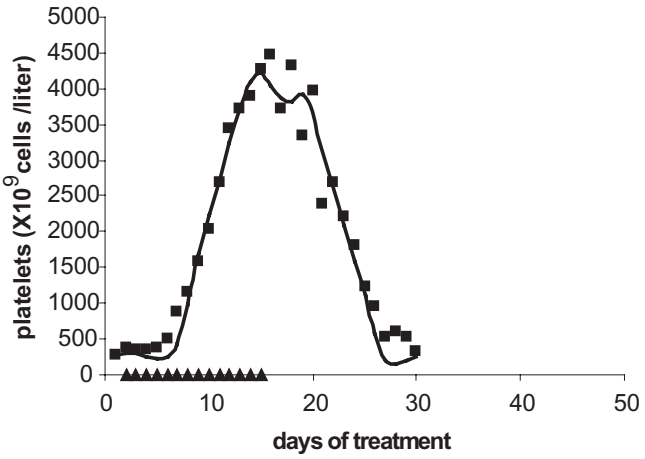


FIGURE 36.7 Comparison of model predictions to empirical data of TPO therapy in a rhesus monkey. Daily experimental measurements (rectangles) are shown as well as model simulations (solid line) of platelet counts of one monkey treated by TPO. Fourteen daily doses of 5 μg/kg TPO were applied, administration days marked by triangles. (Data adapted from Refs. 37 and 38.)

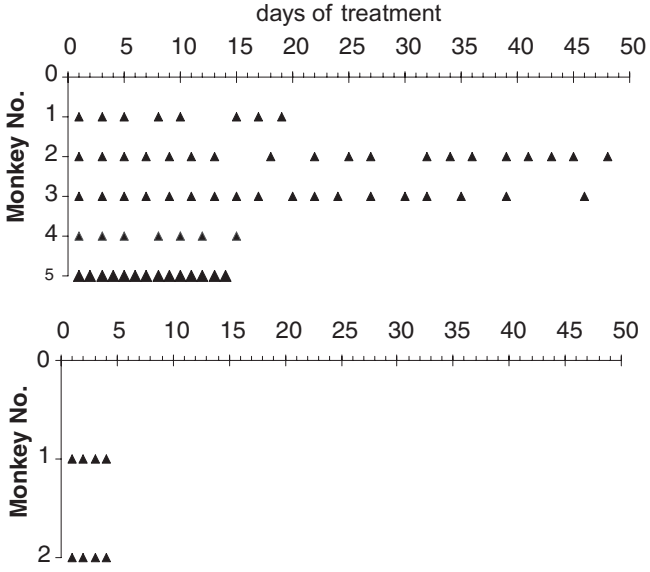


FIGURE 36.8 TPO administration schedules applied in simians for model validation. (Upper panel) Five different schedules, comprising various combinations of 5 μg/kg doses of recombinant full-length rhesus monkey TPO (each dose indicated by triangles), were individually applied to the studied monkeys. (Lower panel) Model-suggested TPO schedules (also using doses of 5 μg/kg) applied to two monkeys.

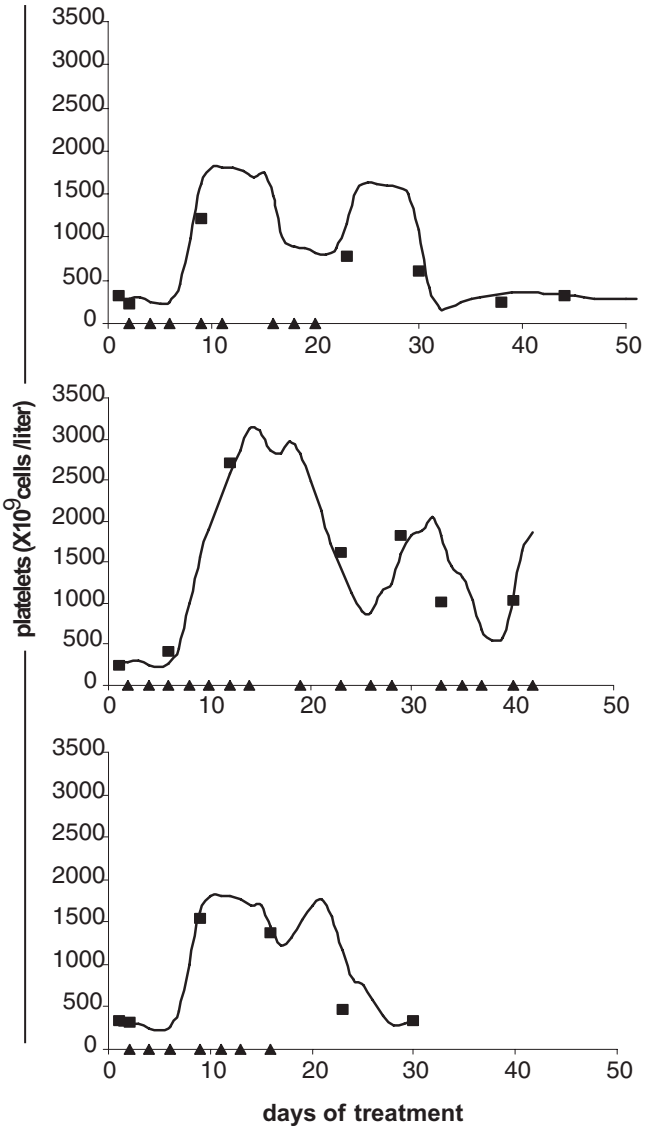


FIGURE 36.9 Comparison of model predictions to experimental platelet profiles of rhesus monkeys under various TPO treatment schedules. Three monkeys (upper, middle, and lower panels) were subjected to individual TPO regimens, consisting of multiple dosing treatments of 5μg/kg TPO, administration days marked by triangles. Experimental measurements of platelet counts in blood were performed weekly or biweekly (squares) and are plotted against model simulations (solid line).

2400×10^9/L following each treatment cycle. The results of a second cycle of the same treatment were similar to those of the first one in showing no neutralizing antibodies. Only when the dosing cycle was applied for the third time were low antibody titers detectable, which did not jeopardize TPO's efficacy and did not result in decreased platelet counts. The individual empirical responses of the two monkeys

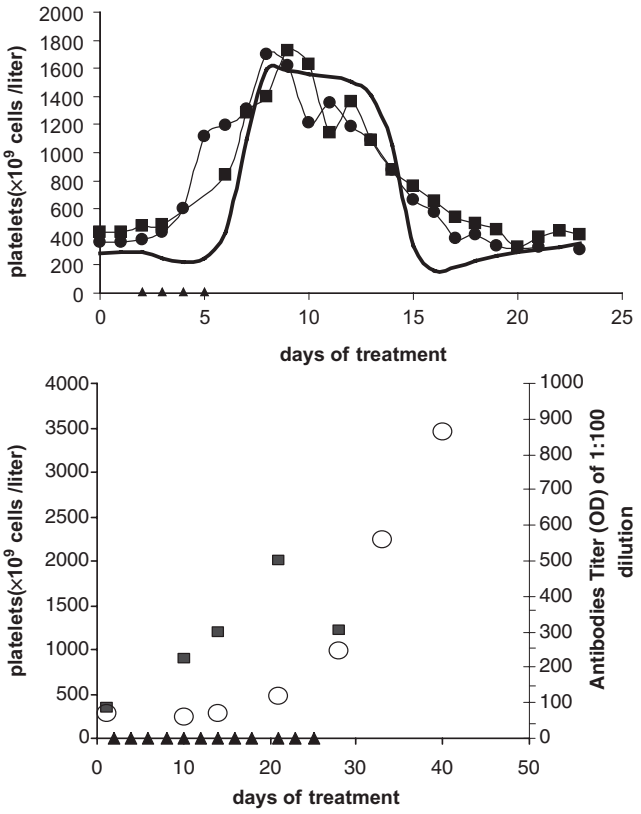


FIGURE 36.10 Superiority of the model-suggested TPO treatment schedule validated in rhesus monkeys, as compared to other regimens. (Upper panel) Empirical platelet profiles of monkeys under the model-suggested TPO regimen of four daily 5 μg/kg doses (solid squares and circles) are plotted; administration days are marked by triangles. (Lower panel) Antibody titer and platelet profiles of a monkey undergoing an arbitrary treatment by 12 TPO doses.

to the first treatment cycle are shown in Fig. 36.10 (top panel) (to be compared with a highly immunogenic response of a monkey who underwent another TPO treatment, Fig. 36.9, bottom panel).

These results show that the model-predicted administration regimen of smaller TPO doses with an interval of 24 hours yields platelet counts that are equal in effect to the more than double dose regimen, administered as a bolus injection. This experiment joins previous *in vivo* experiments with other drugs in verifying a mathematical theory discussed in Section 36.1.1, which essentially suggests that treatment efficacy can be decisively influenced by modulating the interdosing interval according to the internal cell kinetics. The monkey experiment supports the model prediction of an equally efficient and nonimmunogenic treatment, if dose is fractionated by an appropriate dosing interval. Importantly, this schedule, adopted for improving safety of TPO administered for platelet harvesting in monkeys, has been in use for the last five years or so. No adverse effects have been associated with this model-suggested treatment.

In general terms, the experimental results in both animal species supported and validated the predictions of the mathematical model that more efficacious treatment with TPO can be implemented. Although intuitively it may not seem beneficial for the patient to replace a single injection by multiple doses, it is clearly of significance for safety considerations.

The computerized mathematical model is capable of successfully predicting treatment scenarios not yet tested experimentally, as well as of identifying safer regimens. This tool is expected to be of aid in suggesting improved drug strategies for an individual or for a patient population. Human trials are necessary for testing the suggested improved TPO strategies, possibly in conjunction with chemotherapy.

36.6 USING THE THROMBOPOIESIS MODEL FOR PREDICTING AN UNKNOWN ANIMAL TOXICITY MECHANISM

Several pathophysiological mechanisms can account for drug-induced TP (see Section 36.3), and the actual underlying mechanism in each particular case can have important therapeutic implications. Yet, no easily applicable noninvasive laboratory tests are available for distinguishing between the different mechanisms for TP. In this section, we describe the manner by which mathematical modeling can help in understanding the dynamics and etiology of drug-induced TP.

A monoclonal antibody-based drug, developed against a platelet-unrelated antigen and currently under preclinical evaluation, was found to possess cross-reactive effects eliciting severe TP in monkeys. Despite routine laboratory testing and histological examination of bone marrow of affected monkeys, the drug's mechanism for inducing TP has not been elucidated. In an attempt to decipher the underlying mechanism, we used the mathematical model for TPO-regulated thrombopoiesis [37, 38], which was previously formed (as described in Section 36.2) and validated *in vivo* (as depicted in Sections 36.4 and 36.5). This model was extended to include the effect of the drug on MKs and platelets. Since the mechanism is still unknown, several biologically plausible alternatives were examined. Antibodies can exert their effect either by antibody-assisted phagocytosis or by complement-mediated direct toxicity [56]. In the first mechanism, antibody-covered platelets or platelet-forming MKs would be efficiently removed by macrophages that bear specific antibody-recognizing receptors. In the latter case, platelet-bound antibodies activate the complement pathway that leads to cell membrane perforation and cell destruction (Fig. 36.11).

Mathematical implementation of both antibody-mediated killing mechanisms into the PD-extended model was performed as follows. For complement-mediated toxicity, an "accumulated hits" model, according to which each platelet suffers from cumulative damage ("hits") induced by antibody-mediated complement binding, was suggested. Upon accumulation of a certain number of "hits," the platelet is permanently damaged. The resulting probability density function, $P(t)$, describing a fraction of platelets with a given number of "hits" in time t postexposure, is given by the gamma function

$$P(t) = \frac{(\alpha t)^m e^{-\alpha t} \alpha}{m!}$$

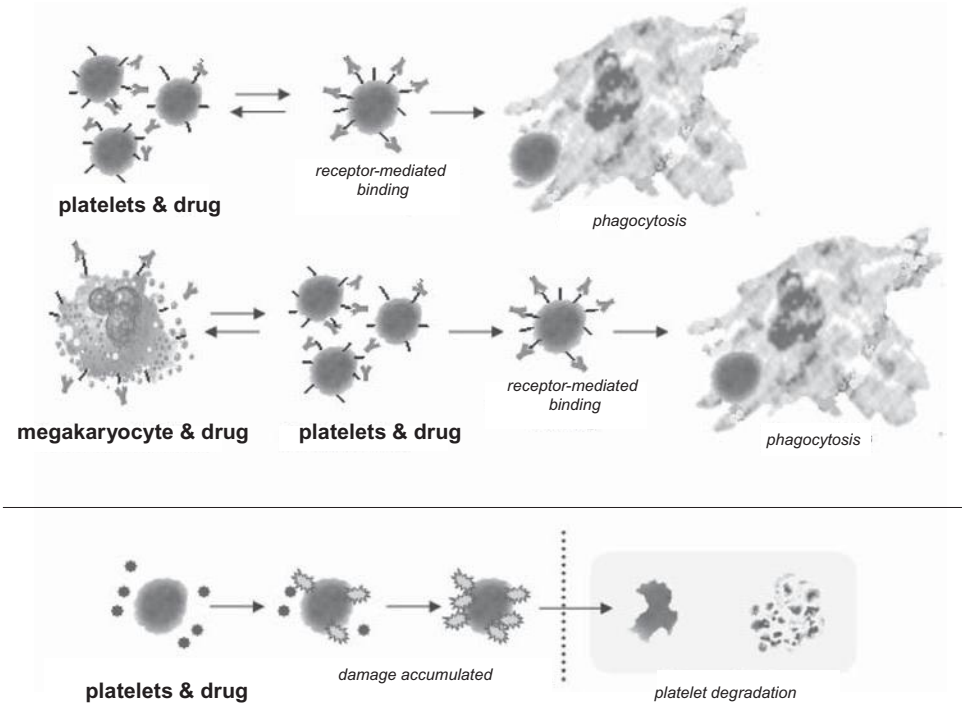


FIGURE 36.11 The "phagocytosis" putative mechanism and the "hits" putative mechanism of drug-induced thrombocytopenia. In the "phagocytosis" mechanism (upper panel), drug molecules bind to platelet and megakaryocyte surface antigens, leading to their phagocytosis by the reticuloendothelial system. In the "hits" mechanism (lower panel), drug molecules bind to platelet surface antigens, leading to complement activation and direct destruction of the cells.

where m is the number of hits needed for platelet destruction, and α is the rate of hit formation. The rate of hits is given by a linear function of the antibody concentration in blood:

$$\alpha = aX + b$$

where X is antibody concentration, and a and b are parameters.

For the case of antibody-mediated phagocytosis, the "phagocytosis" model, it was assumed that the rate of platelet "capture" by macrophages has a Hill's function form, depending on the number of antibodies that are bound to the platelet's surface. This is described as follows:

$$B(i) = \frac{B_{\max} i^z}{K^z + i^z}$$

where $B(i)$ is the rate of capture of platelets that possess i bound antibodies, and K and z are parameters. Since binding and dissociation of antibodies from the

platelet surface are stochastic processes, the distribution of platelets with respect to the number of bound antibodies, V_i, was explicitly calculated, so that the rate of antibody-induced platelet elimination is given by

$$R = \sum_i V_i B_i$$

Antibodies can act against mature platelets, bone marrow-derived MKs, or both. Hence, several combinations of these suggested drug-toxicity mechanisms were implemented in the extended model. Retrospective results of real-life experiments in a number of individual rhesus monkeys [37, 38] were used for comparison with the simulated outcomes of these various alternative models. For each combination, the PD-associated parameters of the extended model were adjusted to best fit to these experimental results. Only one of the combinations was expected to consistently retrieve experimental data, and thus be identified as the preferable mechanism underlying this antibody-mediated TP. Systemic platelet profiles in individual monkeys following administration of multiple or single doses of the drug were compared with the best-fit profiles produced by models with different drug effect mechanisms (Fig. 36.12). The analysis of these simulations indicated that the "hits" model failed to predict dynamics of the drug-induced TP, while the "phagocytosis" model coincided with experimental data. Model results also show that by assuming toxicity to both platelets and MKs, rather than to just platelets, more precise predictions can be yielded.

We conclude that the developed computerized thrombopoiesis model superimposed by mathematical models for putative toxicity mechanisms can retrieve adverse thrombocytopenic effects recorded empirically in simians. Different models of drug-toxicity mechanisms yield different profiles of blood platelets, yet the antibody-mediated phagocytosis of platelets and MKs seems the most plausible mechanism of the drug-induced TP in this situation. In this manner, mathematical modeling can help decipher the underlying mechanisms of other disorders.

36.7 TRANSITION TO PHASE I

Drug development is a costly and time-consuming endeavor, due to its requirement for enormous collections of data concerning the efficacy and safety of the proposed drug. The ability to extrapolate toxicity and efficacy data from animal to human is therefore of great importance for efficiently advancing development of pharmaceuticals. Yet, despite the efforts invested in this direction, and the great advances achieved in recent years, extrapolation of data from animals to humans is still considered unreliable [57–59]. In this section, we provide a detailed description of an algorithm, which in conjunction with data from cell cultures and animal experiments, can be used for the modeling of clinically stimulated (drug-induced) TP in humans, and we show how this method enables good clinical predictability of this disorder.

As discussed in Section 36.3, TP can result from therapeutic intervention, such as anticancer chemotherapy. The mathematical model of thrombopoiesis, described in Section 36.2, was used as a basic model for retrieving clinical cytotoxic drug-

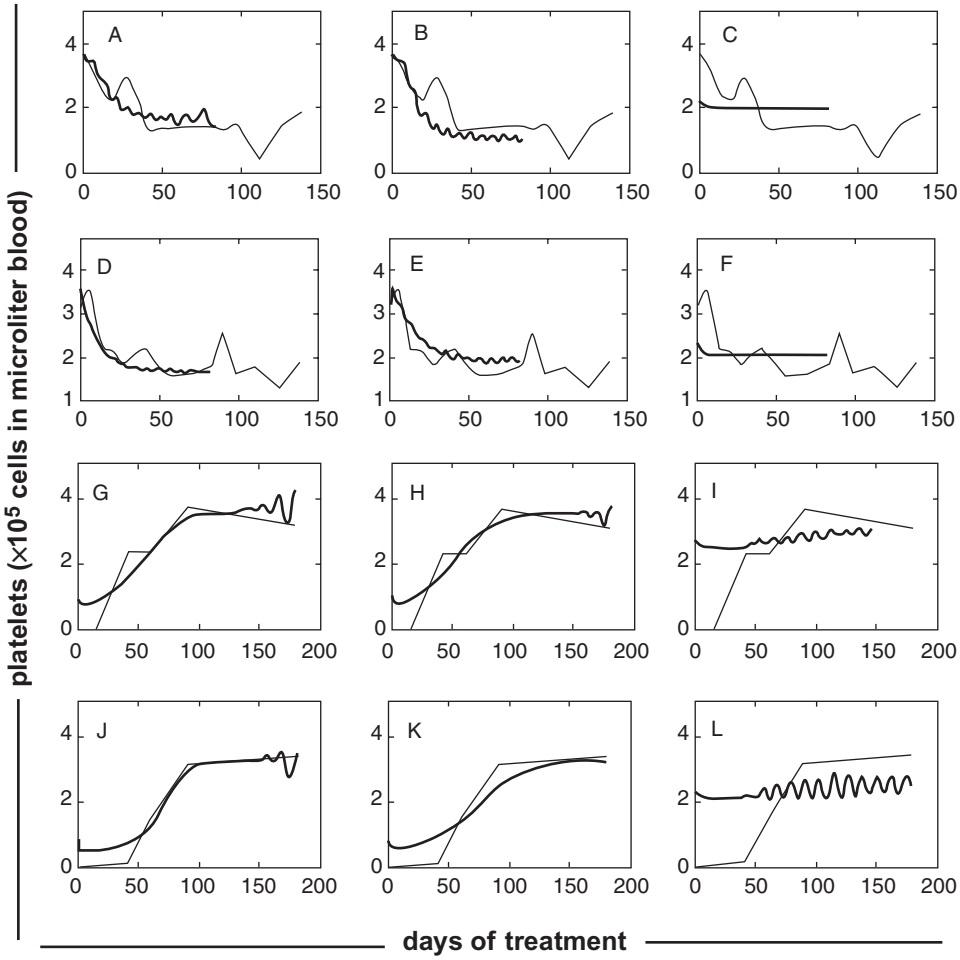


FIGURE 36.12 Model retrieval of drug-induced thrombocytopenia in rhesus monkeys. Platelet dynamics derived from experiments in four monkeys, receiving a treatment of multiple doses (A–F) or a single high dose (G–L) of the drug. The effects of each treatment on the monkey's platelet profile were simulated by the three mathematical models of alternative drug-toxicity mechanisms. Model predictions were then statistically compared with the experimental results. Simulation results are for the "phagocytosis" model assuming that the drug targets platelets alone (left column panels), for the "phagocytosis" model assuming that the drug targets both platelets and megakaryocytes (middle column panels), or for the "hits" model assuming that the drug targets only platelets (right column panels). Panels A–C, D–F, G–I, and J–L correspond to data from each of the four monkeys. Empirical data (thin lines) is shown versus simulation-derived dynamics (thick lines).

induced TP. Yet to obtain a reasonable approximation of the predicted toxicity in humans, based on preclinical data, additional assumptions and simplifications are required. These are detailed next.

First, translation of drug PD from the preclinical to the clinical stage is necessary. One must consider (1) differences between *in vitro* and *in vivo* data and

(2) differences between PD parameters of different species. Both variation types involve built-in inaccuracies. With respect to the comparison between *in vitro* and *in vivo* experiments, a few issues must be taken into account. Cells *in vitro* are more sensitive to a drug, and thus more susceptible to drug-induced apoptosis. They have higher mitotic indices due to less contact inhibition and are usually exposed to constant levels of drug concentration over time. Cells in the physiological, whole-organism context, however, are of lower sensitivity to a drug; the surrounding microenvironment, consisting of high proliferating and less drug-susceptible cells, provides a constant influx of healthy cells into the total pool, thereby limiting the damage caused by the drug [60]. Differences in exposure to growth factors between the two experimental settings exist as well. Drug sensitivity differs not only between *in vitro* and *in vivo* settings, but also in various species, which may differ in size of cells, mitotic indices of various compartments and differential stages of cells, apoptotic indices, transit times, and sensitivity to hormones [61].

In order to replicate clinical use of the drug, the basic mathematical model is extended to incorporate an additional formula for the drug PD. It is assumed that bone marrow cells are exposed to systemic drug concentration at any time, as the tissue is highly vascularized. The model also assumes that cells at different developmental stages, denoted by a subscript X (e.g., UCP, CP, EP), are of diverse sensitivity to the drug. The functional relation between the concentration of the cytotoxic drug in blood (CD_{bl}) and the cytotoxic effect (CE) is given by the equation

$$CE_X(t) = f(CD_{\mathrm{bl}}(t)) \tag{36.14}$$

where CE_X denotes the fraction of bone marrow thrombopoietic cells of a differentiation stage X, eliminated following exposure to CD_{bl} at time t ($CD_{\mathrm{bl}}(t)$). The dependence is represented by function f, where $0 \le f\,(CD_{\mathrm{bl}}(t)) \le 1$ for any t.

Most cytotoxic drugs target mitotic phases of the cell cycle and are thereby more harmful to proliferating, rather than resting, cells. Accordingly, by further subdividing the model compartments into cell-cycle phases (G0-G1 and S-G2-M subcompartments), a more accurate prediction of drug toxicity can be obtained. For example, in the above model, representation of UCP and CP compartments (see Section 36.2) uses cell-cycle length instead of amplification rate. This allows us to calculate, not only the total number of cells remaining at every time point after drug application but also the number of cells at every age and cell-cycle phase. In EP compartments, the age and the position in the endomitotic cycle are synchronized; thus there is no need for additional distribution. The rest of the compartments, consisting of nondividing cells, are not considered susceptible to the standard cytotoxic drug and are therefore not subdivided in this manner. Cytotoxic drugs that selectively target these stages can be addressed after subdivision of those compartments. In this complex form of the model, parameters (e.g., compartments, sizes, transit times) are evaluated differently for all the species examined, while the model equations themselves retain the same structure.

Following adaptation of the model equations to include the PD of the drug, parameters are calibrated using the available experimental information. Preclinical toxicity data to be used by the model consist of the platelet measurements over time in one animal of a chosen species (S), which has shown (in previous *in vitro* studies) higher sensitivity to the drug than other species. Various sets of data are obtained

for a wide range of drug doses, so that different thrombocytopenic responses, from low toxicity to grade 3–4 toxicities, are considered.

The model also exploits data from cell culture assays. For example, for the estimation of the cytotoxic drug concentration, the model uses IC_{20}, IC_{50}, and IC_{90} (the concentrations of the drug leading to inhibition of 20%, 50%, and 90% of *in vitro* cell growth, respectively, as compared to untreated cells). These are obtained from toxicity tests of the platelet lineage-committed bone marrow cells (the CFU-Meg assay), in both human and species S-derived cells [62]. In the complex form of the model, one may also use experimental tools of cell-cycle analysis, such as standard cell-sorting assays.

Based on this data, three functions f (Eq. 36.14), denoted as $f_{\text{inVitroHu}}$, f_{inVitroS}, and f_{inVivoS} for human cell cultures, species S cell cultures, and preclinical S species studies, respectively, can be evaluated. In estimating the function f_{inVivoS}, it is necessary to consider only the drug's killing effect on bone marrow cells of compartment X, the depletion of which is mainly responsible for platelet nadir (see Eq. 36.14). X is identified by the time of the nadir after drug application, taking into account the transit times of the different bone marrow compartments. As a first approximation, only one compartment X of drug-sensitive cells is assumed.

The parameters of function f in the clinical scenario (f_{inVivoHu}), which cannot be estimated as in the other three cases due to lack of data, are thereby calculated according to their counterparts. First, it is assumed that between different species, there is a linear relation between the drug killing effect observed *in vivo* and *in vitro* (i.e., the $f_{\text{inVivo}}/f_{\text{inVitro}}$ ratio is constant between diverse species). The function f_{inVivoHu} is thereby obtained by shifting the IC values on the concentration axis according to this relation, using the *in vitro* data of IC_{50} ($IC_{50\text{inVitroHu}}$) and IC_{90} ($IC_{90\text{inVitroHu}}$). The relation itself is found by comparing the *in vitro* and *in vivo* data for species S. Then the shift of f_{inVivoS} to f_{inVivoHu} on the concentration axis for IC_{50} is computed by the equation

$$IC_{50\,\text{inVivoHu}} = \frac{IC_{50\,\text{inVivoS}} \cdot IC_{50\,\text{inVitroHu}}}{IC_{50\,\text{inVitroS}}} \tag{36.15}$$

The same method can be applied for IC_{90}.

The last step requires simulations of the model with the human parameters, under different regimens, applying the f_{inVivoHu} effect on the same type of bone marrow cells as in species S. The clinical toxicity profile of the drug—that is, the induction and severity of drug-induced TP in humans—is therefore predictable. Importantly, this estimation is a first approximation and a safety factor should be considered prior to initiation of clinical trials.

36.8 CONCLUSION

- Mathematical models are instrumental in increasing the understanding of intricate drug–patient interactions. Specifically, a mathematically based method, termed the Z-method, has been devised for increasing the efficacy/toxicity ratio of chemotherapeutics. The method suggests that safety of cell-cycle-specific drugs can be increased by resonating drug-pulsing with the internal periodicity

of target host cells replication. Experimental verification of the Z-method in mice provides a proof-of-concept for the utility of biomathematics in drug development.

- Increasing model complexity, a prerequisite for the quantitative precision of its conclusions, was performed in order to provide a practical tool for predicting drug effects on platelet counts. To this end, thrombopoiesis models of various mammal species have been developed. Models of TPO supportive treatment have been prospectively validated in mice and monkeys.
- Toxicity effects of IL-11 therapy and chemotherapy have been modeled and various drug regimens were tested. Model validation under data limitation has been examined and the need to collect patient's recovery data has been emphasized. The range of the treatment schedules under which the models could reliably predict the outcomes of drug therapy under obscured biological knowledge has been defined.
- The thrombopoiesis model has been employed for suggesting TPO administration schedules, which would maximize drug safety while maintaining its efficacy. Dose fractionation, having a well-calculated, species-dependent dosing interval, preserves drug effect on platelet counts, yet reduces its immunologic adverse effects below the clinically relevant threshold.
- The above schedule, adjusted by the murine thrombopoiesis model, was validated in mice for efficacy. The monkey-adjusted schedule derived from simulations of the simian thrombopoiesis model, was validated in rhesus monkeys for both efficacy and toxicity. Now the human model may be employed for improving safety of TPO mimetics and other thrombocytopenia-alleviating drugs.
- To the best of our knowledge, this is the first instance of a mathematical model generating quantitative predictions, the precision of which was validated in the preclinical setting.
- The thrombopoiesis model can be used, in conjunction with alternative mathematical models, for deciphering unknown drug-toxicity mechanisms in different species. This can be achieved by comparing preclinical study results with the simulated drug-affected platelet profiles, generated for different models of putative drug-toxicity mechanisms.
- In order to facilitate the transition from preclinical studies to Phase I, the mathematical models for the effect of investigational drugs on different animal species can be adapted accordingly and simulated in the human patient model for predicting parameters, the early estimation of which can economize Phase I clinical trials.

REFERENCES

1. FDA White Paper on Innovation and Stagnation in Drug Industry, Challenges and Opportunities on the Clinical Paths to New Medical Products, March 2004.
2. Agur Z. The effect of drug schedule on responsiveness to chemotherapy. *Ann NY Acad Sci* 1986;504:274–277.
3. Agur Z, Arnon R, Schechter B. Reduction of cytotoxicity to normal tissues by new regimes of cell-cycle phase-specific drugs. *Math Biosci* 1988;92:1–15.

4. Agur Z, Arnon R, Sandak B, Schechter B. The effect of the dosing interval on myelotoxicity and survival in mice treated by cytarabine. *Eur J Cancer* 1992;28A(6/7):1085–1090.
5. Ubezio P, Tagliabue G, Schechter B, Agur Z. Increasing 1-beta-D-arabinofuranosylcytosine efficacy by scheduled dosing interval based on direct measurement of bone marrow cell kinetics. *Cancer Res* 1994;54:6446–6451.
6. Agur Z. Persistence in uncertain environments. In Freedman HI, Strobeck C, Eds. *Population Biology, Lecture Notes in Biomathematics*. Heidelberg: Springer-Verlag; 1982, pp 125–132.
7. Agur Z. Randomness, synchrony and population persistence. *J Theor Biol* 1985;112: 677–693.
8. Agur Z, Deneubourg JL. The effect of environmental disturbances on the dynamics of marine intertidal populations. *Theor Population Biol* 1985;27(1):75–90.
9. Cojocaru L, Agur Z. A theoretical analysis of interval drug dosing for cell-cycle-phase-specific drugs. *Math Biosci* 1992;109:85–97.
10. Kheifetz Y, Kogan Y, Agur Z. Long-range predictability in models of cell populations subjected to phase-specific drugs: growth-rate approximation using properties of positive compact operators. *Math Models Methods Appl Sci* 2006;16(7):1–18.
11. Agur Z, Arnon R, Sandak B, Schechter B. Zidovudine toxicity to murine bone marrow may be affected by the exact frequency of drug administration. *Exp Hematol* 1991; 19:364–368.
12. Arakelyan L, Vainstein V, Agur Z. A computer algorithm describing the process of vessel formation and maturation, and its use for predicting the effects of anti-angiogenic and anti-maturation therapy on vascular tumor growth. *Angiogenesis* 2002;5:203–214.
13. Ribba B, Alarcon T, Marron K, Maini PK, Agur Z. Doxorubicin treatment efficacy on non-Hodgkin's lymphoma: computer model and simulations. *Bull Math Biol* 2005;67: 79–99.
14. Vainstein V, Ginosar Y, Shoham M, Ranmar D, Ianovski A, Agur Z. The complex effect of granulocyte on human granulopoiesis analyzed by a new physiologically-based mathematical model. *J Theor Biol* 2005;234(3):311–327.
15. Agur Z, Ziv I, Shohat R, Wick M, Webb C, Hankins D, Arakelyan L, Sidransky D. Using a novel computer technology for tailoring targeted and chemotherapeutic drug schedules to the individual patient. *First AACR International Conference on Molecular Diagnostic in Cancer Therapeutic Development. Chicago IL*, 2006.
16. Hoffman R, Benz EJ, Shattil SJ, Furie B, Cohen HJ, Silberstein LE, McGlave P. *Hematology*, 3rd ed. London: Churchill Livingstone; 2000.
17. Kaushansky K. The molecular mechanisms that control thrombopoiesis. *J Clin Invest* 2005;115:3339–3347.
18. Kaushansky K. Lineage-specific hematopoietic growth factors. *N Engl J Med* 2006; 354:2034–2045.
19. Schulze H, Shivdasani RA. Mechanisms of thrombopoiesis. *J Thromb Haemost* 2005; 3:1717–1724.
20. Cines DB, Bussel JB, McMillan RB, Zehnder JL. Congenital and acquired thrombocytopenia. In *Hematology, the American Society of Hematology Education Program Book*: 2004, pp 390–406.
21. McCrae KR, Bussel JB, Mannucci PM, Cines DB. Platelets: an update on diagnosis and management of thrombocytopenic disorders. In *Hematology, the American Society of Hematology Education Program Book*: 2001, pp 282–305.
22. Demetri GD. Targeted approaches for the treatment of thrombocytopenia. *Oncologist* 2001;6(Suppl 5):15–23.

23. Schwertschlag US, Trepicchio WL, Dykstra KH, Keith JC, Turner KJ, Dorner AJ. Hematopoietic, immunomodulatory and epithelial effects of interleukin-11. *Leukemia* 1999; 13(9):1307–1315.
24. Tepler I, Elias L, Smith JW 2nd, Hussein M, Rosen G, Chang AY, Moore JO, Gordon MS, Kuca B, Beach KJ, Loewy JW, Garnick MB, Kaye JA. A randomized placebo-controlled trial of recombinant human interleukin-11 in cancer patients with severe thrombocytopenia due to chemotherapy. *Blood* 1996;87(9):3607–3614.
25. Haznedaroglu IC, Goker H, Turgut M, Buyukasik Y, Benekli M. Thrombopoietin as a drug: biologic expectations, clinical realities, and future directions. *Clin Appl Thromb/ Hemost* 2002;8:193–212.
26. Basser R. The impact of thrombopoietin on clinical practice. *Curr Pharm Design* 2002; 8(5):369–377.
27. Elting LS, Rubenstein EB, Martin CG, Kurtin D, Rodriguez S, Laiho E, Kanesan K, Cantor SB, Benjamin RS. Incidence, cost, and outcomes of bleeding and chemotherapy dose modification among solid tumor patients with chemotherapy-induced thrombocytopenia. *J Clin Oncol* 2001;19:1137–1146.
28. Kaushansky K, Lin N, Grossman A, Humes J, Sprugel KH, Broudy VC. Thrombopoietin expands erythroid, granulocyte-macrophage, and megakaryocytic progenitor cells in normal and myelosuppressed mice. *Exp Hematol* 1996;24:265–269.
29. Li J, Yang C, Xia Y, Bertino A, Glaspy J, Roberts M, Kuter DJ. Thrombocytopenia caused by the development of antibodies to thrombopoietin. *Blood* 2001;98(12):3241–3248.
30. Vadhan-Raj S. Recombinant human TPO: clinical experience and *in vivo* biology. *Semin Hematol* 1998;35:261–268.
31. Vadhan-Raj S. Clinical experience with recombinant human thrombopoietin in chemotherapy-induced thrombocytopenia. *Semin Hematol* 2000;37(2 Suppl 4):28–34.
32. Vadhan-Raj S. Recombinant human thrombopoietin in myelosuppressive chemotherapy. *Oncology (Williston Park)* 2001;15(7 Suppl 8):35–38.
33. Vadhan-Raj S, Cohen V, Bueso-Ramos C. Thrombopoietic growth factors and cytokines. *Curr Hematol Rep* 2005;4(2):137–144.
34. Wolff SN, Herzig R, Lynch J, Ericson SG, Greer JP, Stein R, Goodman S, Benyunes MC, Ashby M, Jones DV Jr, Fay J. Recombinant human thrombopoietin (rhTPO) after autologous bone marrow transplantation: a phase I pharmacokinetic and pharmacodynamic study. *Bone Marrow Transplant* 2001;27(3):261–268.
35. Dykstra KH, Rogge H, Stone A, Loewy J, Keith JC Jr, Schwertschlag US. Mechanism and amelioration of recombinant human interleukin-11 (rhIL-11)-induced anemia in healthy subjects. *J Clin Pharmacol* 2000;40(8):880–888.
36. Kheifetz Y, Elishmereni M, Horowitz S, Agur Z. Fluid-retention side-effects of the chemotherapy-supportive treatment interleukin-11: mathematical modelling as affected by data availability. *Comput Math Methods Med* 2006;7(2–3):71–84.
37. Skomorovski K, Agur Z. A new method for predicting and optimizing thrombopoietin (TPO) therapeutic protocols in thrombocytopenic patients and in platelet donors [abstract]. *Hematol J* 2001;1(Suppl 1):185.
38. Skomorovski K, Harpak H, Ianovski A, Vardi M, Visser TP, Hartong S, Van Vliet H, Wagemaker G, Agur Z. New TPO treatment schedules of increased safety and efficacy: preclinical validation of a thrombopoiesis simulation model. *Br J of Haematol* 2003; 123(4):683–691.
39. Vadhan-Raj S, Murray LJ, Bueso-Ramos C, Patel S, Reddy SP, Hoots WK, Johnston T, Papadopolous NE, Hittelman WN, Johnston DA, Yang TA, Paton VE, Cohen RL, Hellmann SD, Benjamin RS, Broxmeyer HE. Stimulation of megakaryocyte and platelet

production by a single dose of recombinant human thrombopoietin in patients with cancer. *Ann Intern Med* 1997;126:673–681.

40. Vadhan-Raj S, Patel S, Bueso-Ramos C, Folloder J, Papadopolous N, Burgess A, Broemeling LD, Broxmeyer HE, Benjamin RS. Importance of predosing of recombinant human thrombopoietin to reduce chemotherapy-induced early thrombocytopenia. *J Clin Oncol* 2003;21:3158–3167.
41. Castiglione F, Selitser V, Agur Z. The analyzing hypersensitive to chemotherapy in a cellular automata model of the immune system. In Preziosi L. Ed. *Cancer Modelling and Simulation*. Boca Raton, FL: CRC Press; 2003.
42. Arnold JT, Daw NC, Stenberg PE, Jayawardene D, Srivastava DK, Jackson CW. A single injection of pegylated murine megakaryocyte growth and development factor (MGDF) into mice is sufficient to produce a profound stimulation of megakaryocyte frequency, size, and ploidization. *Blood* 1997;89:823–833.
43. Ebbe S, Stohlman F. Megakaryocytopoiesis in the rat. *Blood* 1965;26:20–35.
44. Luoh S, Stephanich E, Solar G, Steinmetz H, Lipari T, Pestina TI, Jackson CW, de Sauvage FJ. Role of the distal half of the c-Mpl intracellular domain in control of platelet production by thrombopoietin *in vivo*. *Mol Cell Biol* 2000;20:507–515.
45. Schermer S. *Blood Morphology of Laboratory Animals*. Philadelphia: FA Davis Co; 1967.
46. Siegers MP, Feinendegen LE, Lahiri SK, Cronkite EP. Relative number and proliferation kinetics of hemopoietic stem cells in the mouse. *Blood Cells* 1979;5:211–236.
47. Ulich TR, del Castillo J, Senaldi G, Cheung E, Roskos L, Young J, Molineux G, Guo J, Schoemperlen J, Munyakazi L, Murphy-Filkins R, Tarpley JE, Toombs CF, Kaufman S, Yin S, Nelson AG, Nichol JL, Sheridan WP. Megakaryocytopoiesis: the prolonged hematologic effects of a single injection of PEG-rHuMGDF in normal and thrombocytopenic mice. *Exp Hematol* 1999;27:117–130.
48. De Serres M, Yeager RL, Dillberger JE, Lalonde G, Gardner GH, Rubens CA, Simkins AH, Sailstad JM, McNulty MJ, Woolley JL. Pharmacokinetics and hematological effects of the pegylated thrombopoietin peptide mimetic GW395058 in rats and monkeys after intravenous or subcutaneous administration. *Stem Cells* 1999;17:316–326.
49. Farese AM, Hunt P, Boone T, MacVittie TJ. Recombinant human megakaryocyte growth and development factor stimulates thrombopoiesis in normal nonhuman primates. *Blood* 1995;86:54–59.
50. Harker LA, Hunt P, Marzec UM, Kelly AB, Tomer A, Hanson SR, Stead RB. Regulation of platelet production and function by megakaryocyte growth and development factor in nonhuman primates. *Blood* 1996;87:1833–1844.
51. Harker LA, Marzec UM, Hunt P, Kelly AB, Tomer A, Cheung E, Hanson SR, Stead RB. Dose–response effects of pegylated human megakaryocyte growth and development factor Of platelet production and function in nonhuman primates. *Blood* 1996;88: 511–521.
52. Neelis KJ, Hartong SC, Egeland T, Thomas GR, Eaton DL, Wagemaker G. The efficacy of single-dose administration of thrombopoietin with coadministration of either granulocyte/macrophage or granulocyte colony-stimulating factor in myelosuppressed rhesus monkeys. *Blood* 1997;90:2565–2573.
53. Sola MC, Christensen RD, Hutson AD, Tarantal AF. Pharmacokinetics, pharmacodynamics, and safety of administering pegylated recombinant megakaryocyte growth and development factor to newborn rhesus monkeys. *Pediatr Res* 2000;47:208–214.
54. Wagemaker G, Hartong SC, Neelis KJ, Egeland T, Wognum AW. *In vivo* expansion of hemopoietic stem cells. *Stem Cells* 1998;16(Suppl 1):185–191.

55. Kabaya K, Akahori H, Shibuya K, Nitta Y, Ida M, Kusaka M, Kato T, Miyazaki H. *In vivo* effects of pegylated recombinant human megakaryocytes growth and development factor on hematopoiesis in normal mice. *Stem Cells* 1996;14:651–660.
56. Janeway CA, Travers P, Walport M, Shlomchik M. *Immunobiology*, 6th ed. New York: Garland Science; 2005.
57. Al-Dabbagh SG, Smith RL. Species differences in oxidative drug metabolism: some basic considerations. *Arch Toxicol Suppl* 1984;7:219–231.
58. Kararli TT. Comparison of the gastrointestinal anatomy, physiology, and biochemistry of humans and commonly used laboratory animals. *Biopharm Drug Dispos* 1995;16(5): 351–380.
59. Lin JH. Species similarities and differences in pharmacokinetics. *Drug Metab Dispos* 1995;23(10):1008–1021.
60. Phillips RM, Bibby MC, Double JA. A critical appraisal of the predictive value of *in vitro* chemosensitivity assays. *J Nat Cancer Inst* 1990;82:1457–1468.
61. Harker LA, Finch CA. Thrombokinetics in man. *J Clin Invest* 1969;48:963–974.
62. Ratajczak J, Machalinski B, Samuel A, Pertusini E, Majka M, Czajka R, Ratajczak MZ. A novel serum free system for cloning human megakaryocytic progenitors (CFU-Meg). The role of thrombopoietin and other cytokines on bone marrow and cord blood CFU-Meg growth under serum free conditions. *Folia Histochem Cytobiol* 1998;36(2) 61–66.
63. Agur Z. Population dynamics in harshly varying environments; evolutionary, ecological and medical aspects. In Hallam TG, Gross LJ, Levin SA, Eds. *Mathematical Ecology*. River Edge, NJ: World Scientific; 1988, pp 440–454.
64. Agur Z. Resonance and anti-resonance in the design of chemotherapeutic protocols. *J Theor Biol* 1998;1:237–245.
65. Vainstein V, Ginosar Y, Shoham M, Ianovski A, Rabinovich A, Kogan Y, Selitser V, Ariad S, Chan S, Agur Z. Clinical validation of a physiologically-based computer model of human granulopoiesis and its use for improving cancer therapy by doxorubicin and granulocyte colony-stimulating factor (G-CSF). *Annual Meeting American Society of Hematology (ASH), Orlando, FL*, 2006.